NASA CR-72138

SECOND QUARTERLY REPORT

ELECTROCHEMICAL CHARACTERIZATION OF SYSTEMS FOR SECONDARY BATTERY APPLICATION

August - October, 1966

by

M. Shaw, N. K. Gupta, A. H. Remanick, R. J. Radkey

prepared for

NATIONAL AERONAUTICS AND SPACE ADMINISTRATION

November 18, 1966

CONTRACT NAS 3-8509

Technical Management
Space Power Systems Division
National Aeronautics and Space Administration
Lewis Research Center, Cleveland, Ohio
Mr. Robert B. King

NARMCO RESEARCH AND DEVELOPMENT DIVISION
OF
WHITTAKER CORPORATION
3540 Aero Court
San Diego, California 92123

TABLE OF CONTENTS

CYCLIC VOLTAMMOGRAMS

LIST OF TABLES

ELECTROCHEMICAL CHARACTERIZATION OF SYSTEMS FOR SECONDARY BATTERY APPLICATION

by

M. Shaw, N. K. Gupta, A. H. Remanick, R. J. Radkey

ABSTRACT

Multisweep cyclic voltammograms have been obtained for one hundred and fifty-three systems comprising silver, copper, nickel, zinc, cadmium, and molybdenum in acetonitrile, butyrolactone, dimethylformamide, and propylene carbonate solutions of chlorides and fluorides. Voltammograms are presented for fifty-six of these systems. Tabular data includes peak current density, sweep index, charge-discharge efficiency, and discharge capacity.

SUMMARY

The electrochemical characterization of systems by the method of multi-sweep cyclic voltammetry has continued. Cyclic voltammograms are now available on over two hundred systems comprising silver, copper, nickel, zinc, cadmium, and molybdenum in chloride and fluoride solutions of acetonitrile, butyrolactone, dimethylformamide, and propylene carbonate. The solutes consisted of $AlCl_3$, LiCl, $MgCl_2$, $LiClO_4$, LiF, MgF_2, $LiPF_6$, $LiBF_4$, and KPF_6. The cyclic voltammograms of fifty-six systems are included in this report.

A new procedure for data analysis has been adopted, which has greatly facilitated interpretation of the curves, and permits better correlation of the electrochemical systems.

Tables are presented listing system parameters derived from the cyclic voltammograms. These tables present data on peak current densities, sweep index, cathode reaction type and solution compatibility, anodic to cathodic peak displacement, charge-discharge efficiency, and discharge capacity. Nearly all systems demonstrate reduction of a solid state material during discharge, this material being anodically-formed during the voltage sweep. Where exceptions are found, these generally contain perchlorate ion as the sole solute species. In such uses, reduction of a dissolved species is indicated.

The effect of sweep rate on the anodic to cathodic peak ratio gives a relative measure of anodically-formed cathode material stability to electrolyte dissolution. In general, silver chloride is insoluble, copper chloride and silver fluoride are soluble, and copper fluoride systems mostly insoluble.

Some preliminary voltammograms are presented on zinc, cadmium, and molybdenum electrodes. In general, excellent sweep curves were obtained for zinc and cadmium. Molybdenum failed to form an anodic product.

Chemical characterization of LiCl, LiF, MgF_2, and $LiClO_4$, and silver, copper, and nickel wire, has been recorded. Analysis was made by emission spectroscopy.

INTRODUCTION

The purpose of this program is to conduct a molecular level screening by the cyclic voltammetric method on a large number of electrochemical systems in nonaqueous electrolytes, and to characterize them as to their suitability for use in high energy density secondary batteries.

Since the release and storage of energy in a battery is initiated at the molecular level of the reaction, and therefore dependent on the charge and mass transfer processes, it is essential that screening be conducted at this level, in order to eliminate those systems whose electrode processes are inadequate for secondary battery operation.

I. RESULTS

A. MATERIAL PURIFICATION AND CHARACTERIZATION

During this period, further purification and characterization of materials has been accomplished.

1. Solvent Purification and Characterization

The solvents employed during this period were dimethylformamide, butyrolactone, propylene carbonate, and acetonitrile. With the exception of dimethylformamide, purification of each of these materials was accomplished by distillation under conditions previously described (Ref. 1). Variation in the amount of water found in propylene carbonate necessitated a double distillation with drying over calcium sulfate between the first and second distillation.

Analysis of the solvents was usually carried out by vapor phase chromatography (VPC). The conditions for the VPC analysis have been previously detailed,[1] however two phases of the VPC analysis were investigated further. It has been shown that the use of a polyethylene glycol (PEG) 1540 column allowed resolution of water in butyrolactone. However, a peak appeared in the VPC analysis of a head fraction of butyrolactone which could not be resolved below about 0.05 mole %. Even though this impurity was only apparent in the head fraction, and not in the "as received" material or in the main cuts, resolution of this impurity was attempted on a triscyanoethoxy-propane column (TCEP) and a diethyleneglycol stearate (DEGS) column. Neither of these substrates afforded resolution of the impurity. In order to insure reasonable purity of butyrolactone, a relatively large head cut was taken.

acetonitrile was not possible on a PEG column. Recently, it has been found that VPC analysis using a TCEP column or DEGS column did not afford resolution of water in acetonitrile. Analysis of water by the Karl Fischer method (Ref. 2) showed that acetonitrile distilled under the conditions previously indicated contained 60-80 ppm water. Unless a VPC method becomes available, analysis for water in acetonitrile will be carried out by the Karl Fischer titration.

2. Solute Purification and Characterization

In the initial portion of the program, most of the solutes chosen for screening could be obtained in sufficient purity, with purification limited to drying. Analysis of these materials (Table I) indicated that they were reasonably pure, and that expected impurities would not markedly affect the interpretation of the cyclic voltammograms.

In addition to the common salts shown in Table I, two additional materials were used in the screening program. Potassium hexafluorophosphate (Ozark-Mahoning), 99.6% pure by fluoride analysis, was dried at 120° C for three days. Since this material was not of primary importance in the program, no further characterization was made. However, since the salt may be recrystallized from water, it was not expected that appreciable hydrolysis or dissociation would occur under the drying conditions. The small amount of impurity indicated by the analysis is probably due to the presence of lithium oxide which would not be expected to interfere with the sweep determinations.

Since it was expected that commercially available aluminum chloride was of doubtful purity, purification of this material was accomplished by sublimation at approximately 170° C. Although the material was not analyzed at this time, such treatment should preclude the presence of major impurities.

TABLE I

ANALYSIS OF METAL SALTS*

ppm

Element	LiCl	LiF	MgF_2	$MgCl_2$	$LiClO_4$
Fe	60	4.2	170	52	nil
Al	92	1.7	nil	nil	nil
Cu	1.2	2.5	3.3	27	.54
Ni	nil	1.4	nil	nil	nil
Ca	260	16	430	24	20
Si	36	15	510	51	nil
Mg	3.8	1.2	nil	nil	6.1
Na	nil	nil	nil	nil	nil
K	nil	nil	nil	nil	nil
Mn	nil	.48	110	110	nil
B	nil	nil	330	nil	nil
Ti	nil	nil	55	22	nil
Sr	nil	nil	nil	nil	< 2

* Analysis by emission spectroscopy (Truesdail Laboratories, Inc., Los Angeles, Calif.) Limits of detection of sodium and potassium by this method approximately 0.02%.

The metal electrodes, copper, silver, and nickel were obtained from laboratory supply houses. Analysis of these materials is given in Table II. Although one may not state with complete assurance that the indicated impurities do not affect the nature of the electrochemical processes involved in the electrochemical measurements, it is not expected that the use of extremely high purity materials would markedly affect the sweep curves, sufficient to justify their cost in a screening program.

Since the electrodes, molybdenum, zinc, and cadmium were only used in preliminary screening, no analysis of these materials was made. However, data furnished from the suppliers indicated 99.9% purity.

Copper oxide and nickel oxide electrodes were prepared by heating the metals in a stream of air for a specified time. Attempted preparation of silver oxide electrodes by this method was not successful, so that these electrodes were prepared by electrolytic oxidation in 30% KOH followed by vacuum drying. Although the specific composition of the oxide electrodes was not investigated, these electrodes gave reproducible results in the voltage sweep measurements.

Solution conductivities are given in Table III. A value of 5×10^{-4} ohm^{-1} cm^{-1} had been previously established as a useful limit for systems to be screened, however, a few systems having a lower value were measured in order to ascertain the effect of poor conductivity.

TABLE II

ANALYSIS OF WIRE ELECTRODES*

ppm

Element	Cu	Ag	Ni
Co	nil	nil	1600
Ti	nil	nil	140
Cu	-	91	< 320
Al	nil	nil	30
Fe	9.1	< 10	540
Si	nil	nil	500
Mn	nil	nil	1300
Mg	1.9	2.4	320
B	nil	nil	63
Ag	13	-	nil
Ni	< 10	nil	-
Ca	7.8	< 2	nil
Pb	nil	< 40	nil

* Analysis by emission spectroscopy (Truesdail Laboratories, Los Angeles, California)

TABLE III

ELECTROLYTE CONDUCTIVITIES

Electrolyte	Molality m	Conductivity $ohm^{-1}\ cm^{-1}$
Acetonitrile		
LiCl	< 0.5(s)	4.1×10^{-4}
$AlCl_3$	1.0	4.5×10^{-2}
$LiCl + AlCl_3$	0.082(1)	7.6×10^{-3}
$LiClO_4$	1.0	4.4×10^{-2}
KPF_6	0.75	3.3×10^{-2}
$KPF_6 + LiF$	0.75	3.5×10^{-2}
Butyrolactone		
LiCl	0.75	1.3×10^{-3}
$AlCl_3$	0.5	1.3×10^{-2}
$LiCl + AlCl_3$	0.5(1)	8.1×10^{-4}
$MgCl_2$	(2)	5.5×10^{-3}
$MgCl_2 + LiCl$	0.75(1)	7.3×10^{-3}
$LiClO_4$	0.75	1.7×10^{-2}
$LiClO_4 + LiCl$	(3)	3.2×10^{-3}
$LiClO_4 + AlCl_3$	0.5(1)	1.7×10^{-2}
MgF_2	< 0.5(s)	2.0×10^{-6} *
$MgF_2 + LiF$	< 0.5(s)	4.6×10^{-5}
KPF_6	0.5	1.2×10^{-2}
$KPF_6 + LiF$	(4)	1.57×10^{-2}

* Probably reported in error

TABLE III - Cont'd

Electrolyte	Molality m	Conductivity $ohm^{-1}\ cm^{-1}$
Dimethylformamide		
LiCl	0.75	1.4×10^{-2}
$MgCl_2$	< 0.5(s)	1.7×10^{-2}
$MgCl_2$ + LiCl	< 0.5(s)	1.5×10^{-2}
$LiClO_4$	0.75	3.4×10^{-2}
$LiClO_4$ + LiCl	0.75(1)	2.1×10^{-2}
$LiClO_4$ + $AlCl_3$	< 0.5(s)	1.8×10^{-2}
MgF_2	< 0.5(s)	2.2×10^{-6}
KPF_6	0.75	2.5×10^{-2}
KPF_6 + LiF	(4)	2.3×10^{-2}
Propylene Carbonate		
$MgCl_2$	< 0.5(s)	2.9×10^{-3}
$MgCl_2$ + LiCl	< 0.5(s)	5.8×10^{-3}
$LiClO_4$	1.0	2.0×10^{-3}
KPF_6	0.75	9.1×10^{-3}
KPF_6 + LiF	(4)	1.0×10^{-2}

(s) Saturated

(1) Concentration with respect to each salt

(2) Saturated between 0.75 and 1.0 m

(3) Solution was 0.75 m in $LiClO_4$ and saturated with LiCl at greater than 0.5 m

(4) Solution initially 0.75 m in KPF_6 and saturated with LiF. Solution was stirred overnight to equilibrate.

B. ANALYSIS OF CYCLIC VOLTAMMOGRAMS

Tables IV and V list the electrochemical systems screened during the second quarter of this program. This represents a total of 153 systems. Curve analysis was accomplished by dividing all systems into two major groups:

1. Systems involving chloride electrolytes
2. Systems involving fluoride electrolytes

Each main group was then subdivided according to the identity of the working electrode. Each of these subgroups was further broken down according to the identity of the solvent portion of the solution. The cyclic voltammograms are then discussed in terms of the total solution. This classification has not only facilitated analysis of the data, but more important, has vastly improved interpretation of the data, and has permitted a more significant correlation among the electrochemical systems.

Except in those cases where the metal is converted to a cathodic material prior to assembly in the measuring cell, the working electrode is the base metal itself. During the voltage sweep, the metal is oxidized to some species, this anodic product then serving as the cathode which is subsequently reduced during the cathodic portion of the sweep. Each sweep cycle thus corresponds to a charge-discharge cycle. In the absence of complicating factors, it is assumed that chloride cathodes would be formed in chloride electrolytes, and fluoride cathodes in fluoride electrolytes. This assumption is made with no allusion to reaction mechanism, and the curves generally analyzed on this basis.

Each cyclic voltammogram is identified by a CV number and labelled according to the electrochemical system, sweep rate, temperature, and zero reference, representing the open circuit voltage (ocv) of the working electrode with respect to the indicated reference electrode. The current axis is in units of ma/cm^2, each unit being of variable scale depending on the X-Y

TABLE IV ELECTROCHEMICAL SYSTEMS SCREENED - CHLORIDE ELECTROLYTES*

Solute \ Solvent	Acetonitrile	Butyrolactone	Dimethylformamide	Propylene Carbonate
LiCl	Ag	AgO, NiO, CuO	Ag, Ni, Cu, AgO, NiO, CuO	-
$AlCl_3$	Ag, Ni, Cu	Ag, Ni, Cu	-	-
$LiCl+AlCl_3$	Ag, Ni, Cu, AgO, NiO, CuO	AgO, NiO, CuO	Ag, AgO, NiO, CuO	-
$MgCl_2$	-	Ag, Ni, Cu	Ag, Ni, Cu	Ag, Ni, Cu
$MgCl_2+LiCl$	-	Ag, Ni, Cu	Ag, Ni, Cu	Ag, Ni, Cu
$LiClO_4$	AgO, NiO, CuO	AgO, NiO, CuO, Mo	Ag, Ni, Cu, AgO, NiO, CuO	Ag, Ni, Cu, Mo, AgO, NiO, CuO
$LiClO_4+LiCl$	-	Ag, Ni, Cu	Ag, Ni, Cu	-
$LiClO_4+AlCl_3$	-	Ag, Ni, Cu	Ni, Cu, AgO	-

* Oxide formulas not intended to indicate composition.

TABLE V ELECTROCHEMICAL SYSTEMS SCREENED - FLUORIDE ELECTROLYTES**

Solute \ Solvent	Acetonitrile	Butyrolactone	Dimethylformamide	Propylene Carbonate
MgF_2	-	Ag, Ni, Cu, Mo	Ag, Ni, Cu	-
MgF_2+LiF	-	Ag, Ni, Cu	-	-
KPF_6	Ag, Ni, Cu, Ag*, AgO, NiO, CuO, Zn, Cd, Mo	Ag, Ni, Cu, AgO, NiO, CuO, Zn, Cd, Mo	Ag, Ni, Cu, AgO, NiO, CuO, Zn, Cd, Mo	Ag, Ni, Cu, AgO NiO, CuO, Zn, Cd Mo
KPF_6+LiF	Ag, Ni, Cu, AgO, NiO, CuO, Zn, Cd, Mo	Ag, Ni, Cu, AgO, NiO, CuO, Zn, Cd, Mo	Ag, Ni, Cu	Ag, Ni, Cu
$LiPF_6$	-	-	NiO	-
$LiBF_4$	-	-	Ag, Cu	-

* 1000 ppm water in electrolyte

** Oxide formulas not intended to indicate composition

recorder sensitivity setting. A maximum sensitivity of 0.1 ma/cm^2/cm division has been established to avoid exaggerating the current background of poor systems. The sweep is always in a clockwise direction, the potential becoming more positive to the right. Positive currents represent anodic (charge) reactions, and negative currents represent cathodic (discharge) reactions. The voltage axis units are relative to the ocv so that voltage units are in terms of electrode polarization.

For comparative purposes, current density magnitude is classified according to very high (more than 300 ma/cm^2), high (100-300 ma/cm^2), medium high (50-100 ma/cm^2), medium low (10-50 ma/cm^2), low (1-10 ma/cm^2), and very low (less than 1 ma/cm^2).

Analysis is based on the cyclic voltammograms obtained at the lowest sweep rate, 40 mv/sec, except where additional information is required from the higher sweep rate curves to aid in the analysis.

Designation of Solid State or Dissolved Species Reduction Process

In this, and in an earlier report (Ref. 1), tables are given indicating whether a solid state material or a dissolved species is involved during the cathodic portion of the sweep, and whether the product formed during the anodic portion is soluble or insoluble. For purposes of clarification, this is now discussed in detail.

We consider the following reaction

$$M + X^- \longrightarrow MX + e^-$$

where M is a solid metal electrode, X^- is a soluble anion, and MX is a relatively insoluble solid product. This situation is therefore schematically represented as

M	MX	X^-
Metal	Insoluble Compound	Solution

The layer MX is represented as having some finite depth since prior work at Narmco has demonstrated a thickness of at least 5 monolayers existing at solid electrodes. This representation requires that the MX layer also contains some M species. Charge transfer may therefore be possible either at the M-MX or at the MX-solution interfaces. Determination of which occurs involves consideration of the characteristics of the MX layer. Current must be accompanied by transport through the MX phase of M, M^+, or X^-. It is generally accepted (though not proven) that only M and M^+ are transportable. In metal-excess types, the metal atoms are assumed to migrate interstitially with electron transfer occurring at the MX-solution interface. The electrons must then also cross the MX phase, constituting a semiconductor process. In metal-defect materials, it is assumed that the M^+ ion is the migrating species (via defect lattice sites), and that electron transfer occurs at the M-MX interface. This does not require the electron to be carried across the MX layer. If one assumes that the X^- ion is also mobile, then two additional mechanisms are conceivable analogous to the M and M^+ species. The activational energy losses associated with electron transfer, electron migration across the MX layer, and migration of M or M^+ across the MX layer, must be considered together as one since they cannot be individually measured.

The essential point to be made, is that whenever a solid product is formed at a metal electrode and remains there during the period of the sweep measurement, then a M-MX-X' situation exists, which involves an entirely different electrochemical environment than is to be found in the case of electro-oxidation or reduction of dissolved species at an inert electrode such as mercury, platinum, or pyrolytic graphite. The presence of the MX layer requires that both mass transfer and charge transfer processes within this layer be considered, as well as those normally found at metal-solution interfaces in the case of inert electrodes.

For a reversible dissolved species and an inert electrode, and where the electrode reaction is limited only by mass transfer of ions, the cyclic voltammogram would be typified by the following:

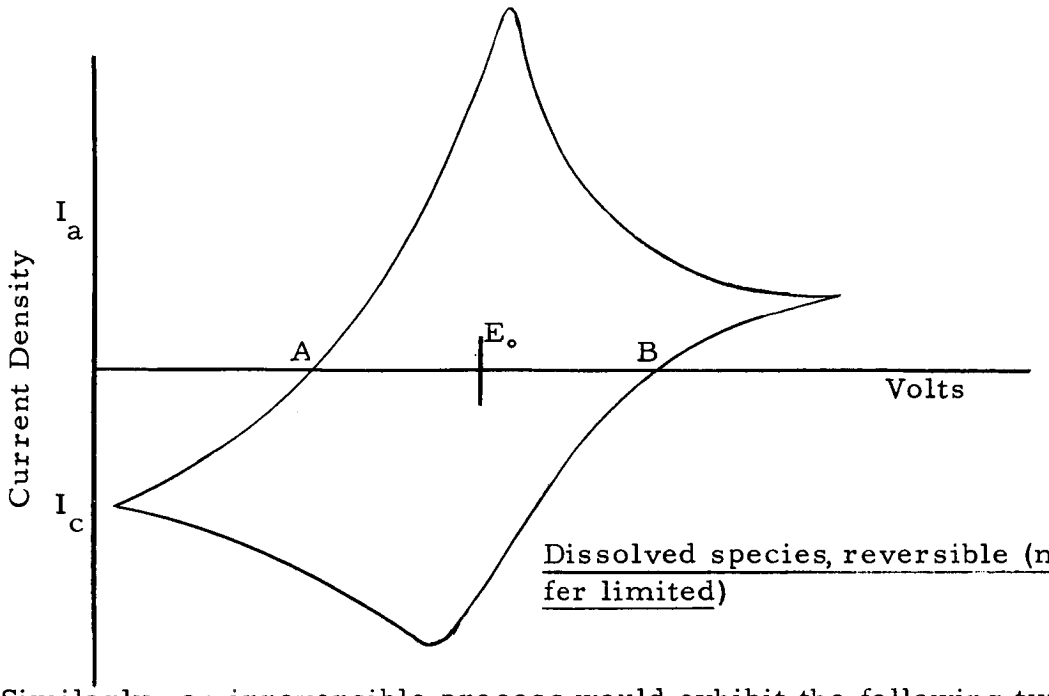

Dissolved species, reversible (mass transfer limited)

Similarly, an irreversible process would exhibit the following type of curve:

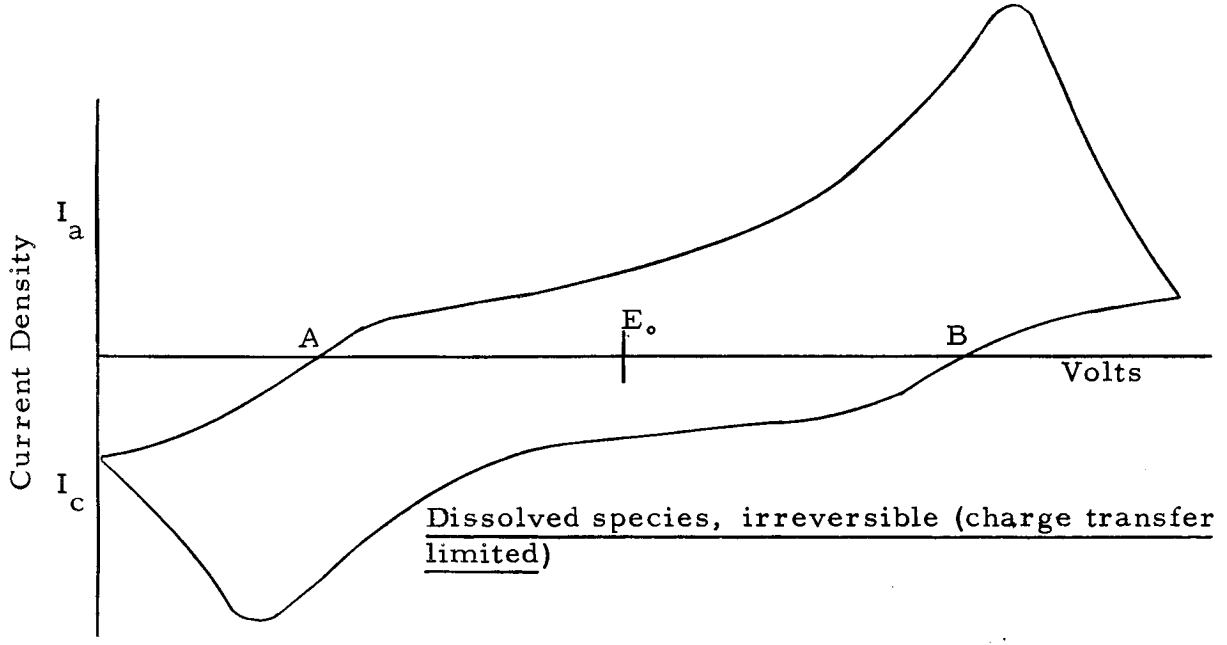

Dissolved species, irreversible (charge transfer limited)

in which the peaks are considerably displaced from the ocv (E_o) value, and from each other. In general, the distance between the two points (A and B) where the curve intersects the zero-current axis, is a relative measure of the concentration polarization.

The presence of a solid product at the metal electrode results in a cyclic voltammogram of the type

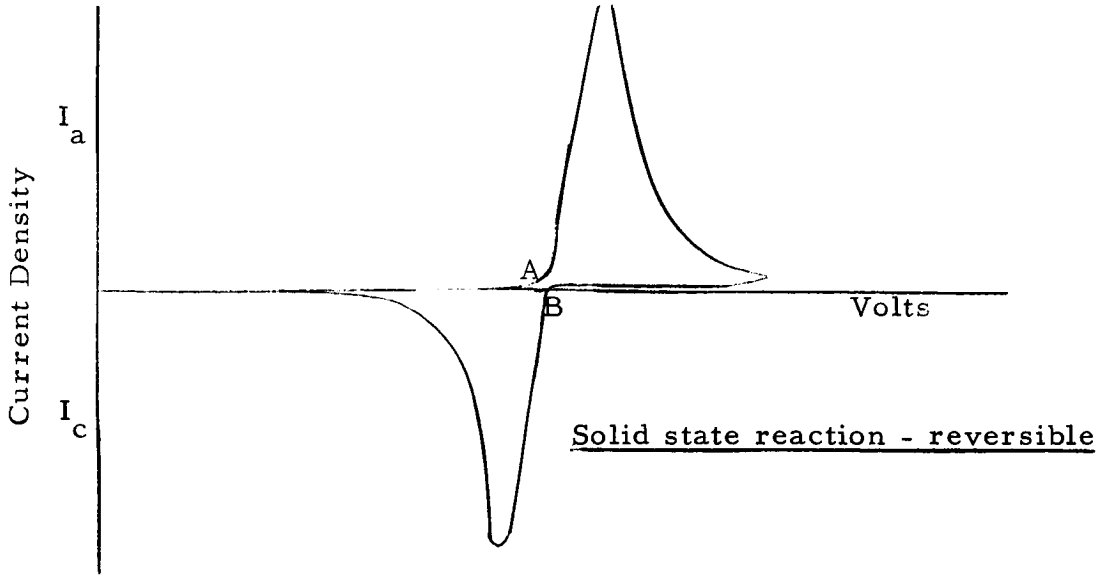

Solid state reaction - reversible

for relatively reversible systems (low activation polarization). For irreversible systems, where the charge transfer process is limiting, the following type of curve will result:

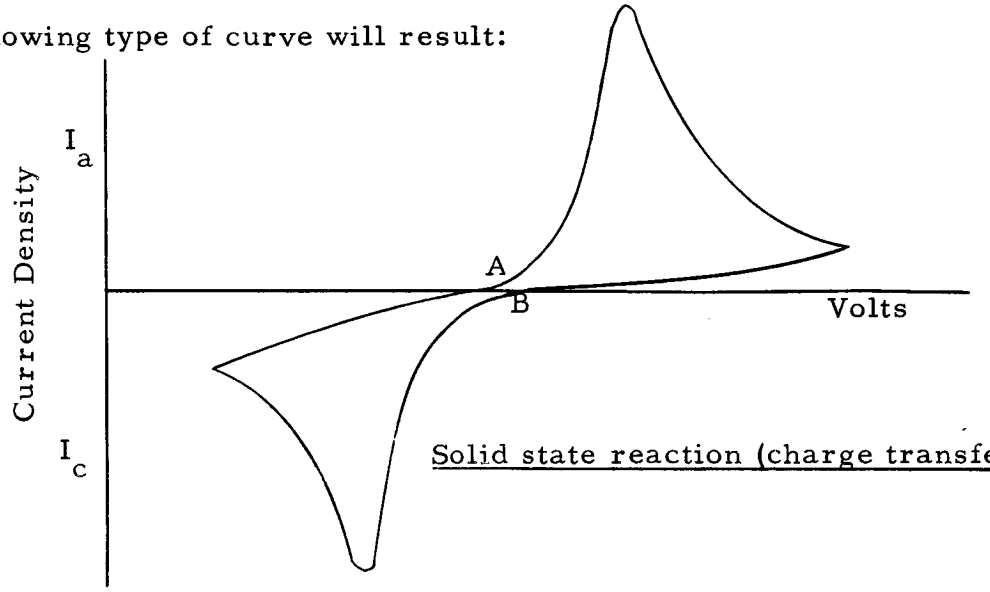

Solid state reaction (charge transfer limited)

The relatively small displacement between points A and B indicates the low degree of concentration polarization. This displacement will become larger with increasing concentration polarization.

Most of the systems screened to date indicate the solid state type of cyclic voltammogram. In addition to this however, the cyclic voltammograms of a large number of systems exhibit a decrease in the cathodic peak current density (with respect to the anodic peak current density) with decreasing sweep rate. These systems also exhibit visual streaming out from the working electrode, as well as solution discoloration. At sufficiently low sweep rates, many systems fail to show any cathodic current. Apparently the product formed during the anodic portion of the sweep is less available, or no longer exists, at the lower sweep rates for subsequent reduction.

If the cathodic reaction involved reduction of a dissolved species in solution no such pronounced effect by sweep rate would be evident, since a sufficient amount would be available for reaction. If, however, the cathodic reaction involved reduction of a solid state product, then at slower sweep rates more of the anodic product has had time to dissolve, resulting in less material available for reduction. At sufficiently slow sweeps, little or none is left at the electrode for the discharge reaction. The effect of sweep rate on the height of the cathodic peak is therefore an indication of relative solubility within the time period of the measurement. Such systems are designated as having a solid state cathodic reaction with the cathode material (product formed during the anodic sweep) being soluble in the electrolyte.

It is of great interest that no reduction of dissolved material occurs (evidenced by the absence of a cathodic current at low sweep rates) even though the solution is heavily contaminated with dissolved oxidized metal species. No explanation is offered at this time, but the answer may lie in the complexation and solvation of these ions preventing their reduction within the voltage range limits, or possibly their complete non-reactivity due to inability to be adsorbed at the electrode surface.

A number of systems have been found in which the anode-cathode peak ratio remains invariant with sweep rate, and the solution remains unchanged during the measurements. In these cases, the cathode is designated as being insoluble, and again the cathodic reaction involves reduction of a solid state material.

In a fewer number of cases dissolution of electrode material is observed, and yet the cathodic peak height remains invariant (relative to the anodic peak height) with decreasing sweep rate. This is often accompanied by extensive concentration polarization (large displacement between A and B). Since the cathodic current density does not decrease, in spite of electrode

dissolution, it has been assumed that the reduction reaction involves a dissolved species. This is in agreement with the significant concentration polarization. In a limited number of cases, however, cyclic voltammograms typical of solid state reduction reactions, with minimal concentration polarization, have been obtained, and designated as dissolved species reduction, because of the invariance of the cathode peak. Such cases may actually involve a solid state reduction reaction, the solution discoloration being due only to slow dissolution of cathode material. In order to establish this fact, more detailed measurements (electrode rotation, use of a pyrolytic graphite electrode) would have to be performed, which is not conducive to a broad screening program. Designation of a "dissolved species" reduction for any system must therefore still be considered suspect, and may only imply formation of an anodic product which is partially soluble (again, relative to the time period of the measurement).

The inclusion of tabular data designating cathode reaction type (solid state or dissolved species) and cathode compatibility (soluble or insoluble) is continued in this report since it serves as another indication for system recommendation, since obviously the most desirable positive plate for battery application is one which is insoluble in the electrolyte, and which (similar to AgO, AgCl, etc. in aqueous solution) involves an electrochemical conversion via a solid state material MA, where M is the reduced metal, and A is the anion common with the electrolyte species.

1. Systems Involving Chloride Electrolytes

a. Silver Chloride - Anodically Formed During Cyclic Voltammetry

Cyclic voltammograms obtained with metallic silver in chloride solutions are assumed to represent the reaction

$$Ag + Cl^- \rightleftharpoons AgCl + e^-$$

This assumption is valid based on the observation that only a single anodic or cathodic peak is generally obtained, except in dimethylformamide solutions, and the cathodic reaction represents reduction of a solid state mater-

ial insoluble in the electrolyte. We now discuss the individual electrochemical systems under the headings of the various solvents.

(1) Butyrolactone solutions

Figure 1 (CV-444) represents the cyclic voltammogram of silver metal in butyrolactone-LiCl electrolyte. No anodic peak was obtained in the voltage range scanned, and only a low cathodic peak was obtained. The substitution of $MgCl_2$ for LiCl results in a curve exhibiting a typical anodic peak for the oxidation of Ag to AgCl, and a typical cathodic peak for the reduction of AgCl to metallic silver. This is shown in Figure 2 (CV-673). The addition of LiCl to butyrolactone-$MgCl_2$ decreases the peak current densities from medium high to medium low as shown in Figure 3 (CV-685). The curves shown in Figures 2 and 3 represent a desirable type of cyclic voltammogram (the ideal would be even sharper peaks with still less displacement). The smooth and directly descending portion of the cathodic peaks to the zero-current axis represents a clean non-complicated reaction. Both curves also exhibit a low degree of concentration polarization, indicated by the small displacement in volts where the ascending portions of the anodic and cathodic peaks intersect the zero-current axis. In addition, the initiation of both the anodic and cathodic reactions at close to the same potential indicates a relative low activation polarization.

The substitution of $AlCl_3$ (Figure 4, CV-782) for either $MgCl_2$ or LiCl results in a system having high peak current densities, e.g. 260 ma/cm^2 for the cathodic current density compared with 74 and 34 ma/cm^2 for $MgCl_2$ and $MgCl_2$+LiCl respectively. $AlCl_3$, however, increases the activation polarization (indicated by an increase in ΔV_p) by nearly 0.3 volts. Concentration polarization is negligible.

The effect of adding $LiClO_4$ to butyrolactone-LiCl is shown in Figure 5 (CV-865) indicating that the perchlorate ion may act separately from the chloride ion in its reaction with silver, its anodic and cathodic reactions occurring at a more positive potential than with chloride. A second

obvious possibility is the existence of a higher oxidation state of silver. Unlike the case for LiCl alone (Figure 1) an anodic peak typical for silver oxidation to AgCl is exhibited at +0. 3 volts, and a typical cathodic peak at -0. 2 volts. A voltage inflection at about -0. 4 volts indicates reduction of some other species.

Figure 6 (CV-1058) shows the curve for butyrolactone-$LiClO_4$+$AlCl_3$. This curve compares well with that obtained for $AlCl_3$ alone (Figure 4) except that a slight anodic inflection occurs just prior to the main oxidation peak. Absent however, is the secondary peak attributed to the perchlorate ion.

Voltammetric measurements were also made using silver wire electrodes electrolytically oxidized in aqueous solution. Figure 7 (CV-756) shows the curve obtained in butyrolactone-LiCl solution. Unlike the corresponding case of silver, an anodic peak is now obtained, although somewhat broader, as well as a much higher cathodic peak. In addition, the peak-to-peak separation is much greater for the oxide electrode than for metallic silver (see Figures 2 and 3).

Pre-oxidized silver in LiCl+$AlCl_3$ represents an excellent electrochemical system for secondary battery application. The cyclic voltammogram is shown in Figure 8 (CV-1081). The extremely high cathodic peak, very high anodic peak, with a peak-to-peak displacement (ΔV_p) of only 230 mv are desirable voltammetric parameters in terms of potential secondary battery systems. Other requirements are high charge-discharge efficiency and discharge capacity. For the AgO/butyrolactone-LiCl+ $AlCl_3$ system these are 100% and 4. 4 coulombs/cm^2, respectively, the latter being of the highest measured to date. No results were available for untreated silver in this solution, so it cannot be stated at this time whether pre-oxidation has any influence on the desirable properties of this system. In any case, this system is recommended for further study.

Silver oxide in butyrolactone-$LiClO_4$ (Figure 9, CV-888) gave comparable results with untreated silver in the same solution, in that the cathodic reaction involved reduction of dissolved species. This implies that at no time was a solid state anodic product formed, but that the oxidation of silver was immediately followed by the reduction of silver ions in solution.

(2) Acetonitrile solutions

Silver in acetonitrile-LiCl (Figure 10, CV-477) exhibits medium low current densities. The anodic reaction, although exhibiting a peak, unlike the butyrolactone case, is accompanied by a conflicting reaction at the higher anodic potentials. The low conductance, 4.7×10^{-4} $ohm^{-1}cm^{-1}$ is indicative of a low availability of chloride ions, probably accounting for the medium low currents, and poor charge performance. Addition of $AlCl_3$ causes voltage overload of the equipment indicative of high currents, (in excess of 1.4 $amps/cm^2$). The high reaction rate resulted in anodic product becoming detached from the electrode and dropping to the bottom of the cell. High current and resulting overload also existed in acetonitrile solution containing $AlCl_3$ alone. Pre-oxidized silver wire in acetonitrile-LiCl+$AlCl_3$ also caused instrument overloading.

The effect of $LiClO_4$ is shown in Figure 11 (CV-808) for pre-oxidized silver in acetonitrile-$LiClO_4$. The presence of multiple anodic peaks indicates a complex oxidation in perchlorate solution. The absence of a cathodic peak is a result of anodic product dissolution in the electrolyte. A cathodic peak is observed at the higher sweep rates of 80 and 200 mv/sec. This observation complies with the designation of a solid state cathodic reaction, with the cathode material being soluble in the electrolyte.

(3) Dimethylformamide solutions

The cyclic voltammograms for silver in dimethylformamide-LiCl, Figure 12 (CV-731), exhibits multiple cathodic peaks, the primary peak occurring

at about +0. 1 volt. An anodic peak occurs at +0. 5 volts, followed by the beginning of a second peak at a more positive potential. It is doubtful whether this second peak represents solvent decomposition, due to the occurrence of multiple anodic peaks in other chloride solutions of this solvent, for example, in dimethylformamide-LiCl+$MgCl_2$, Figure 13 (CV-662). Comparable cathodic peaks are obtained however. $MgCl_2$ alone, (Figure 14, CV-524), shows only a single cathodic peak corresponding to the main reduction reaction.

Addition of $AlCl_3$ to dimethylformamide-LiCl gives a very complex curve (Figure 15, CV-501), although the same reduction peak is evident. $AlCl_3$ alone, shown in Figure 16 (CV-469) shows simpler (but lower) anodic peaks. Again, the primary cathodic peak is predominant. Obviously, the oxidation of silver to the chloride in dimethylformamide represents a complex reaction.

Silver in dimethylformamide-$LiClO_4$ with or without LiCl results in formation of a soluble anodic product. LiCl-$LiClO_4$ resulted in instrument overload due to excessive anodic and cathodic currents.

Pre-oxidized silver gave comparable voltammograms, but with some fine differences. Figure 17 (CV-839) is compared with Figure 12 for silver oxide in dimethylformamide-LiCl. The two anodic peaks are both in the voltage range of the sweep, whereas the cathodic peaks are closer together. In the $AlCl_3$+LiCl solution, (Figure 18, CV-1094) the anodic complexity is eliminated, leaving only the two small initial anodic peaks found for the non-treated silver electrode (Figure 15). The larger current densities may again be due to the increased electrode area caused by surface oxidation.

As before, dimethylformamide-$LiClO_4$ results in larger currents causing instrument overload. The curve for $AlCl_3$+$LiClO_4$ in this solvent, shown in Figure 19 (CV-1071), is somewhat comparable to that obtained for non-treated silver (Figure 15). (The observed dissolution of anodic product

even though the anode-cathode peak ratio remains invariant with decreasing sweep rates, suggests that the cathodic reaction, in the presence of perchlorate ion, may involve a dissolved species.)

(4) Propylene carbonate solutions

Figures 20 and 21 (CV's-700 and -711 respectively) were obtained for silver in propylene carbonate solutions of $MgCl_2$ and $MgCl_2$+LiCl respectively. These curves compare well with butyrolactone solutions of the same salts, (Figures 2 and 3 respectively) except that lower peak-to-peak displacements exists for the butyrolactone solutions, indicating that the latter solvent would be more desirable for secondary battery application. For both types of solvents, the cathodic peak current densities are medium low. In both cases, the $MgCl_2$ electrolyte gave more than double the cathode discharge capacity of the $MgCl_2$+LiCl mixture, 0.7 coulombs/cm^2 compared with 0.3 coulombs/cm^2.

The sweep curve for silver in propylene carbonate-$LiClO_4$, Figure 22 (CV-852) exhibits a very broad anodic peak, barely peaking out at +0.9 volts, representing a much poorer system than the halide. Pre-oxidized silver gave the same performance, but with slightly higher current densities.

b. Copper Chloride - Anodically Formed During Cyclic Voltammetry

Cyclic voltammograms obtained with metallic copper in chloride solutions should at first approximation represent the reaction

$$Cu + Cl^- \rightleftharpoons CuCl + e^-$$

followed by

$$CuCl + Cl^- \rightleftharpoons CuCl_2 + e^-$$

or by the sum of these,

$$Cu + 2Cl^- \rightleftharpoons CuCl_2 + 2e^-$$

Because of the possible complex reactions that may be involved, it is not expected that the voltammograms will exhibit single peaks indicative of the above net reactions.

(1) Butyrolactone solutions

Figure 23 (CV-790) represents a typical curve obtained for copper electrodes in chloride solutions of butyrolactone. Copper in butyrolactone-$AlCl_3$ is shown here. The curve is characterized by a sharp first anodic peak followed by a broad, ill-defined second anodic peak. Only a single low cathodic peak is evident, with a hint of a second reduction beyond -1.0 volt. Addition of $LiClO_4$ to this solution shows the second cathodic peak (Figure 24, CV-1066). The cathodic peaks, still differing by about 0.9 v, are more evident with butyrolactone-$MgCl_2$ and butyrolactone-$MgCl_2$+LiCl. The poor discharge properties of copper chloride in butyrolactone solutions make them undesirable systems. Equally poor results were obtained with pre-oxidized copper.

(2) Dimethylformamide solutions

Copper in chloride solutions of dimethylformamide forms soluble, anodic products, with the cathodic reaction being of the solid state type. Figure 25 (CV-739) represents the sweep curve for dimethylformamide-LiCl. The relatively low cathodic peak is due to dissolution of the anodic product, so that less is available for reduction at the low sweep rate of 40 mv/sec. A nearly identical curve is obtained using pre-oxidized copper in the same electrolyte, as shown in Figure 26 (CV-847), but is characterized by sharper and higher peaks. The sharper peaks and smaller peak displacement evident in Figure 26, are due to the fact that this cyclic voltammogram was obtained in the new measuring cell which eliminated IR drop to an absolute minimum (see Experimental). The considerably higher peaks are probably due to the greater surface area due to etching during the pre-oxidation process. Addition of $LiClO_4$ results in a larger cathodic peak current (Figure 27, CV-883), although $LiClO_4$ alone gives poor performance (low current, broad peaks), as shown in Figure 28

(CV-834). Dimethylformamide-$MgCl_2$, (Figure 29, CV-529), exhibits a sharp, but low, cathodic peak and a flat anodic peak.

Multiple anodic peaks were obtained for dimethylformamide-$LiCl+AlCl_3$, as shown in Figure 30 (CV-1102) using a pre-oxidized copper electrode. This is indicative of the complex oxidation reaction of copper in the presence of $AlCl_4^-$. A very high and sharp cathodic peak is also obtained. Similar high cathodic currents are obtained with $LiClO_4+AlCl_3$ (Figure 31, CV-1078). The cathodic reaction in these last examples may possibly involve reduction of a dissolved species.

(3) Acetonitrile solutions

Copper electrodes in acetonitrile-$AlCl_3$ solution form a soluble anodic product during the sweep measurement, so that only a small cathodic peak is evident at 40 mv (20 ma/cm^2 compared to 490 ma/cm^2 for the anodic peak). This compared with the data for acetonitrile-LiCl. Addition of LiCl results in sufficiently higher currents to give instrument overloading. Pre-oxidation of copper results in much lower current densities for acetonitrile-$LiCl+AlCl_3$, as well as a poorly defined anodic peak, suggesting the poor reactivity of copper oxide in this solution. The CV for pre-oxidized copper in acetonitrile-$LiClO_4$ exhibits a sharp anodic peak, but a poorly-defined cathodic peak (Figure 32, CV-816). Untreated copper wire gives the identical curve.

(4) Propylene carbonate solutions

The CV obtained in propylene carbonate-$MgCl_2$ as shown in Figure 33 (CV-707), represents an extremely poor system. Apparently the anodic product, which is poorly formed (low anodic currents) is immediately dissolved, since the cathodic peak is proportionately smaller at the higher sweep rate of 200 mv/sec. Addition of LiCl (Figure 34, CV-718), although giving a better defined anodic peak, the anodic product is still excessively soluble.

Pre-oxidized copper in $LiClO_4$ (Figure 35, CV-972) solution results in a high and sharp cathodic peak. Because the anodic-to-cathodic peak ratio is invariant with sweep rate, and no solution discoloration was observed, the cathodic reaction must involve reduction of an insoluble solid state material. The voltammogram exhibits a larger degree of concentration polarization than is usually observed. Untreated copper in perchlorate solution exhibits a broad anodic and cathodic peak, each extending over the 1.0 volt range. In addition the peak current densities are considerably smaller.

c. Nickel Chloride - Anodically Formed During Cyclic Voltammetry

(1) Acetonitrile solutions

Nickel undergoes anodic reaction in $AlCl_3$, reaching a maximum current density (no peak) of 164 ma/cm^2 at +1.0 v. No cathodic reaction is evident. Addition of LiCl results in sufficiently high anodic currents to cause instrument overload, even though the solution conductance is considerably decreased. Pre-oxidized nickel in $LiCl+AlCl_3$, however, exhibits much lower anodic currents, reaching a maximum of only 29 ma/cm^2. Nickel oxide in acetonitrile-$LiClO_4$ exhibits a definite but very small (0.25 ma/cm^2) anodic and cathodic peak.

(2) Butyrolactone solutions

Low and very low cathodic currents with no peaks were obtained with nickel and pre-oxidized nickel in LiCl, $AlCl_3$, $LiCl+AlCl_3$, $MgCl_2$, $LiClO_4$, and $LiClO_4$+LiCl solutions. A medium low anodic and cathodic peak was obtained with $LiClO_4$+LiCl. Currents were less than 0.1 $ma/cm^2/cm$ division of current axis, for the $MgCl_2$ and $MgCl_2$+LiCl solutions. $AlCl_3$ solution gave a high anodic current.

(3) Dimethylformamide solutions

Nickel and pre-oxidized nickel gave very low currents in all solutions measured, with no peaks as the general case.

(4) Propylene carbonate solutions

All solutions indicated current densities less than 0.1 ma/cm^2/cm division of current axis.

2. Systems Involving Fluoride Electrolytes

a. Silver Fluoride - Anodically Formed During Cyclic Voltammetry

Cyclic voltammograms obtained with metallic silver in fluoride solutions should at first approximation represent the reactions

$$Ag + F^- \rightleftharpoons AgF + e^-$$

followed by

$$AgF + F^- \rightleftharpoons AgF_2 + 2e^-$$

or by the sum of these,

$$Ag + 2F^- \rightleftharpoons AgF_2 + 2e^-$$

The above reactions can only be assumed to occur if the simple fluoride ion is directly involved. Since the concentration of fluoride ion is apparently quite low based upon solubility product data, in order for the above reactions to occur, fluoride would have to be continually restored by dissociation of the complex fluoride (hexafluorophosphate or tetrafluoroborate). Because this dissociation occurs to a relatively small degree, it is not unlikely that the electrode reactions may proceed according to the net reactions

$$Ag + 2BF_4^- \rightleftharpoons AgF_2 + 2BF_3 + 2e^-$$

or

$$Ag + 2PF_6^- \rightleftharpoons AgF_2 + 2PF_5 + 2e^-$$

in which case the species BF_3 and PF_5 may subsequently be complexed with the solvent molecules.

Since it is the purpose of this program to characterize electrochemical systems as to their suitability for battery application, the cyclic voltammograms of the fluoride systems will be tentatively interpreted on the basis of silver mono- or difluoride formation during the anodic portion of the sweep.

(1) Acetonitrile solutions

The cyclic voltammogram for silver metal in the KPF_6 solution, Figure 36 (CV-580) exhibits very high initial anodic peak, followed by a poorly defined secondary peak. Two high current density cathodic peaks are obtained, with the second anodic peak being better defined at higher sweep rates. Although some dissolution of the anodic product was observed, the anodic-to-cathodic peak ratio was independent of sweep rate. Existence of two cathodic peaks suggests that the anodic product formed is AgF_2. If so, then charging the monovalent silver to the divalent form represents an inefficient process in this system.

Addition of 1000 ppm water to the above system resulted in a similar type of anodic peak, but with a still higher current density. The cathodic peak was reduced markedly, however, and the effect of sweep rate indicated that a solid state cathodic reaction was involved in which the cathode was soluble. The CV at 200 mv/sec was identical to that obtained for the water-free solution. These facts further substantiate the formation and consequence discharge of AgF_2, which would not be compatible with water. The addition of LiF to the KPF_6 solution increased the anodic current density still further, and had a pronounced effect on ΔV_p, the peak-to-peak displacement, decreasing it from 0.6 to 0.2 volts, indicating increased reversibility of the reaction.

Pre-oxidized silver in acetonitrile-KPF_6 exhibited only a single poorly defined anodic peak at the higher oxidation potential, and only a single

cathodic peak, although a slight inflection occurred slightly cathodic to the latter peak. Peak current densities were approximately the same as for the untreated silver. Addition of LiF resulted in extremely high currents and consequent instrument overload. This effect is of interest, and will be investigated further.

(2) Butyrolactone solutions

The sweep curves for silver in KPF_6 solution, with or without LiF, are identical in that only a single broad anodic peak is exhibited, and a single broad cathodic peak. In both cases, the cathodic peak becomes proportionately smaller with decreasing sweep rate, indicating a solid state cathodic reaction in which the cathode is soluble. The anodic peak current density is in the high range (100-300 ma/cm^2) for the KPF_6 solution , and the very high range (more than 300 ma/cm^2) for the KPF_6+LiF solution. Pre-oxidized silver electrodes gave extremely high currents in KPF_6 solution, with or without LiF, resulting in voltage overload of the equipment. Dissolution of material was evident.

Low anodic currents (less than 10 ma/cm^2) with no peaks, are exhibited in MgF_2 solution, with or without LiF additive, although a low cathodic peak exists. This is to be expected, owing to the low availability of fluoride ion, as indicated by the very low conductance.

(3) Dimethylformamide solutions

The sweep curve for silver in MgF_2 solution exhibits currents less than 0. 1 $ma/cm^2/cm$ division current axis which is not surprising in view of the extremely low conductance (2.2×10^{-6}) and the consequent low availability of solute species for reaction. On the other hand, very high anodic currents are obtained with KPF_6 solution, with or without LiF, with the existence of two anodic peaks. Two cathodic peaks are also obtained, although these are proportionately smaller at the 40 mv/sec sweep rate, indicating a soluble anodic product undergoing a solid state reduction reaction.

Similar results were obtained with pre-oxidized silver in KPF_6 solution, with anodic currents in excess of 650 ma/cm^2.

The cyclic voltammogram for silver in dimethylformamide-$LiBF_4$ is shown in Figure 37 (CV-505) where a second anodic peak begins at +0.9 volts. The peculiar return loop represents a type of voltage delay action. The effect of sweep rate indicated a soluble cathode undergoing a solid state reduction reaction. Gassing was observed at the silver electrode.

(4) Propylene carbonate solutions

Figure 38 (CV-547) represents the sweep curve obtained for silver in propylene carbonate-KPF_6 at 40 mv/sec. This is compared with the family of curves shown in Figure 39 (CV-433), obtained earlier in the program using non-distilled propylene carbonate. This set of curves was obtained by raising the X-Y recorder pen for a few minutes each time, but allowing the system to cycle continuously. Successive curves were recorded over a 30-minute period proceeding in the order 1-6 as labelled. Curve 1 corresponds to that shown in Figure 38 (because of the higher sweep rate for the family of curves, no anodic peak is reached within the 1.0 volt range). Of interest is the absence of a lower oxidation peak and corresponding reduction peak during the early cycles, but with continued cycling, these peaks begin to occur and gain in magnitude, indicating the formation of a double oxidation species of silver. Of further interest, and in confirmation of these data, shown as an inset in Figure 39 is a reproduction of an oscillogram of a cyclic voltammogram obtained with non-distilled propylene carbonate at 800 mv/sec, nineteen months previously during an independent investigation by Whittaker Corporation. Because of the still higher sweep rate, the double peaked curve was immediately evident. The curve shown in Figure 38 was run at a much lower sweep rate so that there was insufficient cycling to bring about the double peaks. Measurements will have to be repeated to determine if the presence of water in the non-distilled propylene carbonate has an influence on the formation of the double peaks.

The addition of LiF to the KPF_6 solution results in much lower currents and the absence of an anodic peak, as shown in Figure 40 (CV-722). Pre-oxidized silver in KPF_6 gives a similar curve to that of silver in KPF_6, but with a hint of a preliminary anodic peak. Only a single cathodic peak is obtained, however, corresponding to the main anodic peak observed for the untreated metal.

b. Copper Fluoride - Anodically Formed During Cyclic Voltammetry

Using the same approach as before, we could consider that cyclic voltammograms on copper in fluoride solutions should at first approximation indicate the formation and discharge of mono- and di-valent copper fluoride.

(1) Acetonitrile solutions

The cyclic voltammograms for pre-oxidized copper in KPF_6 solution, (Figure 41, CV-910), is characterized by a high, sharp anodic peak, originating immediately at the ocv, followed by a second broad, flat peak which is spread over the remaining anodic scan. On the return sweep, the current remains constant at approximately the peak value until it reaches the ocv, only at which time it drops towards the negative direction. This straight-back current return is a common characteristic for copper in acetonitrile solutions of both chlorides and fluorides. Only a single cathodic peak is evident, which is somewhat broader than the anodic peak. Addition of LiF has no effect on the voltammogram. Copper metal in KPF_6+LiF (Figure 42, CV-618) gives a similar CV but with current densities less than half of the pre-oxidized metal, again confirming the belief that the effect of pre-oxidation is to essentially increase the surface area. (Again, the greater peak displacement is a result of the measurement being made in the older cell.)

(2) Butyrolactone solutions

Very low currents (no peaks) were obtained with copper in MgF_2 solution, with or without LiF, again indicative of low availability of fluoride ions.

Copper in butyrolactone-KPF_6 solution gave two poorly formed anodic peaks, the second in the high current range. The anodic product was slightly soluble, and a solid state cathodic reaction was indicated. Pre-oxidized copper gave a better formed anodic peak, but still very broad. This represents a poor system however, because of the large peak-to-peak displacement (1. 3 v). Addition of LiF to the KPF_6 solution results in a curve having a single high and sharp anodic peak (Figure 43, CV-630) for copper. Unfortunately, the formed cathode material is soluble. Pre-oxidized copper forms a similar type of curve (Figure 44, CV-1009) but in this case the anodic product appears to be insoluble. A second anodic peak, absent on the forward sweep, appears on the return sweep, but only a single cathodic peak is evident, although a slight deflection precedes this peak, occurring at about +0. 18 volts. This second cathodic peak is evident at higher sweep rates, indicating the solubility of the higher oxidation state cathode material. This system is still undesirable, however, because the cathodic peak is broad and of medium low magnitude (10-50 ma/cm^2).

(3) Dimethylformamide solutions

The poor solubility of MgF_2 in this solvent results in low currents because of the deficiency in electrolytic species. The curve for copper in KPF_6 is shown in Figure 45 (CV-565), indicating low currents and a broad anodic peak, which probably involves two peaks close together, since a double cathodic peak is evident. Low currents and poor charge performance characterize this as a poor system. Addition of LiF gives no improvement. Indeed, still lower currents are obtained. Pre-oxidized copper gives the same poor results.

Copper in $LiBF_4$ solution, shown in Figure 46 (CV-509) exhibits two anodic peaks in the medium high current range (50-100 ma/cm^2) differing by 0. 6 volts. The reduction reaction is accompanied by excessive activation polarization, and the large peak-to-peak displacement, together with formation of soluble cathode, render this system entirely unsuitable for battery application.

(4) Propylene carbonate solutions

Copper in KPF_6 solution exhibits two distinct anodic peaks, the higher oxidation state being of the medium high current density range, whereas the initial peak is medium low. This is shown in Figure 47 (CV-554). The anodically-formed cathode material, however, is soluble in the electrolyte. Pre-oxidized copper failed to give any peaks, and overall currents were very low. Addition of LiF to the KPF_6 solution resulted in voltage overload in the case of copper metal.

c. Nickel Fluoride - Anodically Formed During Cyclic Voltammetry

Nickel and nickel oxide electrodes failed to produce any current peaks for all systems screened, with one exception, and maximum currents were less than 0.1 $ma/cm^2/cm$ division current axis. The one exception ($LiPF_6$ in dimethylformamide) is shown in Figure 48 (CV-517) where pre-oxidized nickel shows a single low current anodic peak, and two low current cathodic peaks fusing together. The inflection at 0.5 volts shows as a definite peak at higher sweep rates. As before, nickel systems are consistently poor because of inability to form an anodic product.

d. Zinc Fluoride - Anodically Formed During Cyclic Voltammetry

The first data are reported here on zinc electrodes in fluoride electrolytes.

(1) Acetonitrile solutions

The sweep curve for Zn in KPF_6 solution is shown in Figure 49 (CV-918). Although high currents are obtained for the anodic and cathodic reactions, no desirable peaks are obtained. Addition of LiF causes excessively high currents and instrument overload.

(2) Butyrolactone solutions

Zinc in butyrolactone-KPF_6 solution presents a very desirable cyclic voltammogram as shown in Figure 50 (CV-992). The sharp symmetric anodic and cathodic peaks are displaced by only 130 millivolts, the entire pattern representing a very reversible system. The solid state cathodic reaction type, with the cathode being insoluble makes this a desirable system, and one to be recommended even though the current densities are in the medium high range. The effect of adding LiF is shown in Figure 51 (CV-1014), the only result being a 50% decrease in peak currents, and a slightly larger peak-to-peak displacement (240 mv).

(3) Dimethylformamide solutions

The only zinc system screened in this solvent involved KPF_6 as the solute, resulting in the excellent cyclic voltammogram shown in Figure 52 (CV-1048). Very high current densities are obtained, with the discharge reaction showing a higher value than the charge reaction (571 ma/cm^2 compared with 439 ma/cm^2). In addition, the peaks are again close together (ΔV_p = 320 mv). This cyclic voltammogram is a classic example of a solid state reaction type, with negligible activation and concentration polarization both. Comparison is made with zinc in a butyrolactone-KPF_6 (Figure 50) which although exhibiting negligible activation polarization, does have some concentration polarization shown by the width of the sweep curve at the zero current axis. Although the charge-discharge efficiency for the dimethylformamide-KPF_6 electrolyte is not as high as for butyrolactone-KPF_6, the discharge capacity is much higher, 2.4 $coulombs/cm^2$ compared with 0.5 $coulombs/cm^2$. This again is a recommended system.

(4) Propylene carbonate solutions

The sweep curve for zinc in KPF_6 solution is shown in Figure 53 (CV-959). A desirable type of curve is again obtained, comparing somewhat with butyrolactone-KPF_6+LiF in current density magnitude. The possibility

exists for two reducible species, indicated by the inflection near the apex of the cathodic peak.

e. Cadmium Fluoride - Anodically Formed During Cyclic Voltammetry

During this second quarter, cyclic voltammograms were initiated using cadmium in fluoride electrolytes.

(1) Acetonitrile solutions

Extremely erratic results were obtained with cadmium in KPF_6 solution, particularly with respect to the anodic peaks which were of a multiple nature, and which were repeated on the return scan. Very high currents were obtained accompanied by excessive dissolution of the anodic product in the electrolyte. Addition of LiF resulted in more reproducible voltammograms, but decreased the current considerably, although still in the high range. With or without the LiF, a single cathode peak was obtained, being much broader in the presence of LiF.

(2) Butyrolactone solutions

Cadmium in butyrolactone-KPF_6 gives an excellent cyclic voltammogram shown in Figure 54 (CV-997). The peaks are sharp and well formed with a displacement of 340 mv. Larger currents are obtained on discharge than on charge. This system has a charge-discharge efficiency of 95%, double that of the Zn/dimethylformamide-KPF_6 system, also a very high current density system. There is some indication that continued cycling increased the current densities still further. Addition of LiF resulted in a large decrease of current, but again, evidence indicated that further cycling would bring a considerable increase of current. A second small cathodic peak occurs at -0.35 volts, which was more pronounced in the presence of LiF, but which decreased with increased cycling. This peak would not interfere in the discharge process of an actual cell since it is much smaller than the

primary peak, and is more negative by 0.4 volts. The system is recommended.

(3) Dimethylformamide solutions

Cadmium in KPF_6 solution (Figure 55, CV-1053) again exhibits closely placed peaks of high and very high current densities. The peaks are not as sharp, however, as for the butyrolactone case. This is indicated in comparing the cathodic sweep indices, 107.4 for dimethylformamide and 193.7 for butyrolactone. The cathodic sweep index for zinc in dimethylformamide-KPF_6 is 332.9, which reflects the larger peak current. The Cd/dimethylformamide-KPF_6 is recommended for further study.

(4) Propylene carbonate solutions

The only cadmium system screened was in propylene carbonate-KPF_6. Extremely high currents were obtained resulting in instrument voltage overload.

f. Cyclic Voltammetry of Molybdenum

During this quarter, cyclic voltammetry was initiated using molybdenum electrodes in fluoride solutions, and in $LiClO_4$ solution of propylene carbonate and butyrolactone. Figure 56 (CV-911), obtained in acetonitrile-KPF_6 solution, is typical of all sweep curves measured in the $LiClO_4$ solutions, butyrolactone-MgF_2, and KPF_6 solutions in butyrolactone, dimethylformamide, and propylene carbonate, as well as KPF_6+LiF in acetonitrile and butyrolactone. Such a curve, with very low current densities, is the result of failure to form an anodic product. Most of the nickel systems also give such voltammograms.

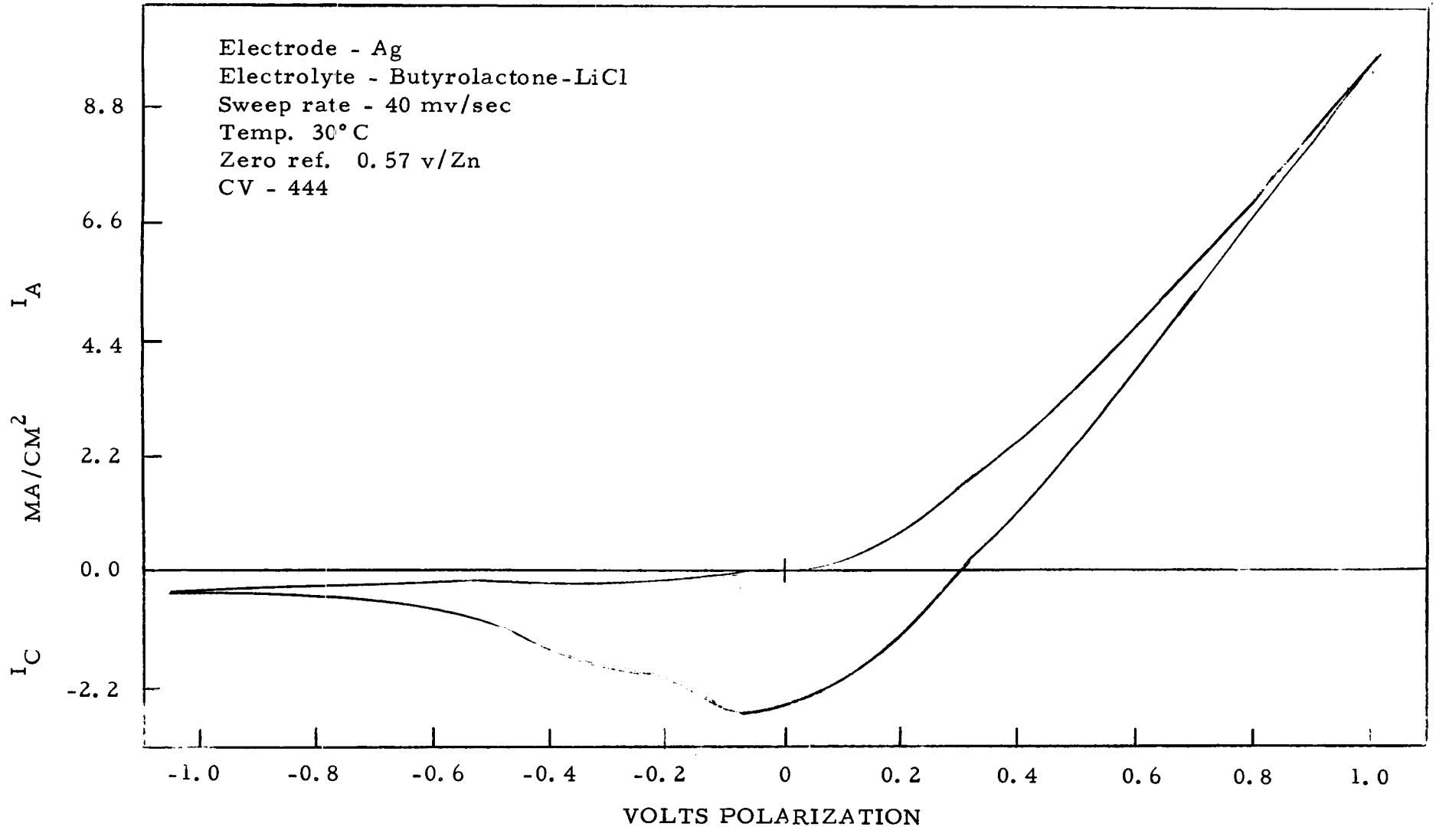
Electrode - Ag
Electrolyte - Butyrolactone-LiCl
Sweep rate - 40 mv/sec
Temp. 30° C
Zero ref. 0.57 v/Zn
CV - 444
8.8
6.6
4.4
2.2
0.0
-2.2
I_A
MA/CM^2
I_C
-1.0
-0.8
-0.6
-0.4
-0.2
0
0.2
0.4
0.6
0.8
1.0
VOLTS POLARIZATION

Figure 1

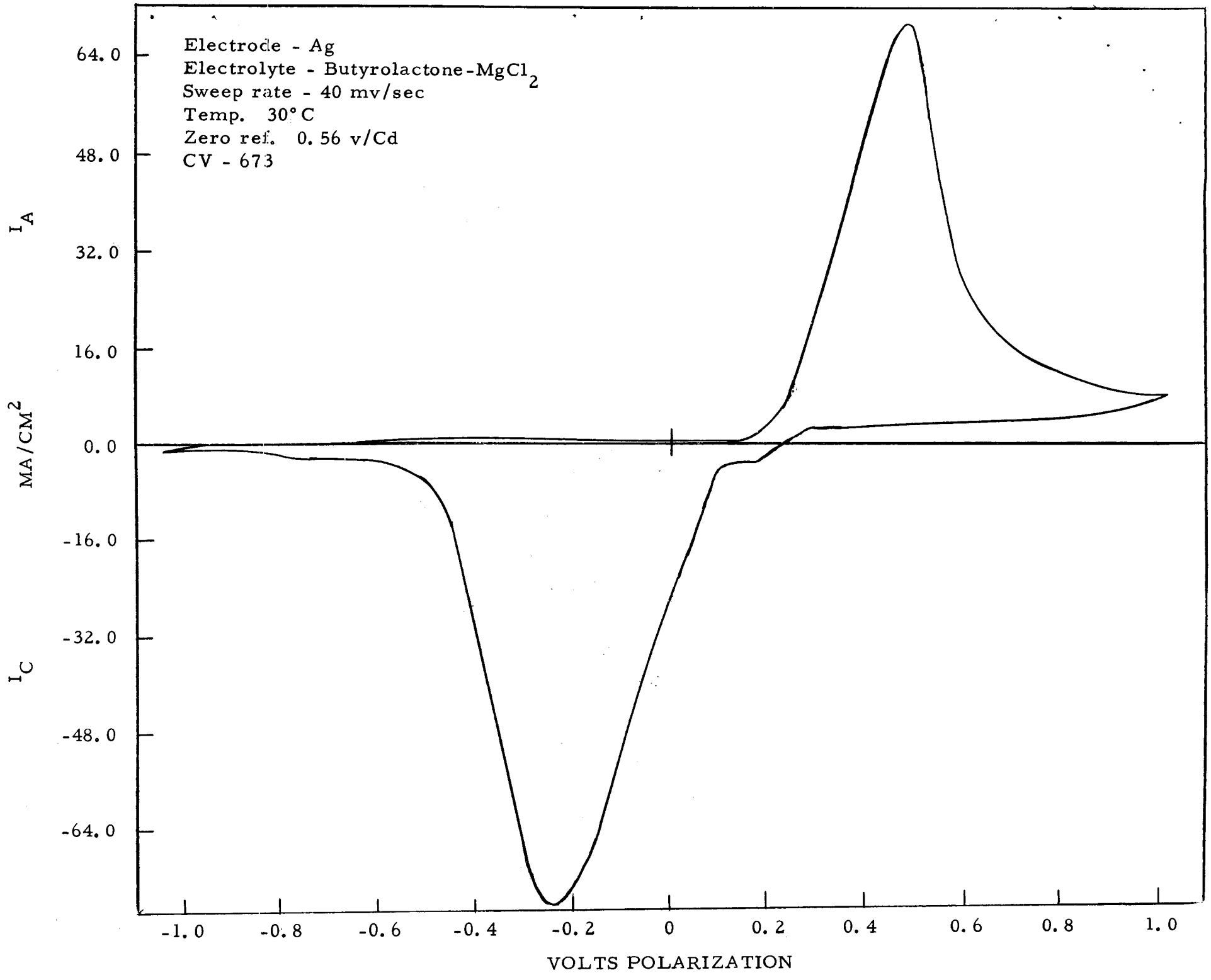
Electrode - Ag
Electrolyte - Butyrolactone-$MgCl_2$
Sweep rate - 40 mv/sec
Temp. 30° C
Zero ref. 0.56 v/Cd
CV - 673
64.0
48.0
32.0
16.0
0.0
-16.0
-32.0
-48.0
-64.0
I_A
MA/CM^2
I_C
-1.0
-0.8
-0.6
-0.4
-0.2
0
0.2
0.4
0.6
0.8
1.0
VOLTS POLARIZATION

Figure 2

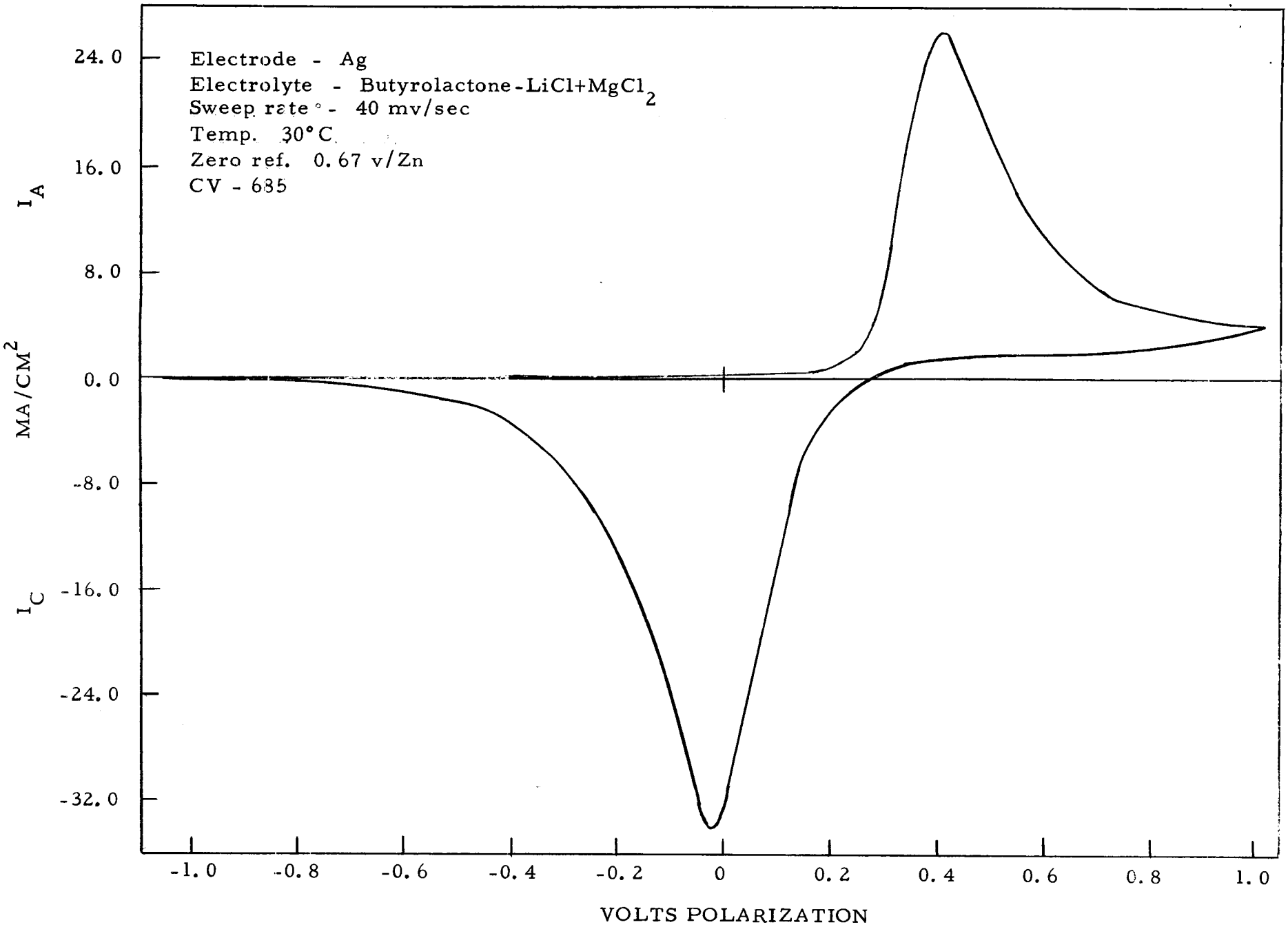
Electrode - Ag
Electrolyte - Butyrolactone-LiCl+MgCl2
Sweep rate - 40 mv/sec
Temp. 30°C
Zero ref. 0.67 v/Zn
CV - 685
24.0
16.0
8.0
0.0
-8.0
-16.0
-24.0
-32.0
IA
IC
MA/CM2
-1.0
-0.8
-0.6
-0.4
-0.2
0
0.2
0.4
0.6
0.8
1.0
VOLTS POLARIZATION

Figure 3

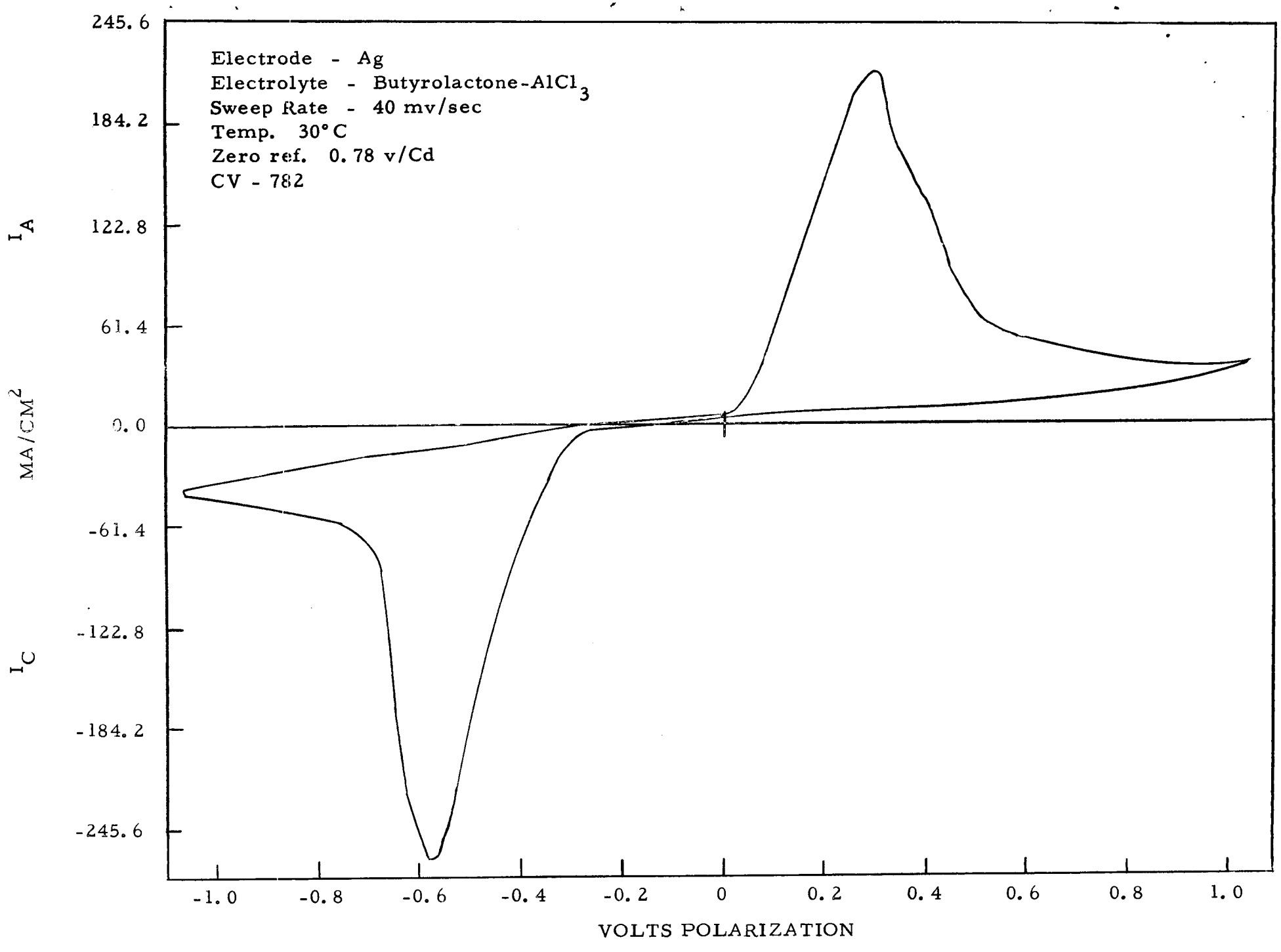
Electrode - Ag
Electrolyte - Butyrolactone-AlCl3
Sweep Rate - 40 mv/sec
Temp. 30°C
Zero ref. 0.78 v/Cd
CV - 782
245.6
184.2
122.8
61.4
0.0
-61.4
-122.8
-184.2
-245.6
IA
MA/CM2
IC
-1.0
-0.8
-0.6
-0.4
-0.2
0
0.2
0.4
0.6
0.8
1.0
VOLTS POLARIZATION

Figure 4

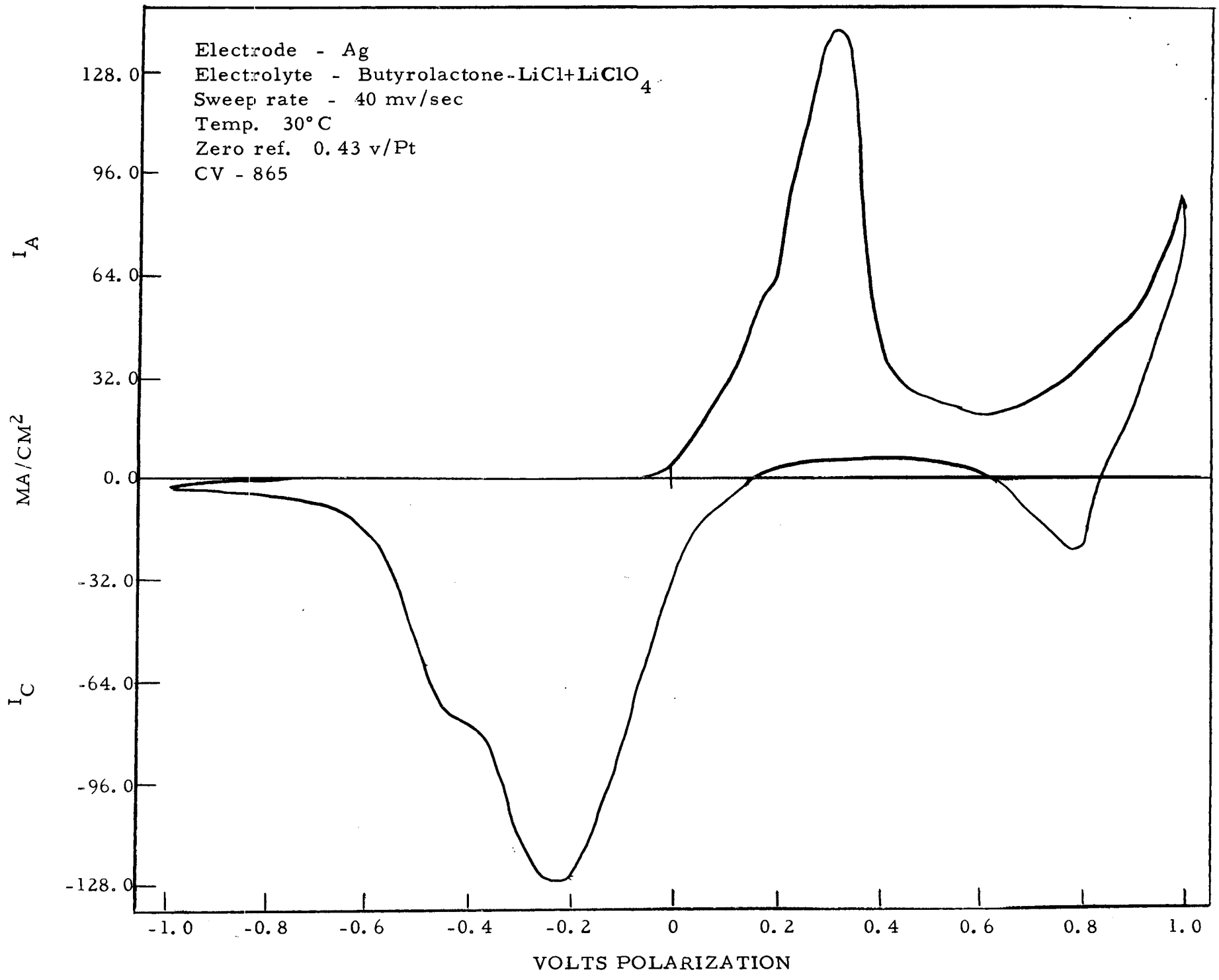
Electrode - Ag
Electrolyte - Butyrolactone-LiCl+LiClO4
Sweep rate - 40 mv/sec
Temp. 30° C
Zero ref. 0.43 v/Pt
CV - 865
128.0
96.0
64.0
32.0
0.0
-32.0
-64.0
-96.0
-128.0
IA
MA/CM2
IC
-1.0
-0.8
-0.6
-0.4
-0.2
0
0.2
0.4
0.6
0.8
1.0
VOLTS POLARIZATION

Figure 5

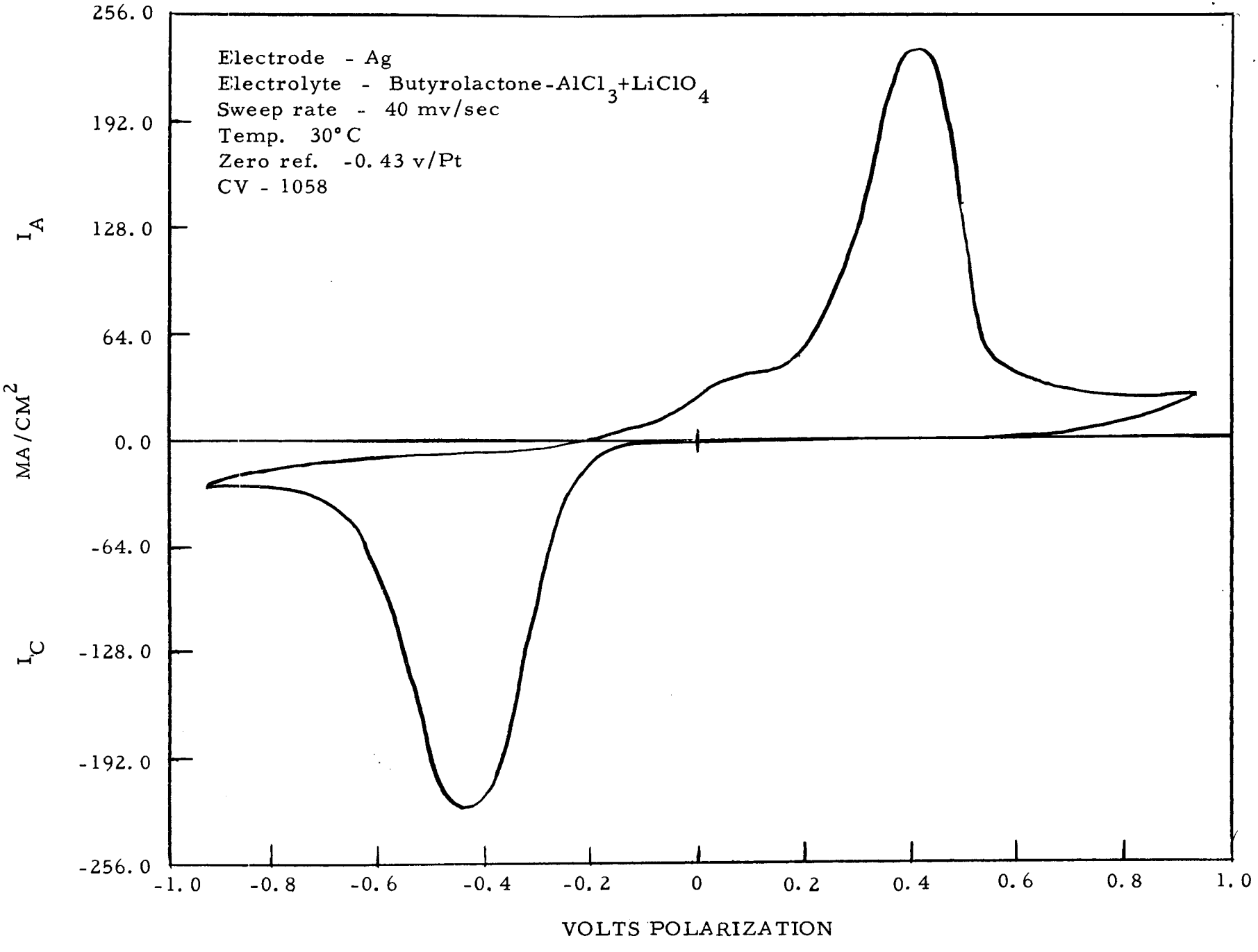
Electrode - Ag
Electrolyte - Butyrolactone-AlCl3+LiClO4
Sweep rate - 40 mv/sec
Temp. 30°C
Zero ref. -0.43 v/Pt
CV - 1058
256.0
192.0
128.0
64.0
0.0
-64.0
-128.0
-192.0
-256.0
IA
MA/CM2
IC
-1.0
-0.8
-0.6
-0.4
-0.2
0
0.2
0.4
0.6
0.8
1.0
VOLTS POLARIZATION

Figure 6

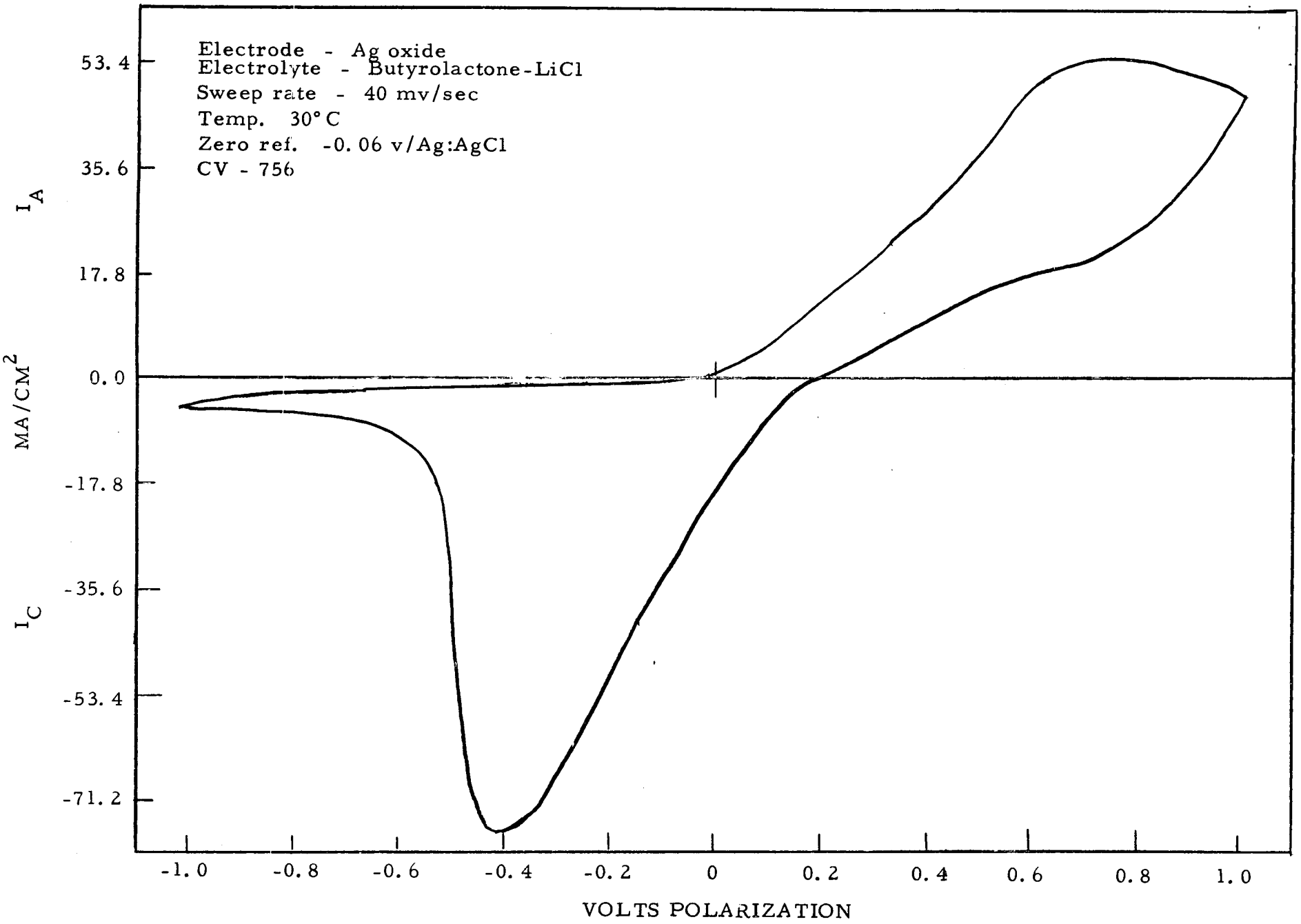
Electrode - Ag oxide
Electrolyte - Butyrolactone-LiCl
Sweep rate - 40 mv/sec
Temp. 30° C
Zero ref. -0.06 v/Ag:AgCl
CV - 756
53.4
35.6
17.8
0.0
-17.8
-35.6
-53.4
-71.2
I_A
I_C
MA/CM^2
-1.0
-0.8
-0.6
-0.4
-0.2
0
0.2
0.4
0.6
0.8
1.0
VOLTS POLARIZATION

Figure 7

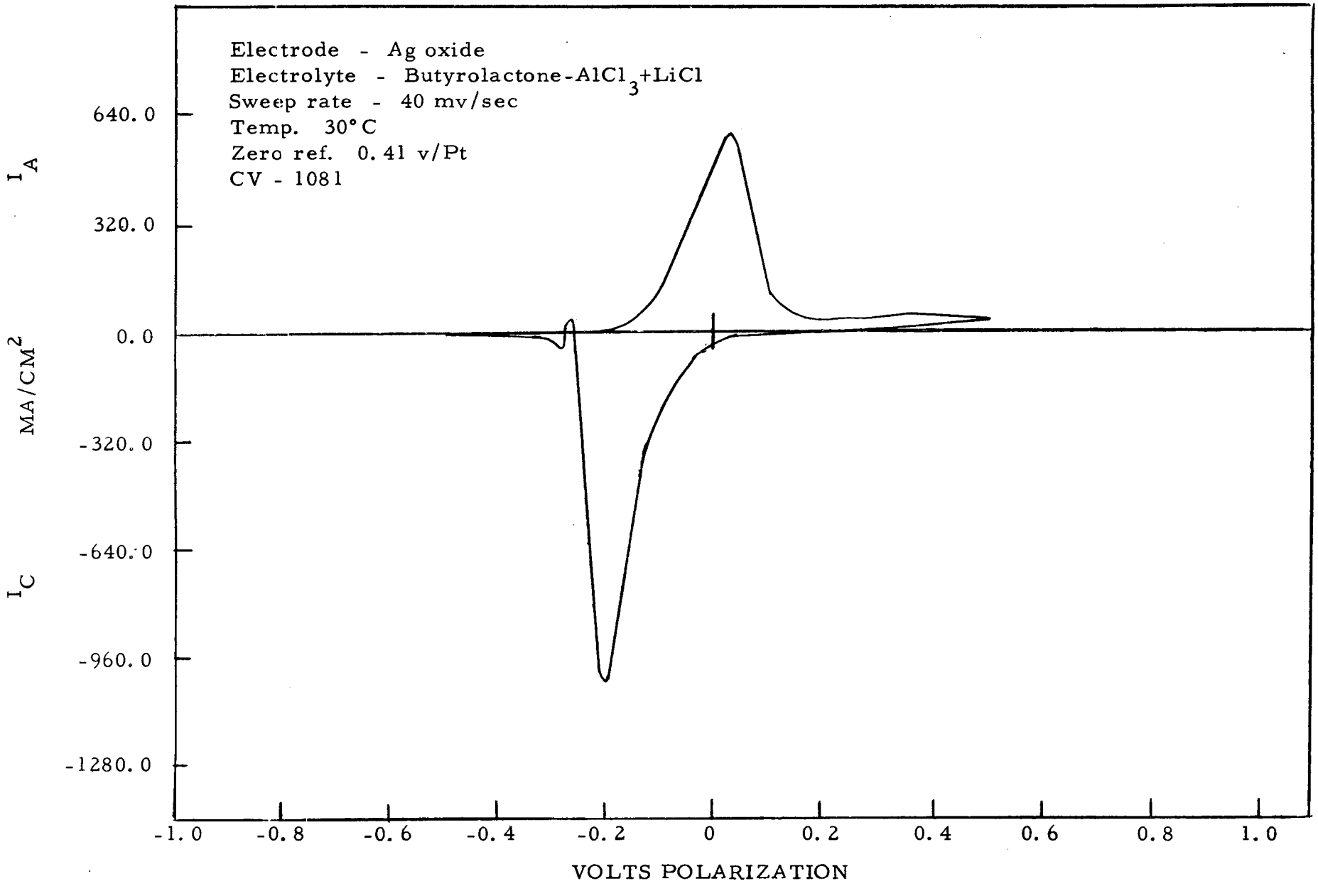
Electrode - Ag oxide
Electrolyte - Butyrolactone-AlCl3+LiCl
Sweep rate - 40 mv/sec
Temp. 30°C
Zero ref. 0.41 v/Pt
CV - 1081
640.0
320.0
0.0
-320.0
-640.0
-960.0
-1280.0
IA
MA/CM2
IC
-1.0
-0.8
-0.6
-0.4
-0.2
0
0.2
0.4
0.6
0.8
1.0
VOLTS POLARIZATION

Figure 8

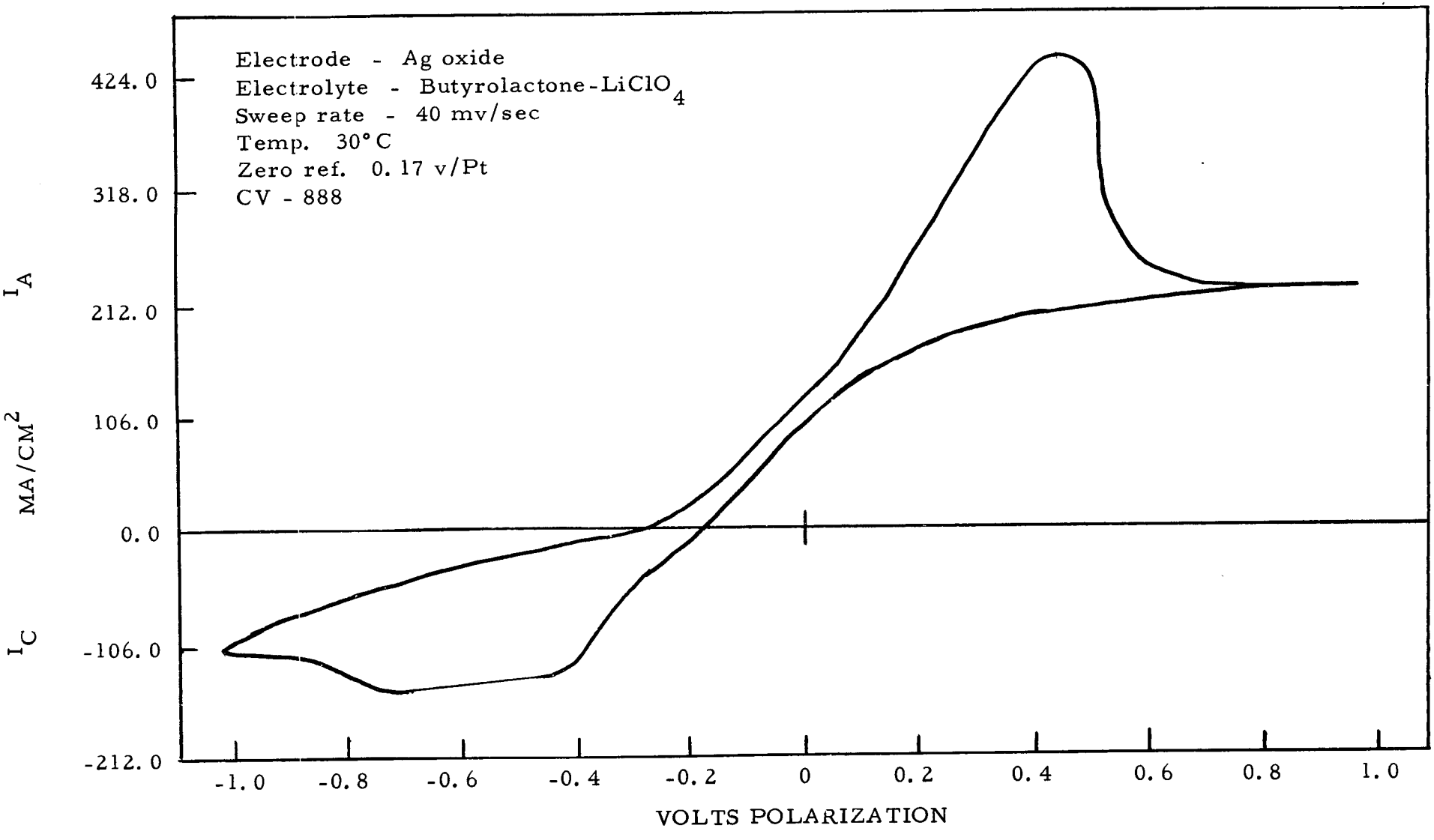
Electrode - Ag oxide
Electrolyte - Butyrolactone-$LiClO_4$
Sweep rate - 40 mv/sec
Temp. 30° C
Zero ref. 0.17 v/Pt
CV - 888
424.0
318.0
212.0
106.0
0.0
-106.0
-212.0
I_A
MA/CM^2
I_C
-1.0
-0.8
-0.6
-0.4
-0.2
0
0.2
0.4
0.6
0.8
1.0
VOLTS POLARIZATION

Figure 9

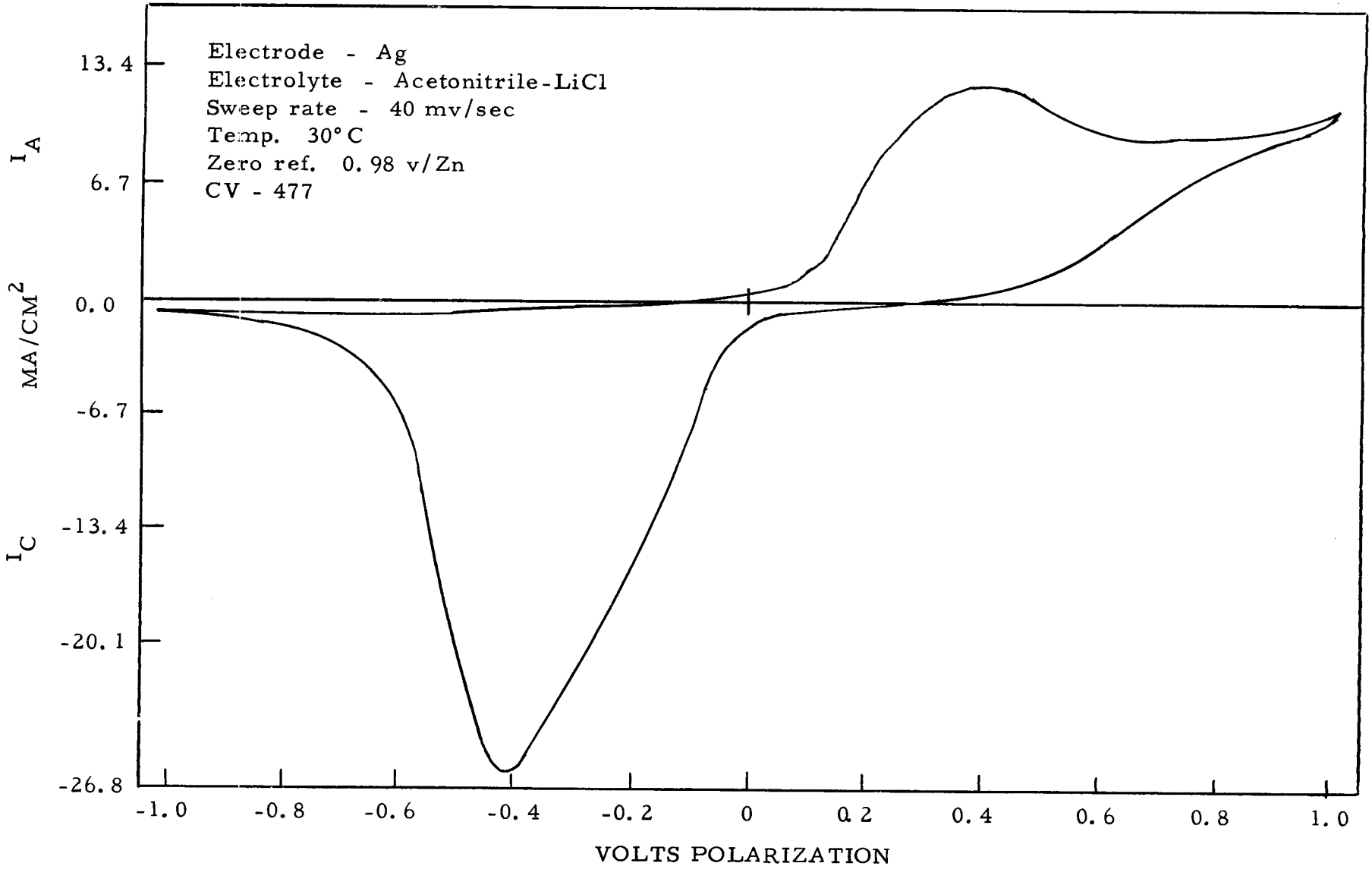
Electrode - Ag
Electrolyte - Acetonitrile-LiCl
Sweep rate - 40 mv/sec
Temp. 30° C
Zero ref. 0.98 v/Zn
CV - 477
13.4
6.7
0.0
-6.7
-13.4
-20.1
-26.8
I_A
I_C
MA/CM^2
-1.0
-0.8
-0.6
-0.4
-0.2
0
0.2
0.4
0.6
0.8
1.0
VOLTS POLARIZATION

Figure 10

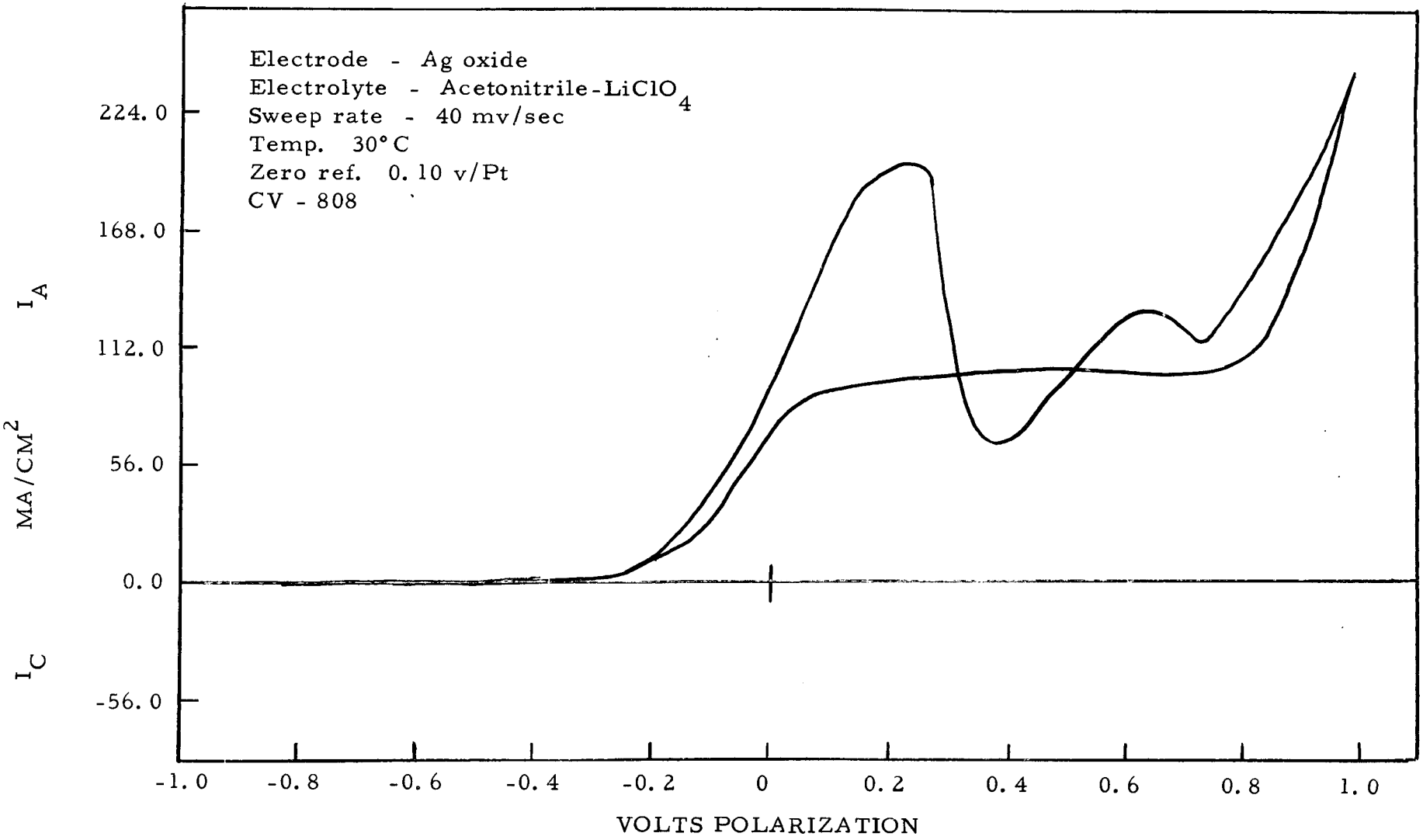
Electrode - Ag oxide
Electrolyte - Acetonitrile-LiClO4
Sweep rate - 40 mv/sec
Temp. 30° C
Zero ref. 0.10 v/Pt
CV - 808
224.0
168.0
112.0
56.0
0.0
-56.0
IA
MA/CM2
IC
-1.0
-0.8
-0.6
-0.4
-0.2
0
0.2
0.4
0.6
0.8
1.0
VOLTS POLARIZATION

Figure 11

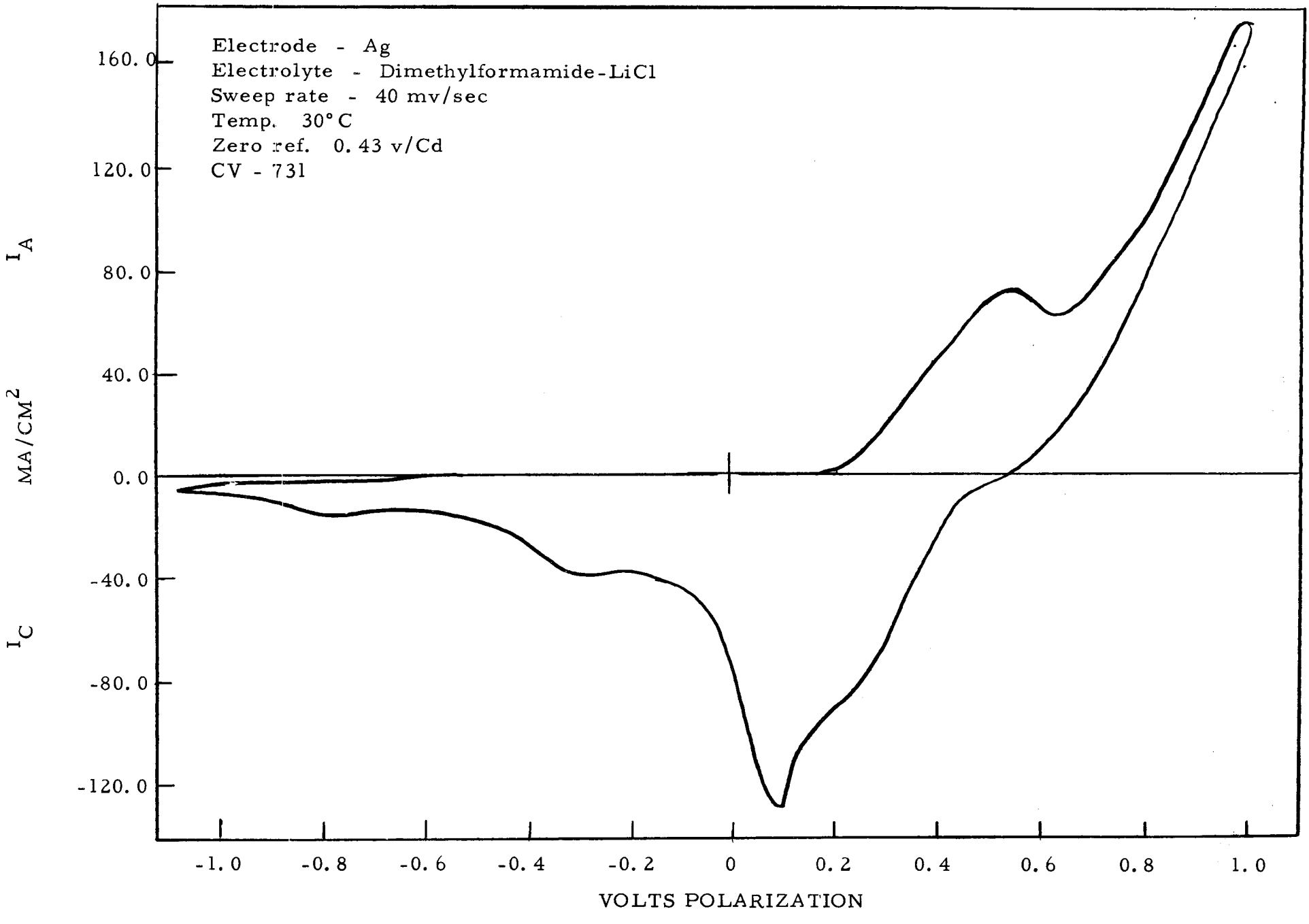
Electrode - Ag
Electrolyte - Dimethylformamide-LiCl
Sweep rate - 40 mv/sec
Temp. 30° C
Zero ref. 0.43 v/Cd
CV - 731
160.0
120.0
80.0
40.0
0.0
-40.0
-80.0
-120.0
I_A
MA/CM^2
I_C
-1.0
-0.8
-0.6
-0.4
-0.2
0
0.2
0.4
0.6
0.8
1.0
VOLTS POLARIZATION

Figure 12

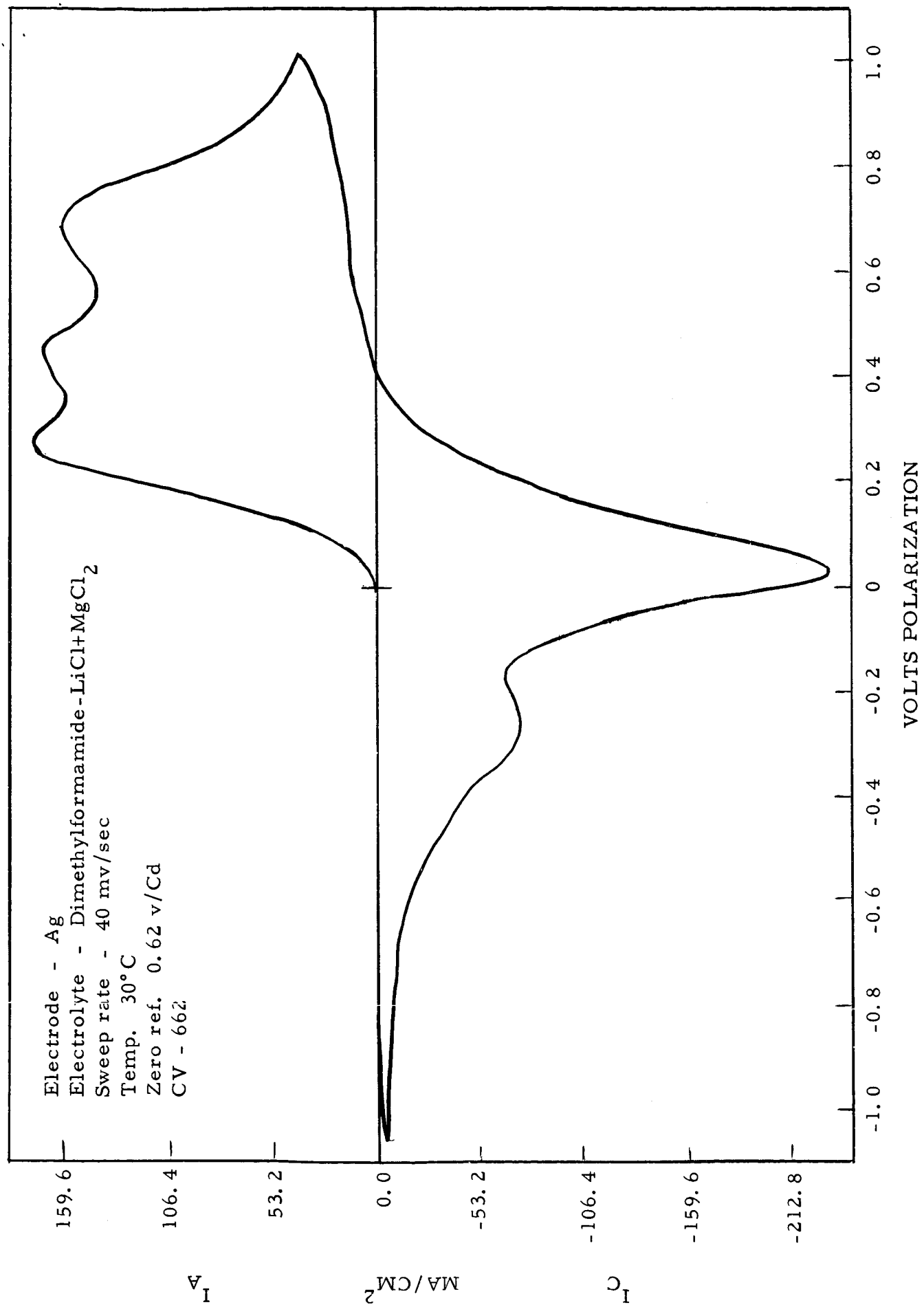
Electrode - Ag
Electrolyte - Dimethylformamide-LiCl+MgCl2
Sweep rate - 40 mv/sec
Temp. 30°C
Zero ref. 0.62 v/Cd
CV - 662
159.6
106.4
53.2
0.0
-53.2
-106.4
-159.6
-212.8
MA/CM2
IA
IC
-1.0
-0.8
-0.6
-0.4
-0.2
0
0.2
0.4
0.6
0.8
1.0
VOLTS POLARIZATION

Figure 13

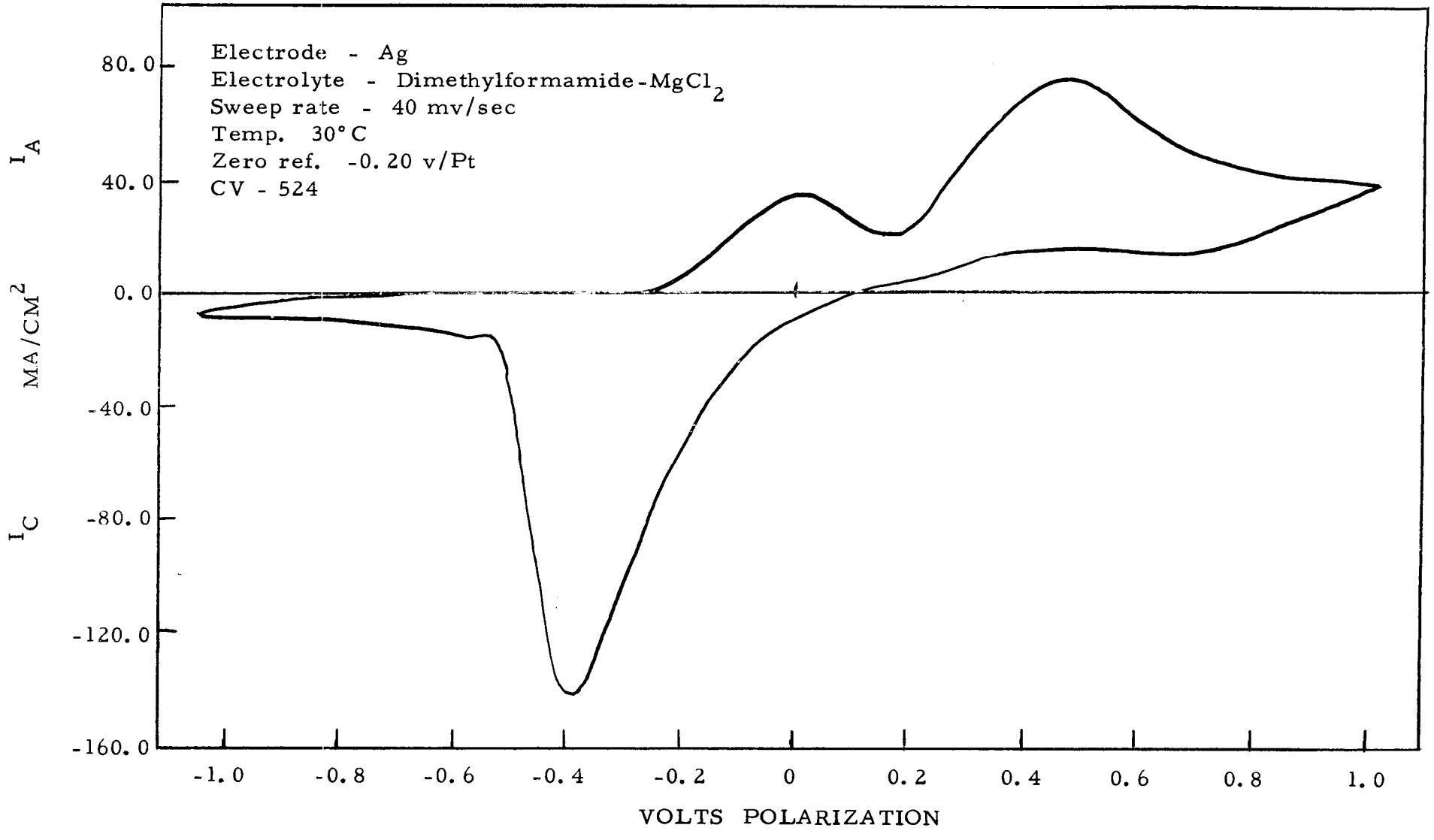
Electrode - Ag
Electrolyte - Dimethylformamide-$MgCl_2$
Sweep rate - 40 mv/sec
Temp. 30°C
Zero ref. -0.20 v/Pt
CV - 524
80.0
40.0
0.0
-40.0
-80.0
-120.0
-160.0
I_A
MA/CM^2
I_C
-1.0
-0.8
-0.6
-0.4
-0.2
0
0.2
0.4
0.6
0.8
1.0
VOLTS POLARIZATION

Figure 14

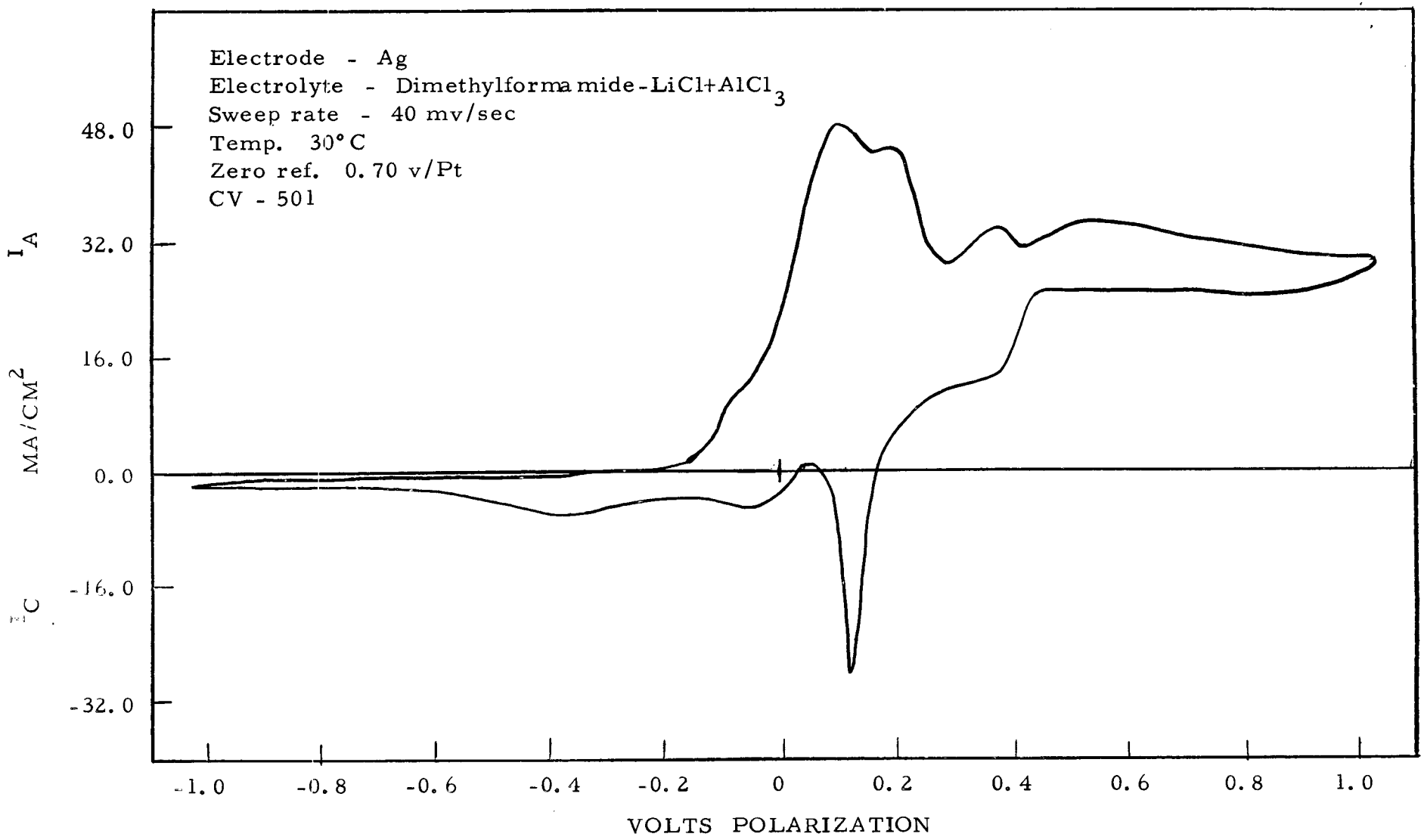
Electrode - Ag
Electrolyte - Dimethylformamide-LiCl+AlCl3
Sweep rate - 40 mv/sec
Temp. 30°C
Zero ref. 0.70 v/Pt
CV - 501
48.0
32.0
16.0
0.0
-16.0
-32.0
I_A
MA/CM^2
I_C
-1.0
-0.8
-0.6
-0.4
-0.2
0
0.2
0.4
0.6
0.8
1.0
VOLTS POLARIZATION

Figure 15

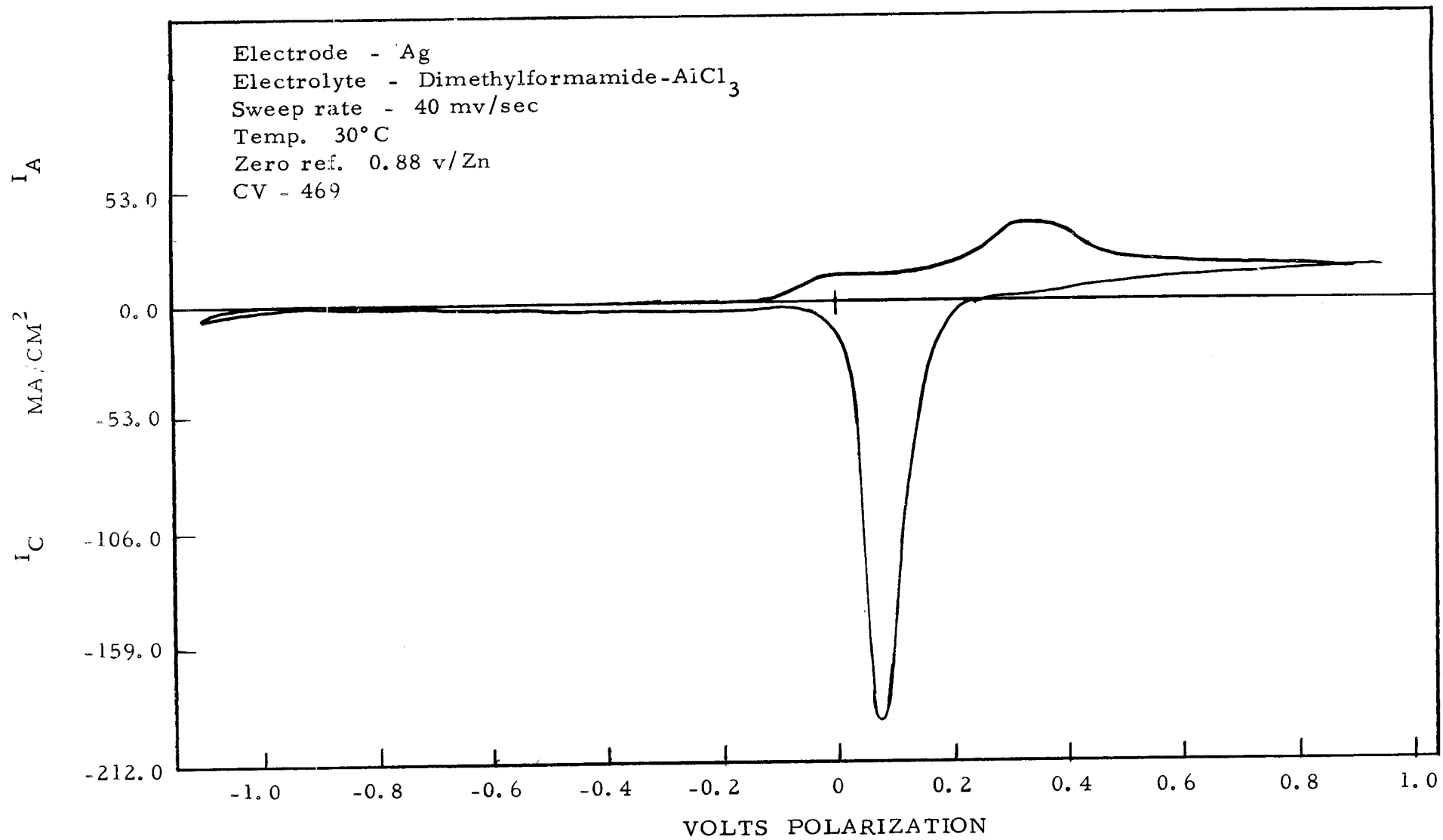
Electrode - Ag
Electrolyte - Dimethylformamide-AiCl3
Sweep rate - 40 mv/sec
Temp. 30° C
Zero ref. 0.88 v/Zn
CV - 469
IA
53.0
0.0
-53.0
IC
-106.0
-159.0
-212.0
MA/CM2
-1.0
-0.8
-0.6
-0.4
-0.2
0
0.2
0.4
0.6
0.8
1.0
VOLTS POLARIZATION

Figure 16

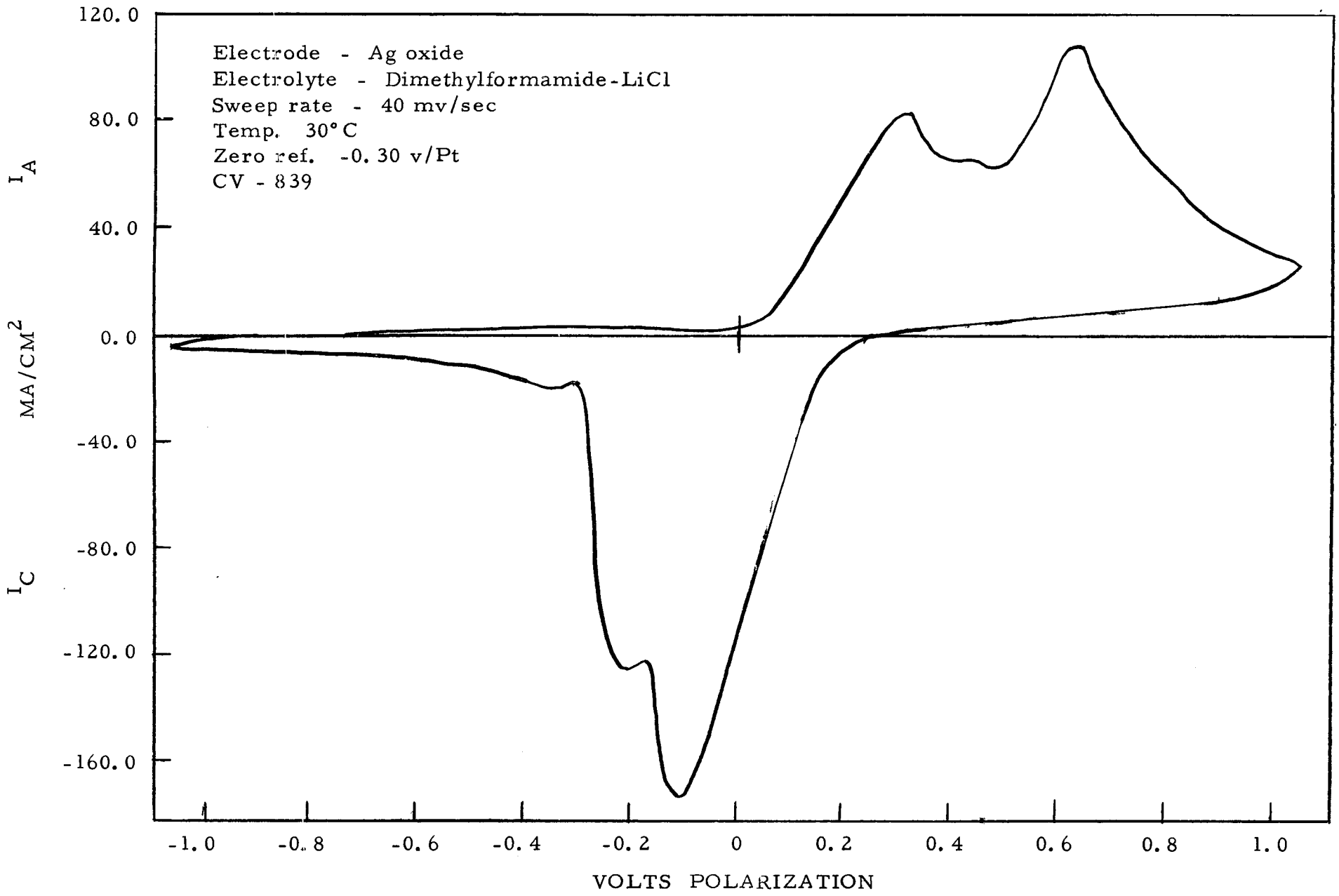
Electrode - Ag oxide
Electrolyte - Dimethylformamide-LiCl
Sweep rate - 40 mv/sec
Temp. 30° C
Zero ref. -0.30 v/Pt
CV - 839
120.0
80.0
40.0
0.0
-40.0
-80.0
-120.0
-160.0
I_A
MA/CM^2
I_C
-1.0
-0.8
-0.6
-0.4
-0.2
0
0.2
0.4
0.6
0.8
1.0
VOLTS POLARIZATION

Figure 17

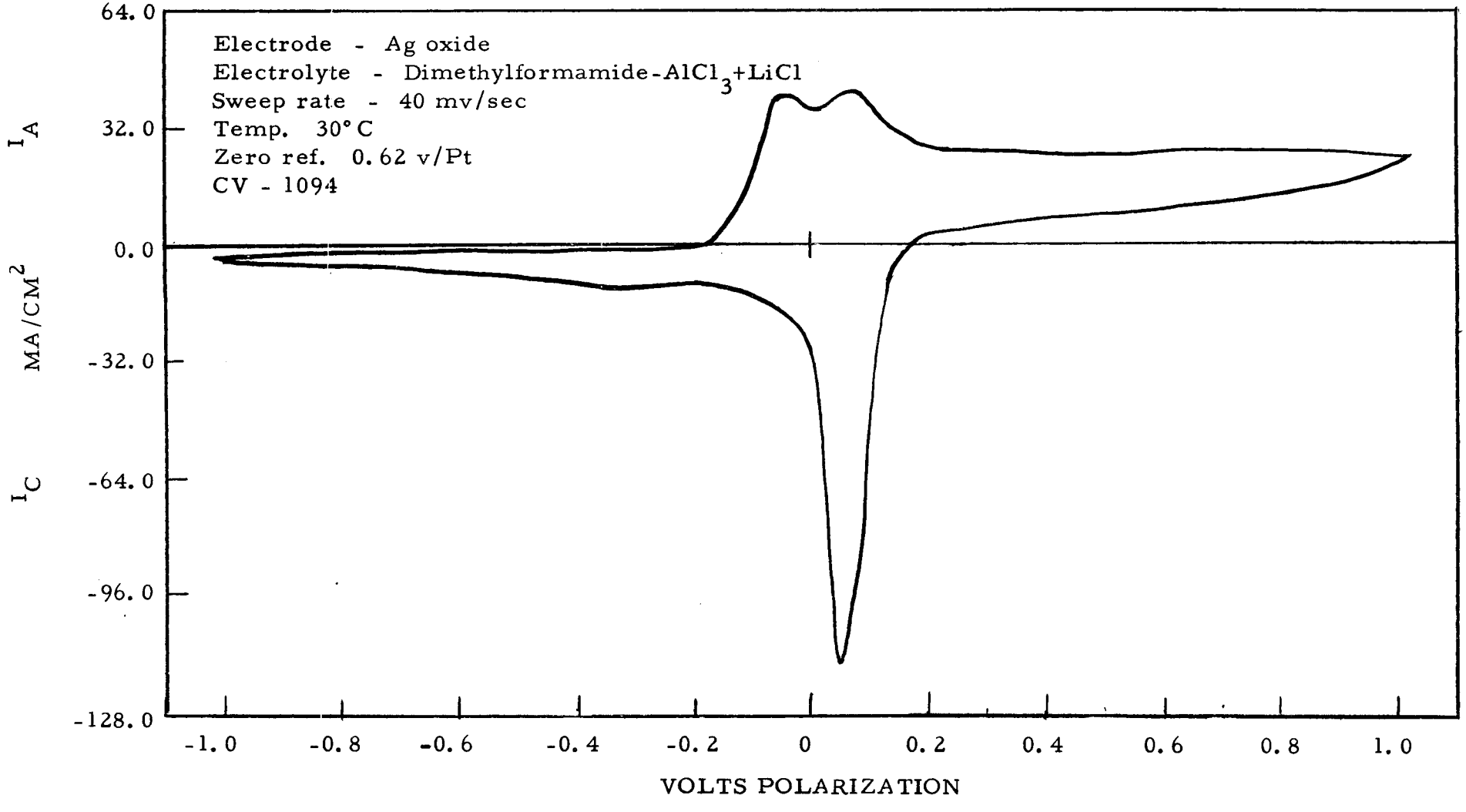
Electrode - Ag oxide
Electrolyte - Dimethylformamide-AlCl3+LiCl
Sweep rate - 40 mv/sec
Temp. 30° C
Zero ref. 0.62 v/Pt
CV - 1094
64.0
32.0
0.0
-32.0
-64.0
-96.0
-128.0
IA
MA/CM2
IC
-1.0
-0.8
-0.6
-0.4
-0.2
0
0.2
0.4
0.6
0.8
1.0
VOLTS POLARIZATION

Figure 18

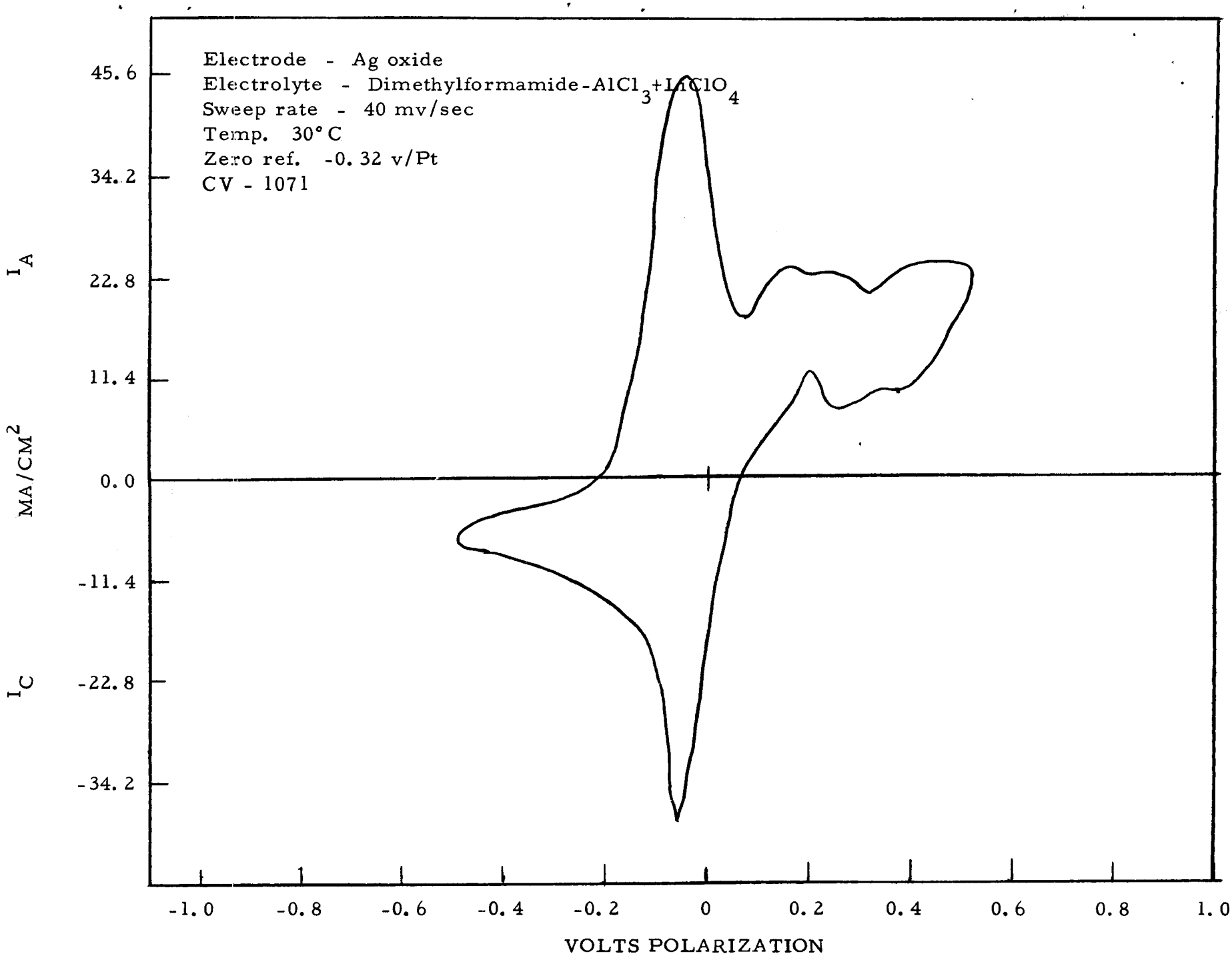
Electrode - Ag oxide
Electrolyte - Dimethylformamide-$AlCl_3$+$LiClO_4$
Sweep rate - 40 mv/sec
Temp. 30° C
Zero ref. -0.32 v/Pt
CV - 1071
45.6
34.2
22.8
11.4
0.0
-11.4
-22.8
-34.2
I_A
I_C
MA/CM^2
-1.0
-0.8
-0.6
-0.4
-0.2
0
0.2
0.4
0.6
0.8
1.0
VOLTS POLARIZATION

Figure 19

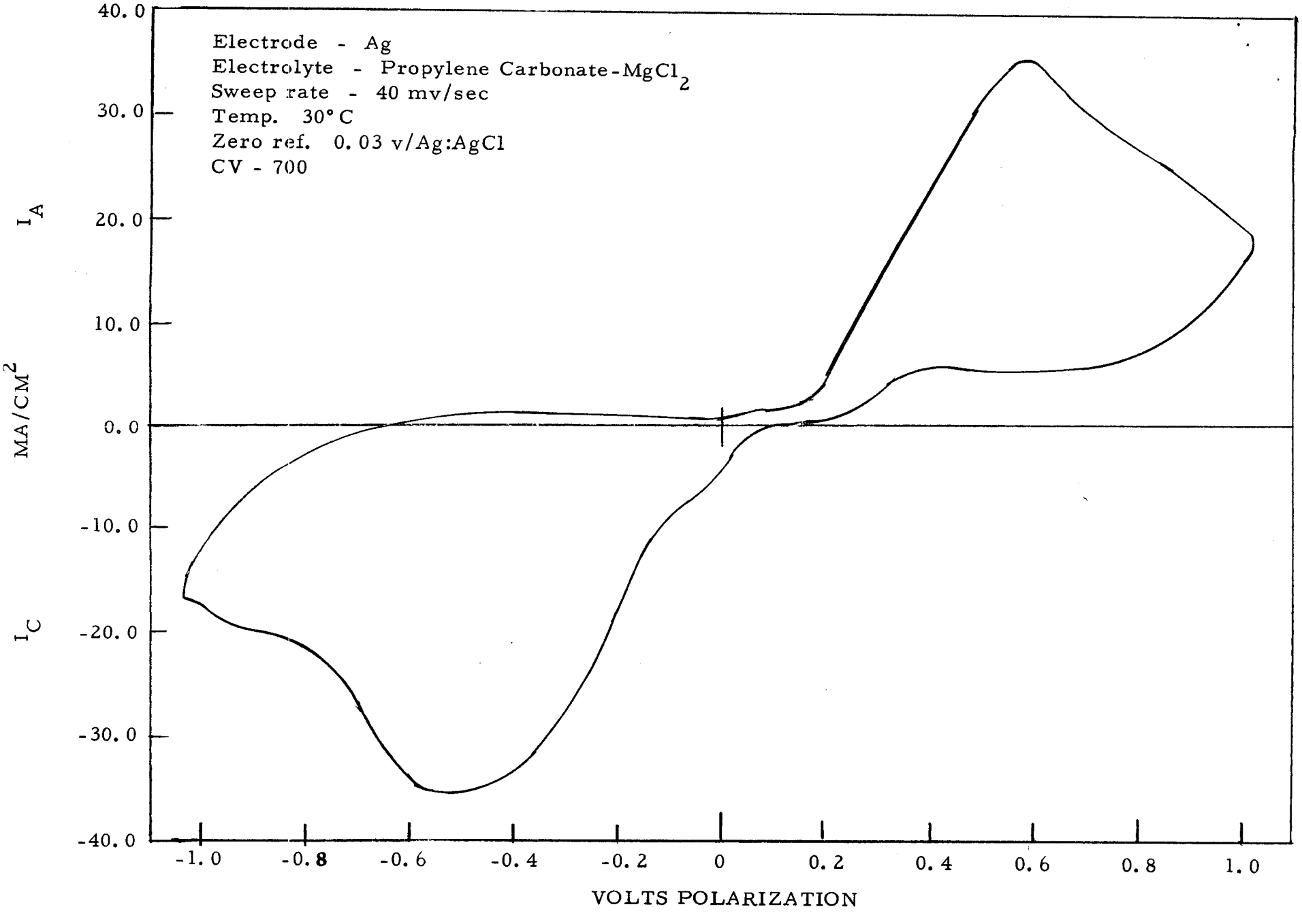
Electrode - Ag
Electrolyte - Propylene Carbonate-$MgCl_2$
Sweep rate - 40 mv/sec
Temp. 30° C
Zero ref. 0.03 v/Ag:AgCl
CV - 700
40.0
30.0
20.0
10.0
0.0
-10.0
-20.0
-30.0
-40.0
I_A
MA/CM^2
I_C
-1.0
-0.8
-0.6
-0.4
-0.2
0
0.2
0.4
0.6
0.8
1.0
VOLTS POLARIZATION

Figure 20

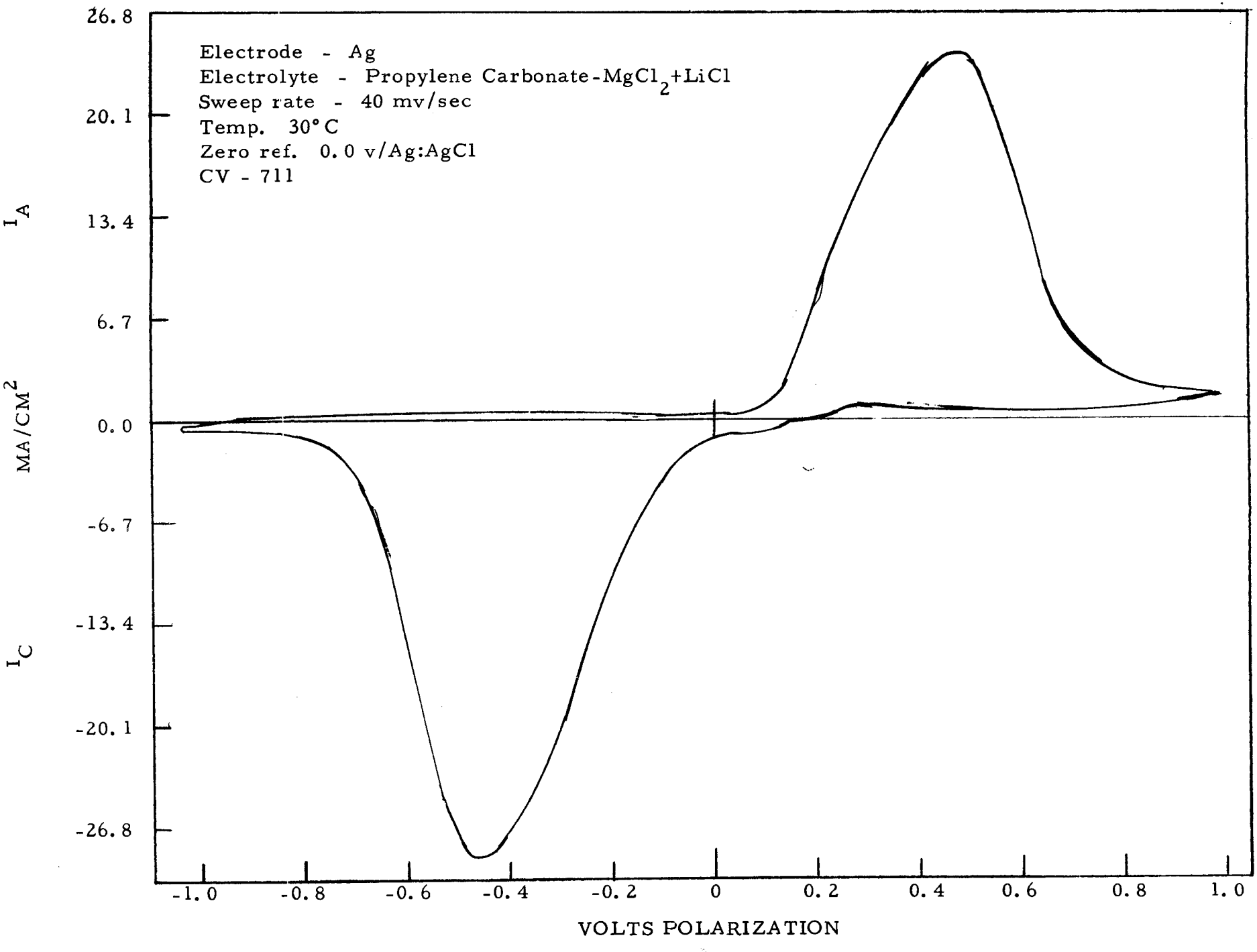
Electrode - Ag
Electrolyte - Propylene Carbonate-$MgCl_2$+LiCl
Sweep rate - 40 mv/sec
Temp. 30° C
Zero ref. 0.0 v/Ag:AgCl
CV - 711
26.8
20.1
13.4
6.7
0.0
-6.7
-13.4
-20.1
-26.8
I_A
MA/CM^2
I_C
-1.0
-0.8
-0.6
-0.4
-0.2
0
0.2
0.4
0.6
0.8
1.0
VOLTS POLARIZATION

Figure 21

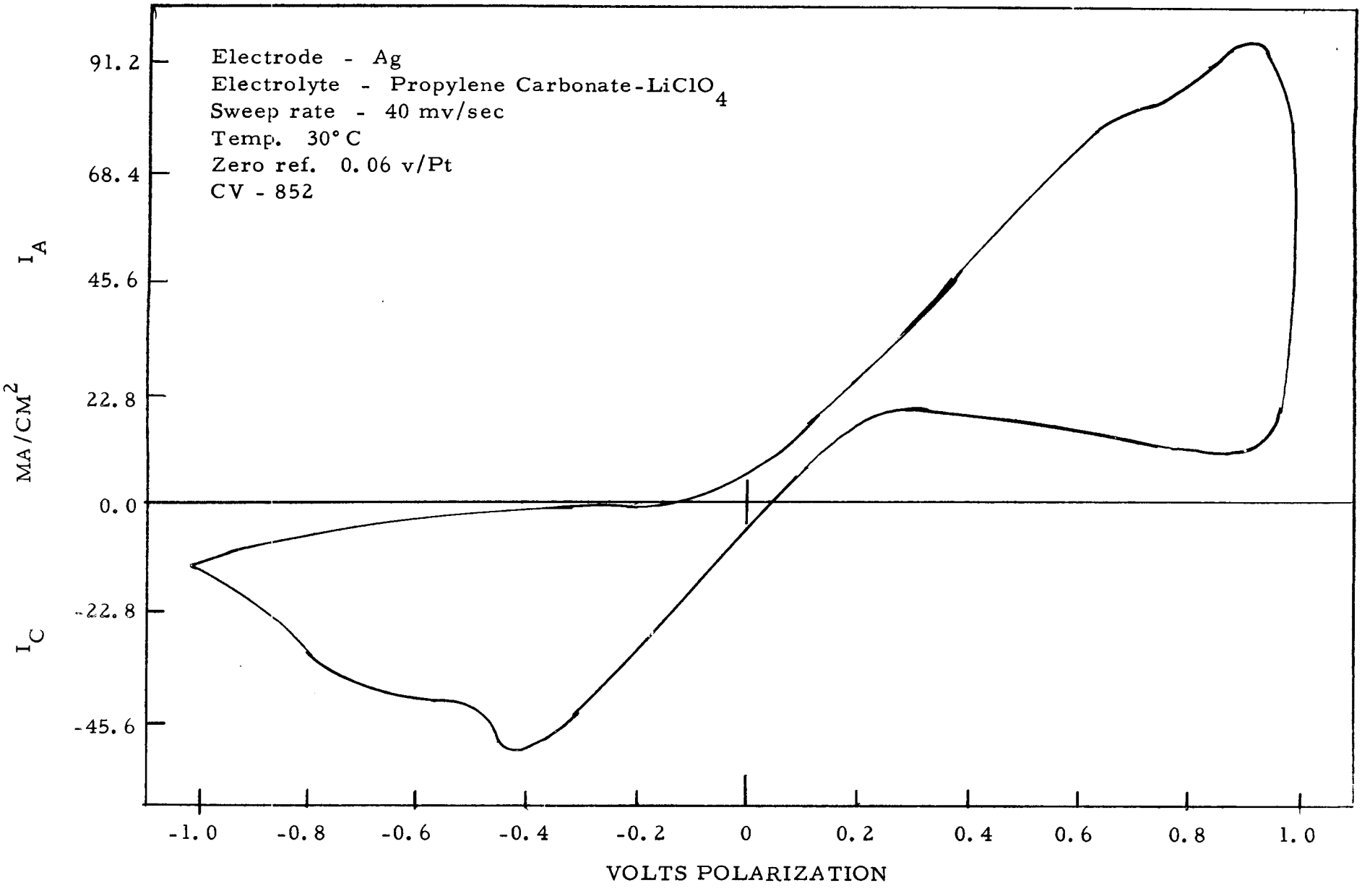
Electrode - Ag
Electrolyte - Propylene Carbonate-$LiClO_4$
Sweep rate - 40 mv/sec
Temp. 30° C
Zero ref. 0.06 v/Pt
CV - 852
91.2
68.4
45.6
22.8
0.0
-22.8
-45.6
I_A
I_C
MA/CM^2
-1.0
-0.8
-0.6
-0.4
-0.2
0
0.2
0.4
0.6
0.8
1.0
VOLTS POLARIZATION

Figure 22

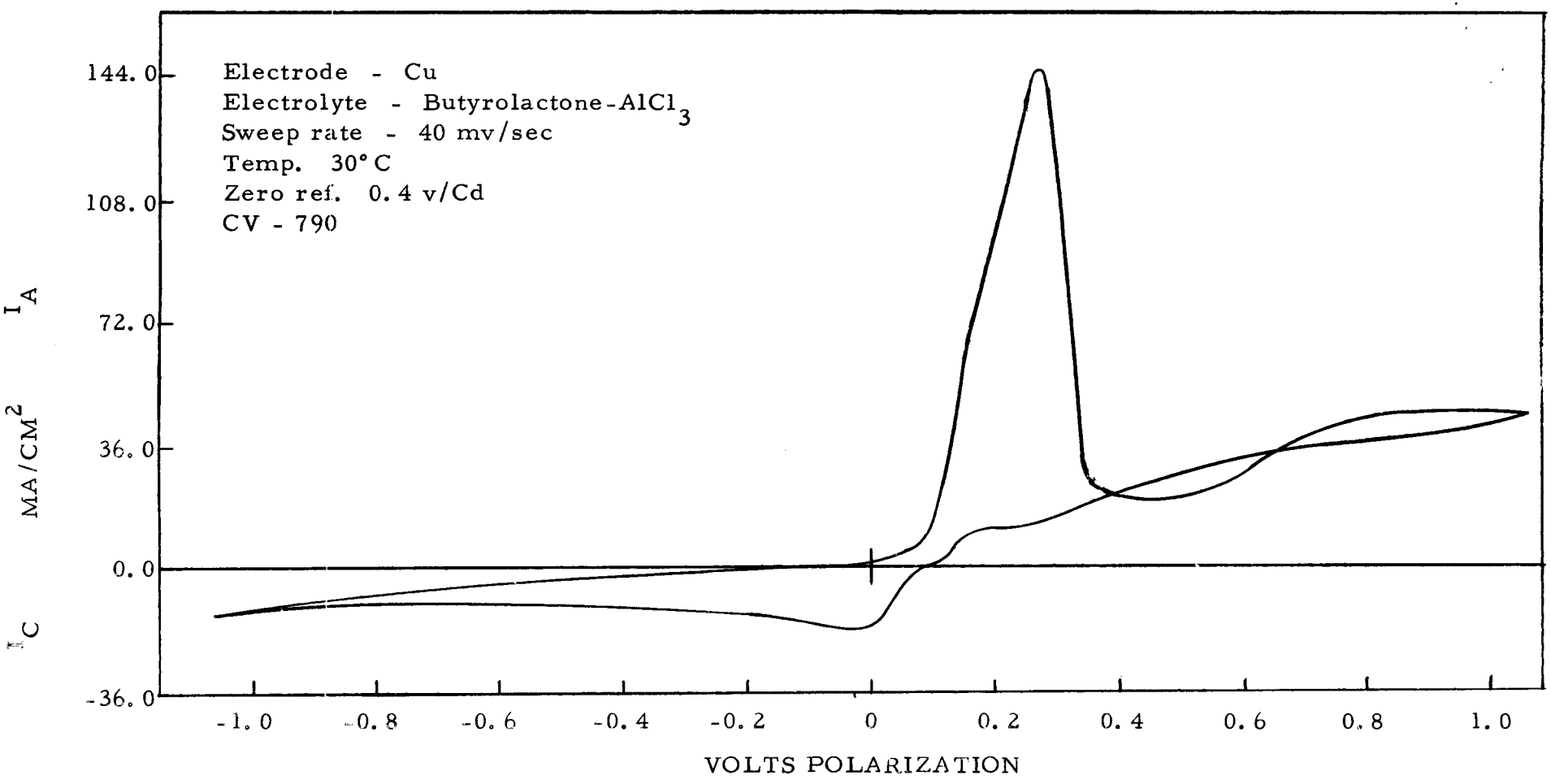
Electrode - Cu
Electrolyte - Butyrolactone-AlCl3
Sweep rate - 40 mv/sec
Temp. 30° C
Zero ref. 0.4 v/Cd
CV - 790
144.0
108.0
72.0
36.0
0.0
-36.0
I_A
MA/CM^2
I_C
-1.0
-0.8
-0.6
-0.4
-0.2
0
0.2
0.4
0.6
0.8
1.0
VOLTS POLARIZATION

Figure 23

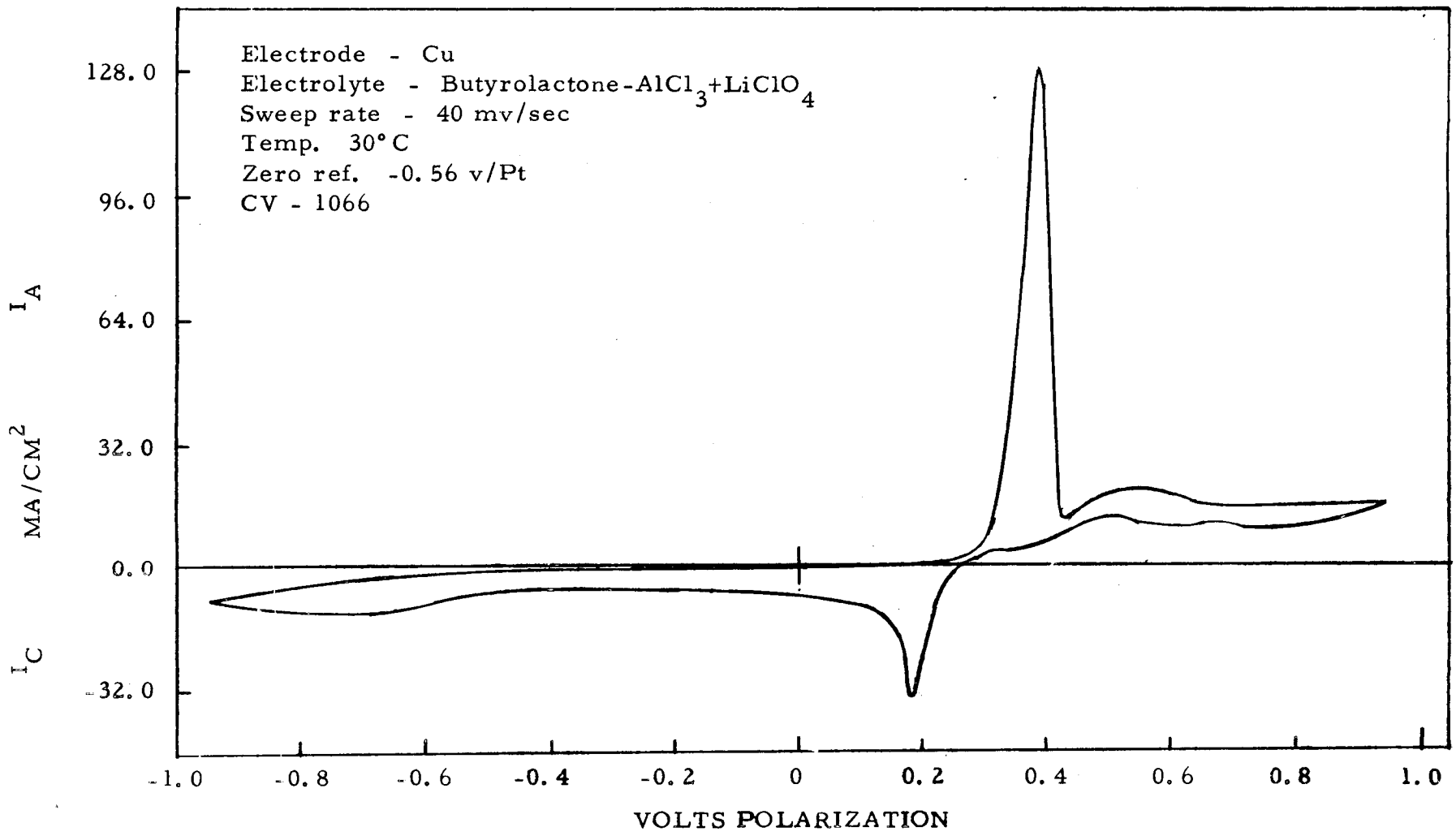
Electrode - Cu
Electrolyte - Butyrolactone-AlCl3+LiClO4
Sweep rate - 40 mv/sec
Temp. 30° C
Zero ref. -0.56 v/Pt
CV - 1066
128.0
96.0
64.0
32.0
0.0
-32.0
IA
MA/CM2
IC
-1.0
-0.8
-0.6
-0.4
-0.2
0
0.2
0.4
0.6
0.8
1.0
VOLTS POLARIZATION

Figure 24

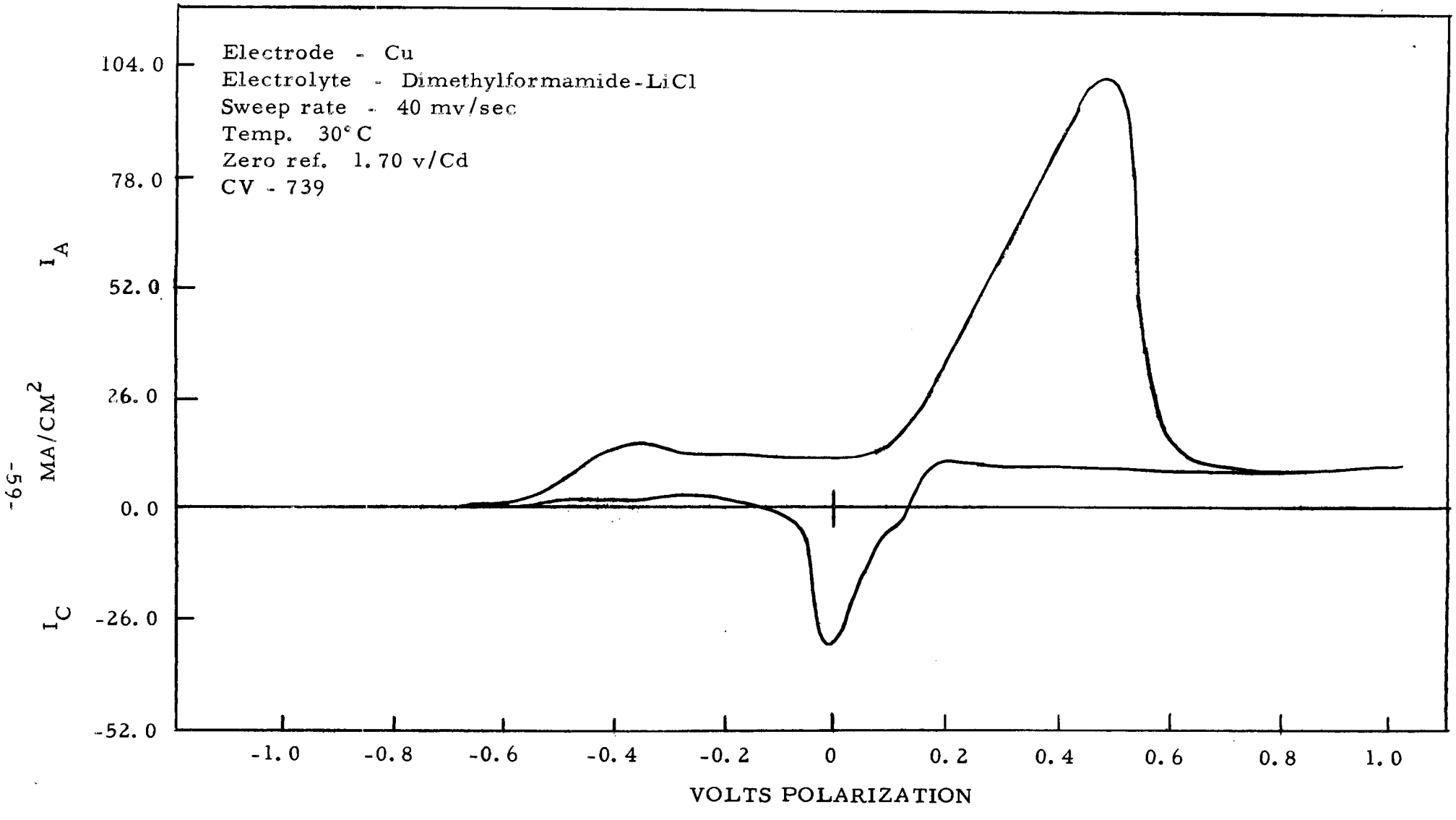
Electrode - Cu
Electrolyte - Dimethylformamide-LiCl
Sweep rate - 40 mv/sec
Temp. 30° C
Zero ref. 1.70 v/Cd
CV - 739
104.0
78.0
52.0
26.0
0.0
-26.0
-52.0
I_A
I_C
MA/CM^2
-1.0
-0.8
-0.6
-0.4
-0.2
0
0.2
0.4
0.6
0.8
1.0
VOLTS POLARIZATION

Figure 25

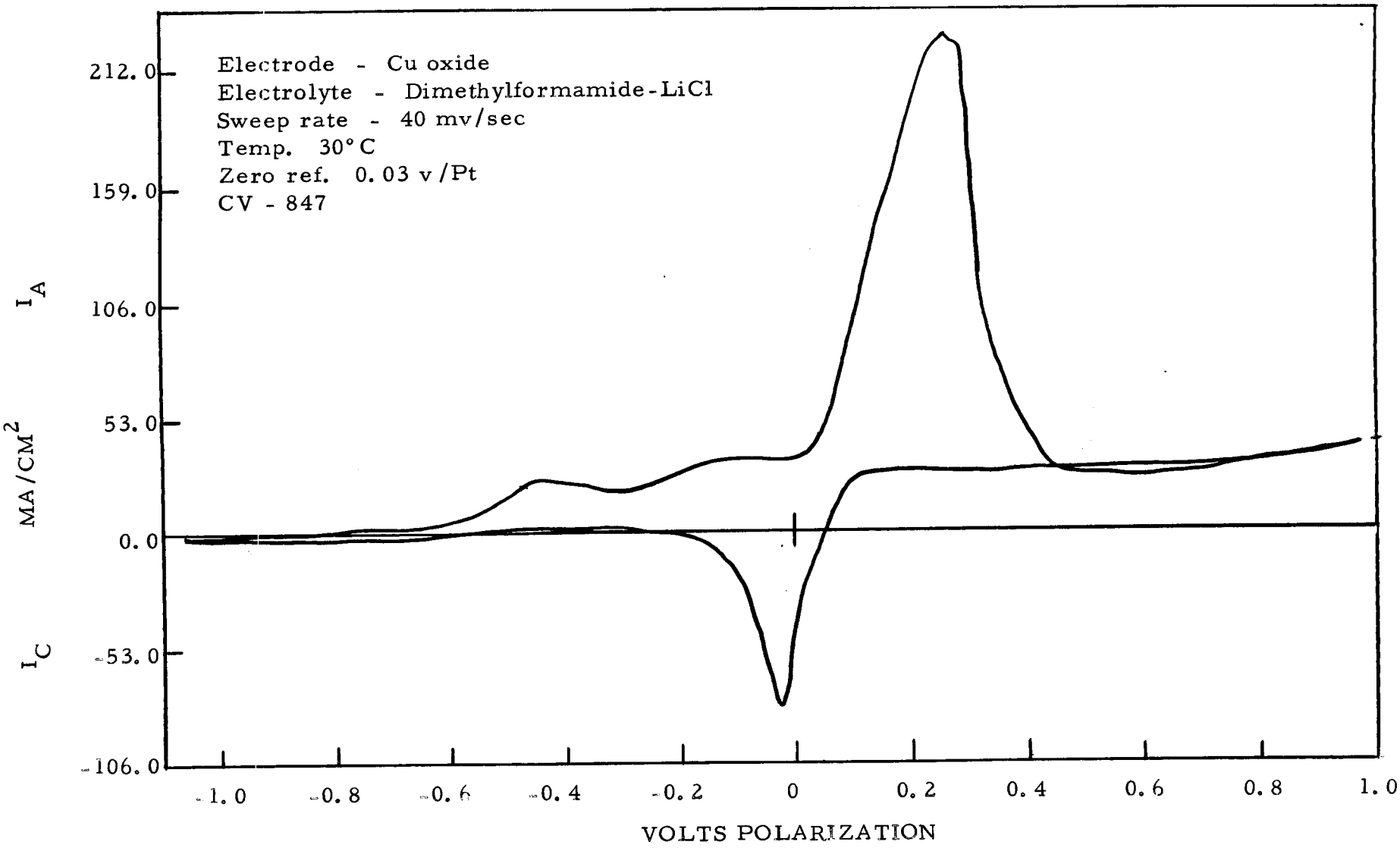
Electrode - Cu oxide
Electrolyte - Dimethylformamide-LiCl
Sweep rate - 40 mv/sec
Temp. 30° C
Zero ref. 0.03 v/Pt
CV - 847
212.0
159.0
106.0
53.0
0.0
-53.0
-106.0
I_A
MA/CM^2
I_C
-1.0
-0.8
-0.6
-0.4
-0.2
0
0.2
0.4
0.6
0.8
1.0
VOLTS POLARIZATION

Figure 26

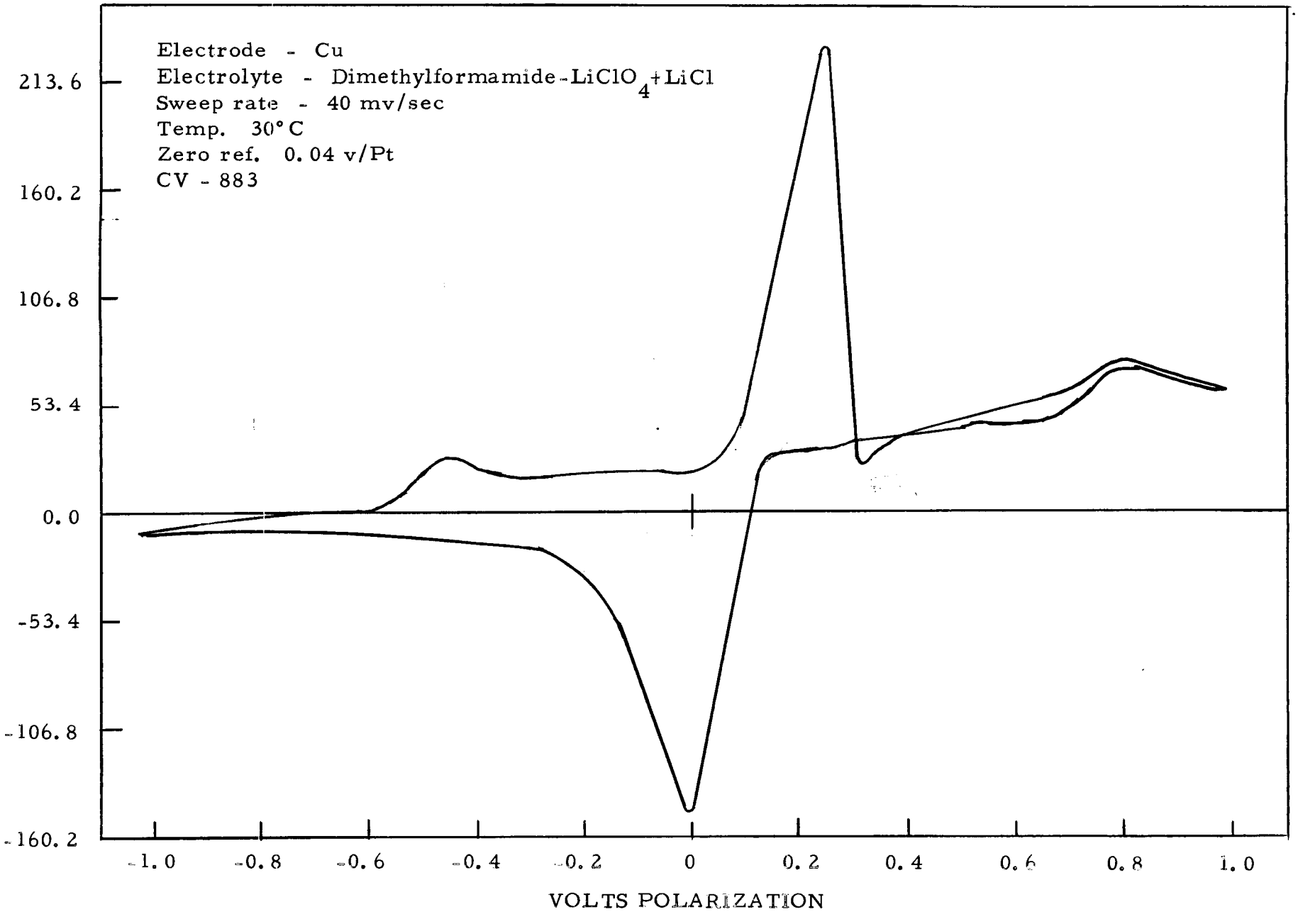
Electrode - Cu
Electrolyte - Dimethylformamide-$LiClO_4$+LiCl
Sweep rate - 40 mv/sec
Temp. 30° C
Zero ref. 0.04 v/Pt
CV - 883
213.6
160.2
106.8
53.4
0.0
-53.4
-106.8
-160.2
I_A
I_C
MA/CM^2
-1.0
-0.8
-0.6
-0.4
-0.2
0
0.2
0.4
0.6
0.8
1.0
VOLTS POLARIZATION

Figure 27

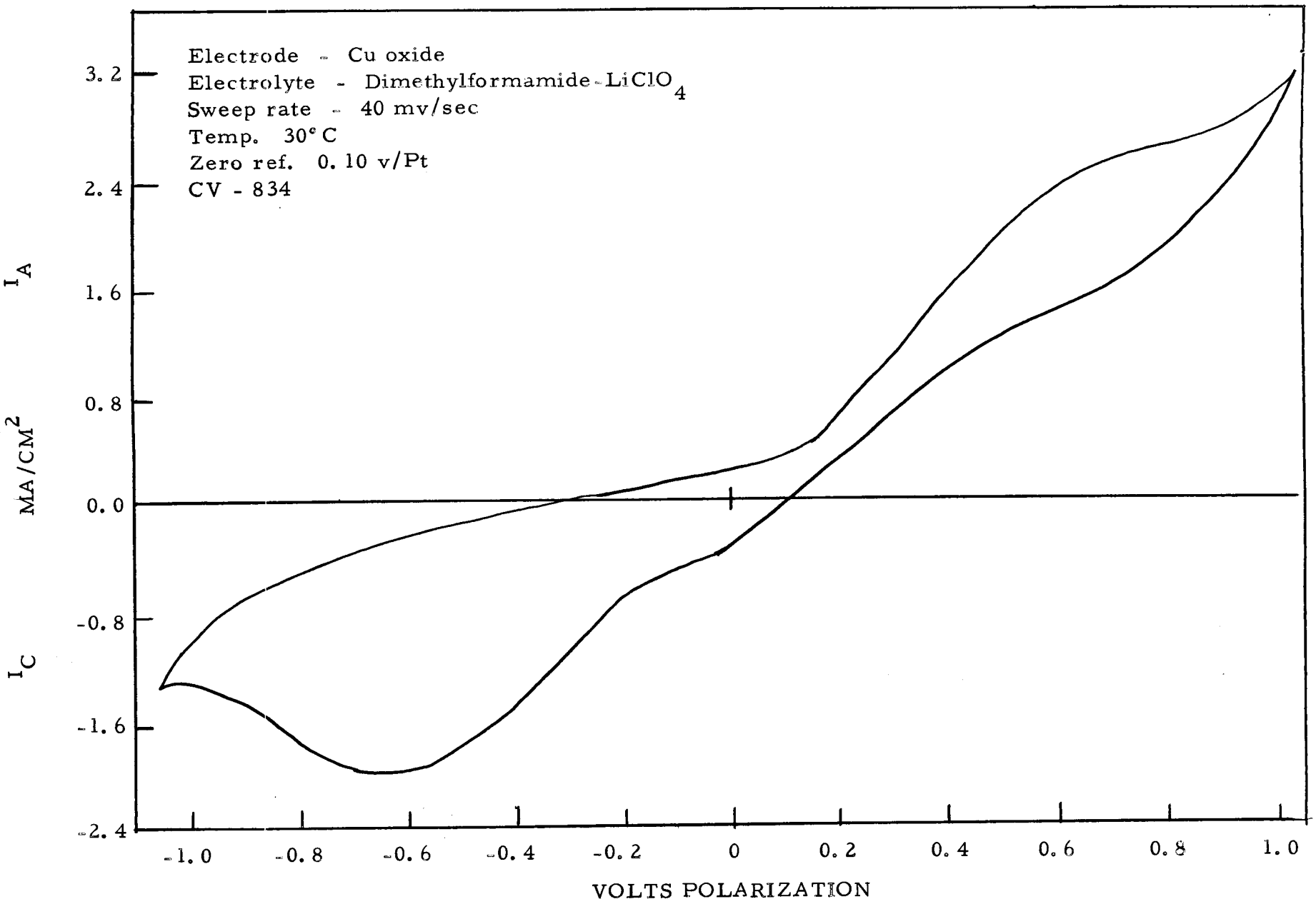
Electrode - Cu oxide
Electrolyte - Dimethylformamide-$LiClO_4$
Sweep rate - 40 mv/sec
Temp. 30° C
Zero ref. 0.10 v/Pt
CV - 834
3.2
2.4
1.6
0.8
0.0
-0.8
-1.6
-2.4
I_A
MA/CM^2
I_C
-1.0
-0.8
-0.6
-0.4
-0.2
0
0.2
0.4
0.6
0.8
1.0
VOLTS POLARIZATION

Figure 28

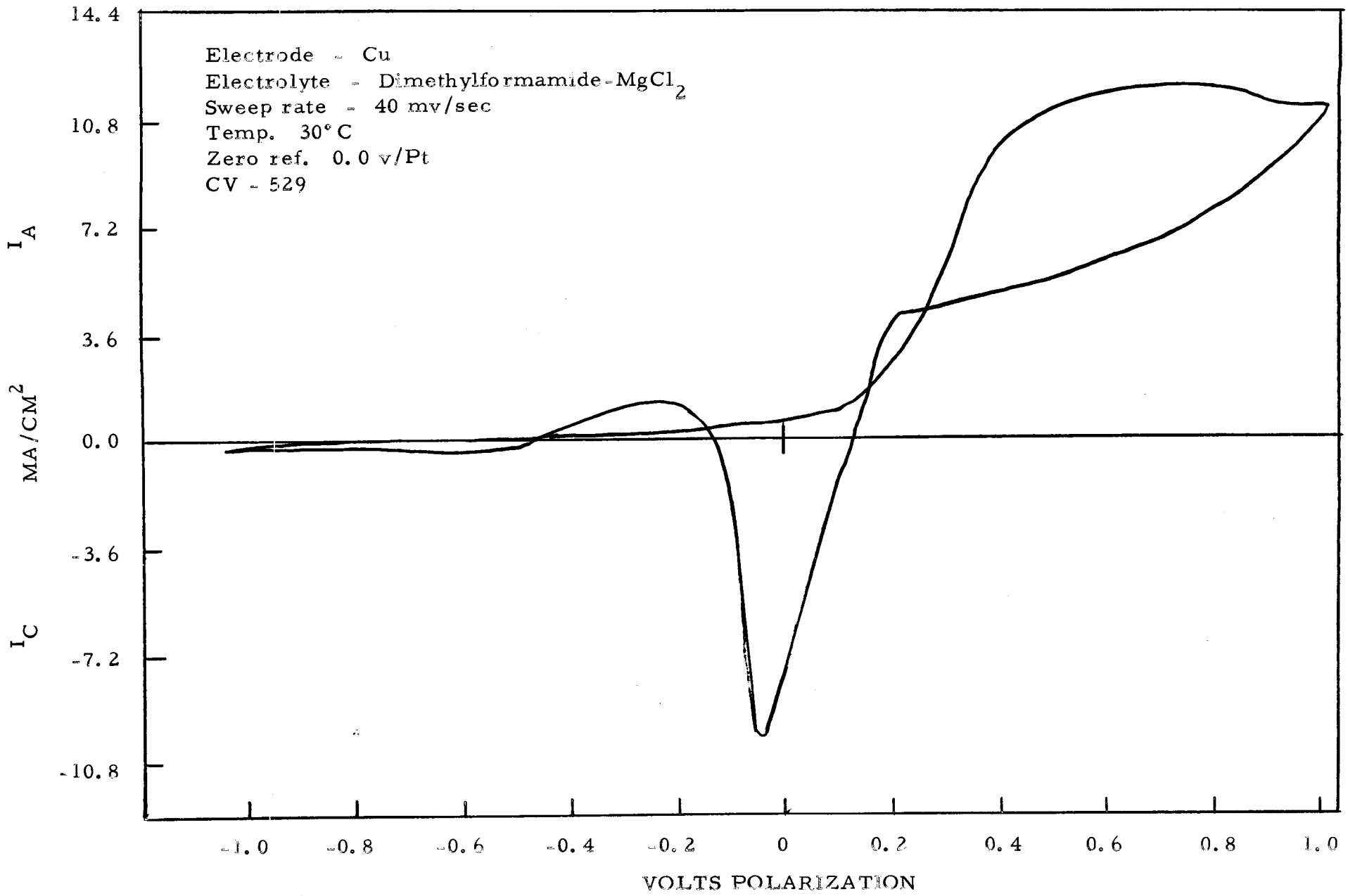
Electrode - Cu
Electrolyte - Dimethylformamide-$MgCl_2$
Sweep rate - 40 mv/sec
Temp. 30° C
Zero ref. 0.0 v/Pt
CV - 529
14.4
10.8
7.2
3.6
0.0
-3.6
-7.2
-10.8
I_A
I_C
MA/CM^2
-1.0
-0.8
-0.6
-0.4
-0.2
0
0.2
0.4
0.6
0.8
1.0
VOLTS POLARIZATION

Figure 29

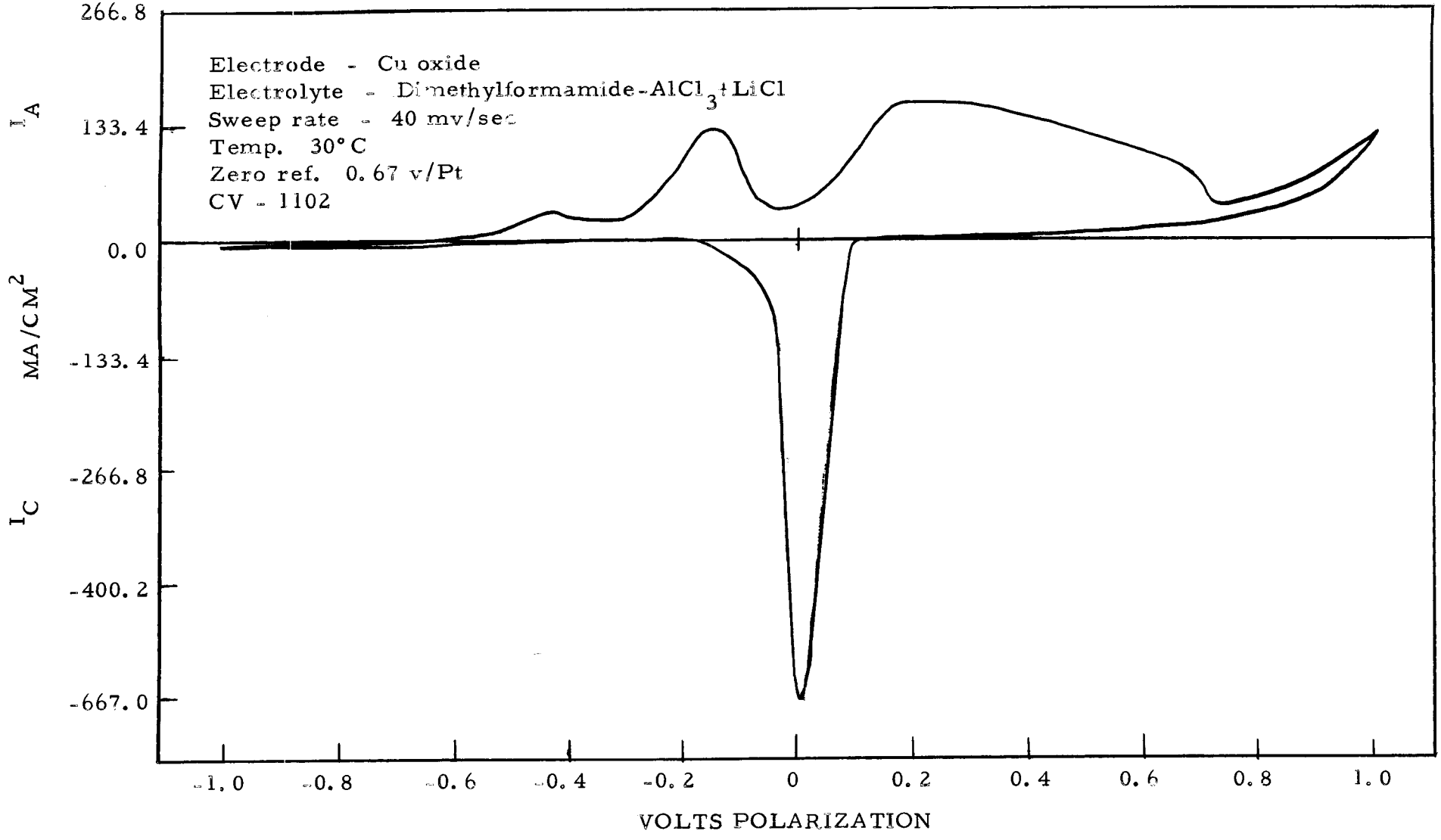
266.8
133.4
0.0
-133.4
-266.8
-400.2
-667.0
I_A
I_C
MA/CM^2
Electrode - Cu oxide
Electrolyte - Dimethylformamide-$AlCl_3$+LiCl
Sweep rate - 40 mv/sec
Temp. 30°C
Zero ref. 0.67 v/Pt
CV - 1102
-1.0
-0.8
-0.6
-0.4
-0.2
0
0.2
0.4
0.6
0.8
1.0
VOLTS POLARIZATION

Figure 30

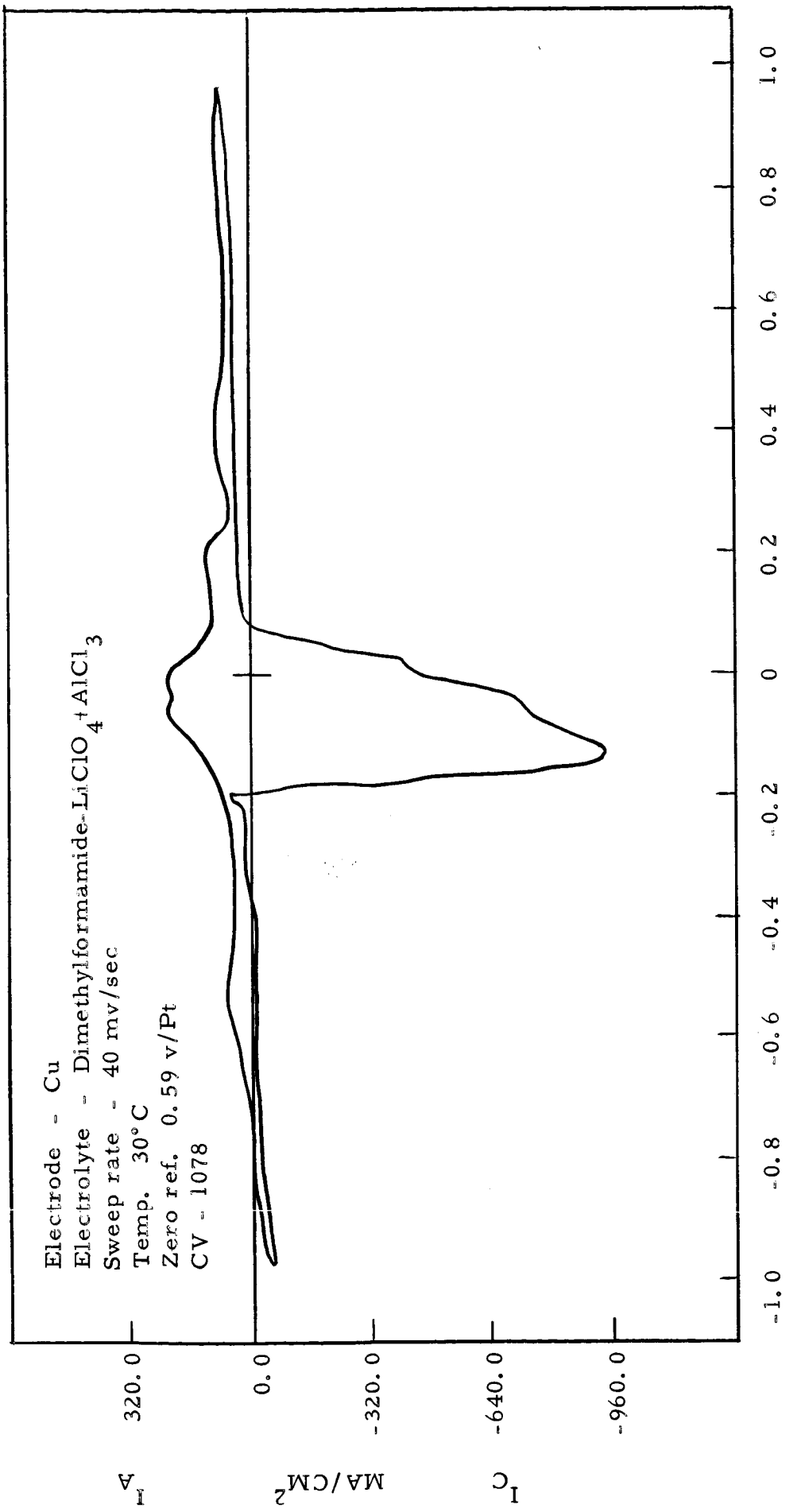
Electrode - Cu
Electrolyte - Dimethylformamide-$LiClO_4$+$AlCl_3$
Sweep rate - 40 mv/sec
Temp. 30°C
Zero ref. 0.59 v/Pt
CV - 1078
320.0
0.0
-320.0
-640.0
-960.0
I_A
I_C
MA/CM^2
-1.0
-0.8
-0.6
-0.4
-0.2
0
0.2
0.4
0.6
0.8
1.0
VOLTS POLARIZATION

Figure 31

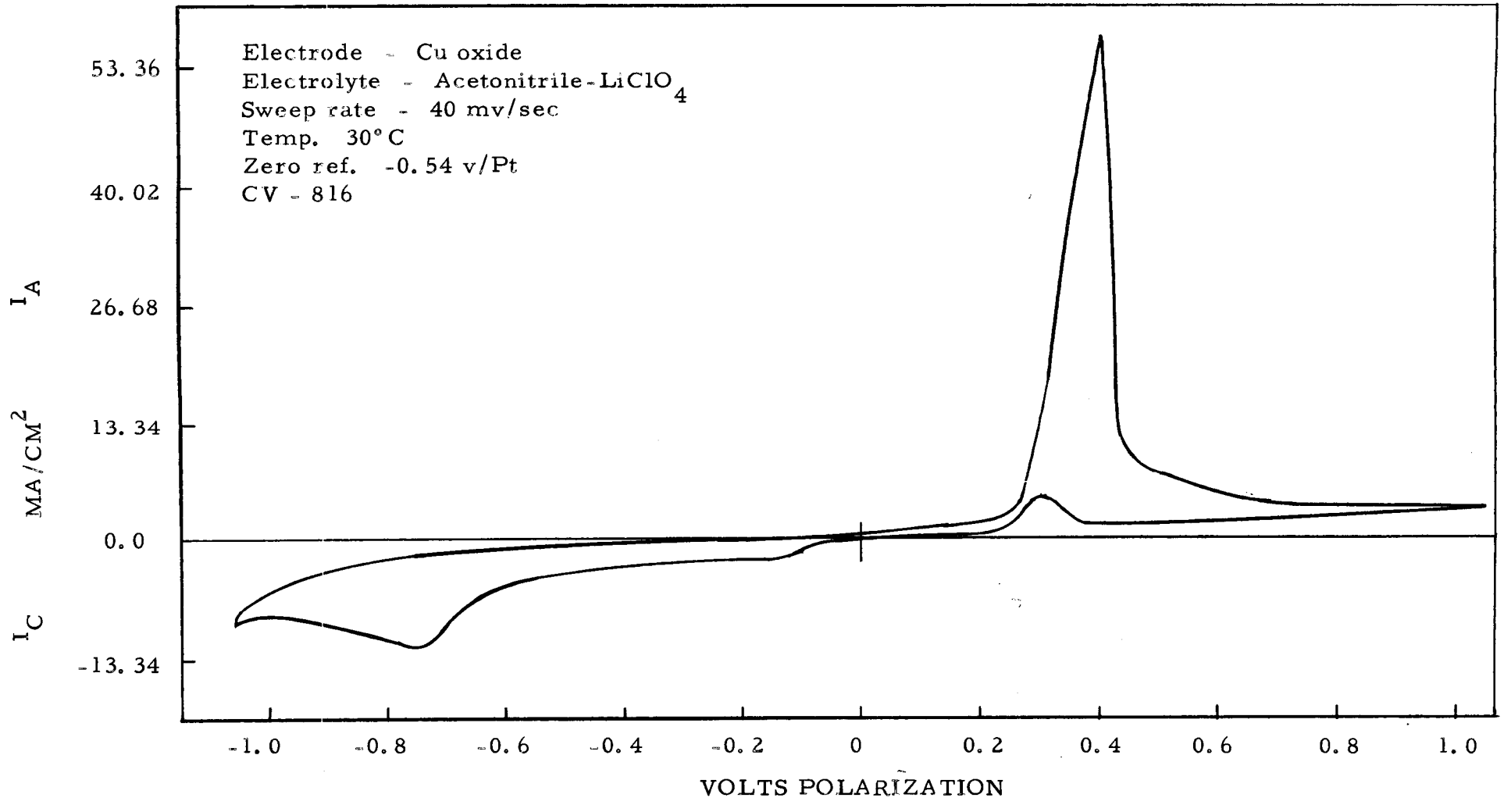
Electrode - Cu oxide
Electrolyte - Acetonitrile-$LiClO_4$
Sweep rate - 40 mv/sec
Temp. 30° C
Zero ref. -0.54 v/Pt
CV - 816
53.36
40.02
26.68
13.34
0.0
-13.34
I_A
MA/CM^2
I_C
-1.0
-0.8
-0.6
-0.4
-0.2
0
0.2
0.4
0.6
0.8
1.0
VOLTS POLARIZATION

Figure 32

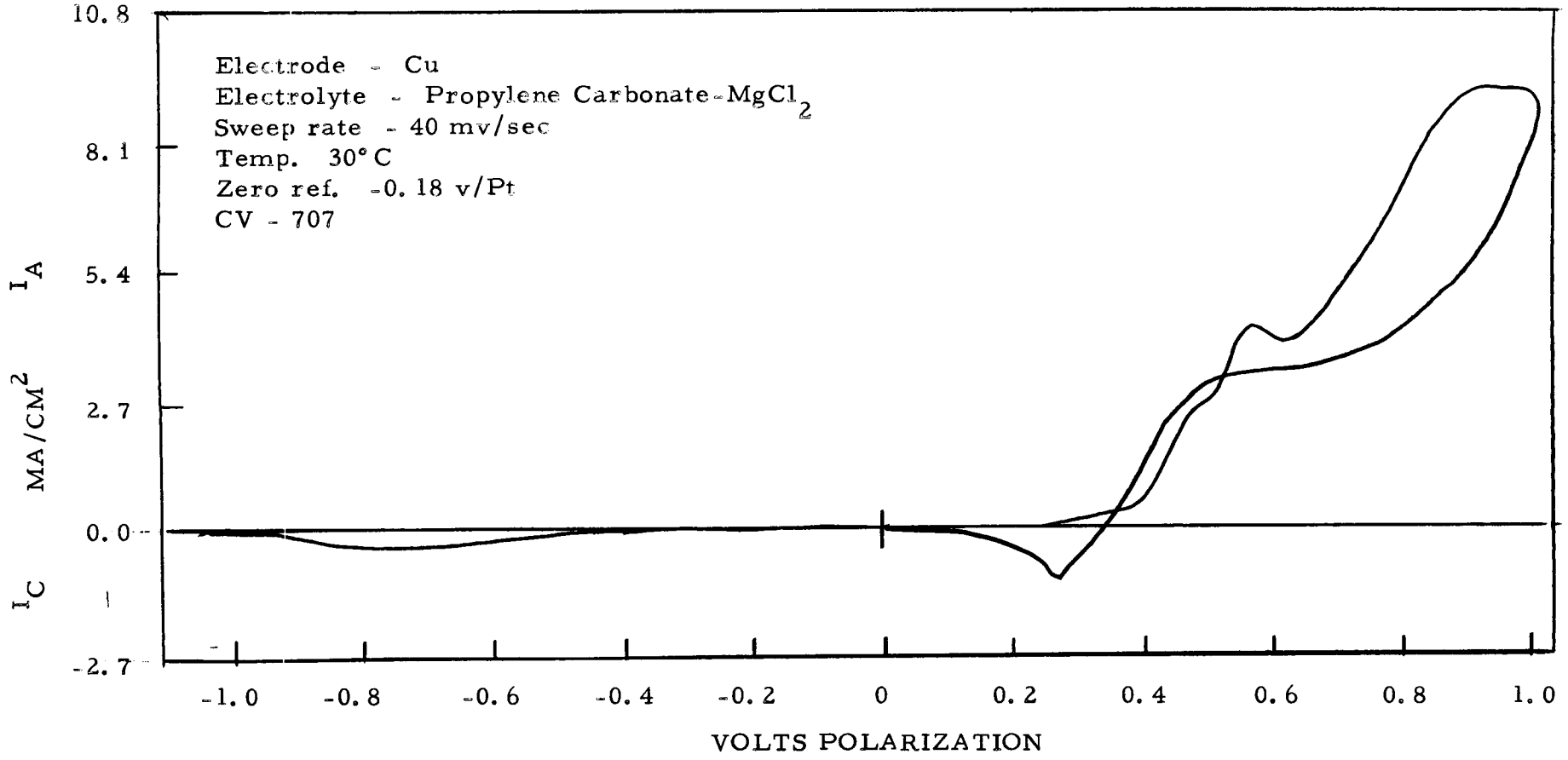
Electrode - Cu
Electrolyte - Propylene Carbonate-$MgCl_2$
Sweep rate - 40 mv/sec
Temp. 30° C
Zero ref. -0.18 v/Pt
CV - 707
10.8
8.1
5.4
2.7
0.0
-2.7
I_A
MA/CM^2
I_C
-1.0
-0.8
-0.6
-0.4
-0.2
0
0.2
0.4
0.6
0.8
1.0
VOLTS POLARIZATION

Figure 33

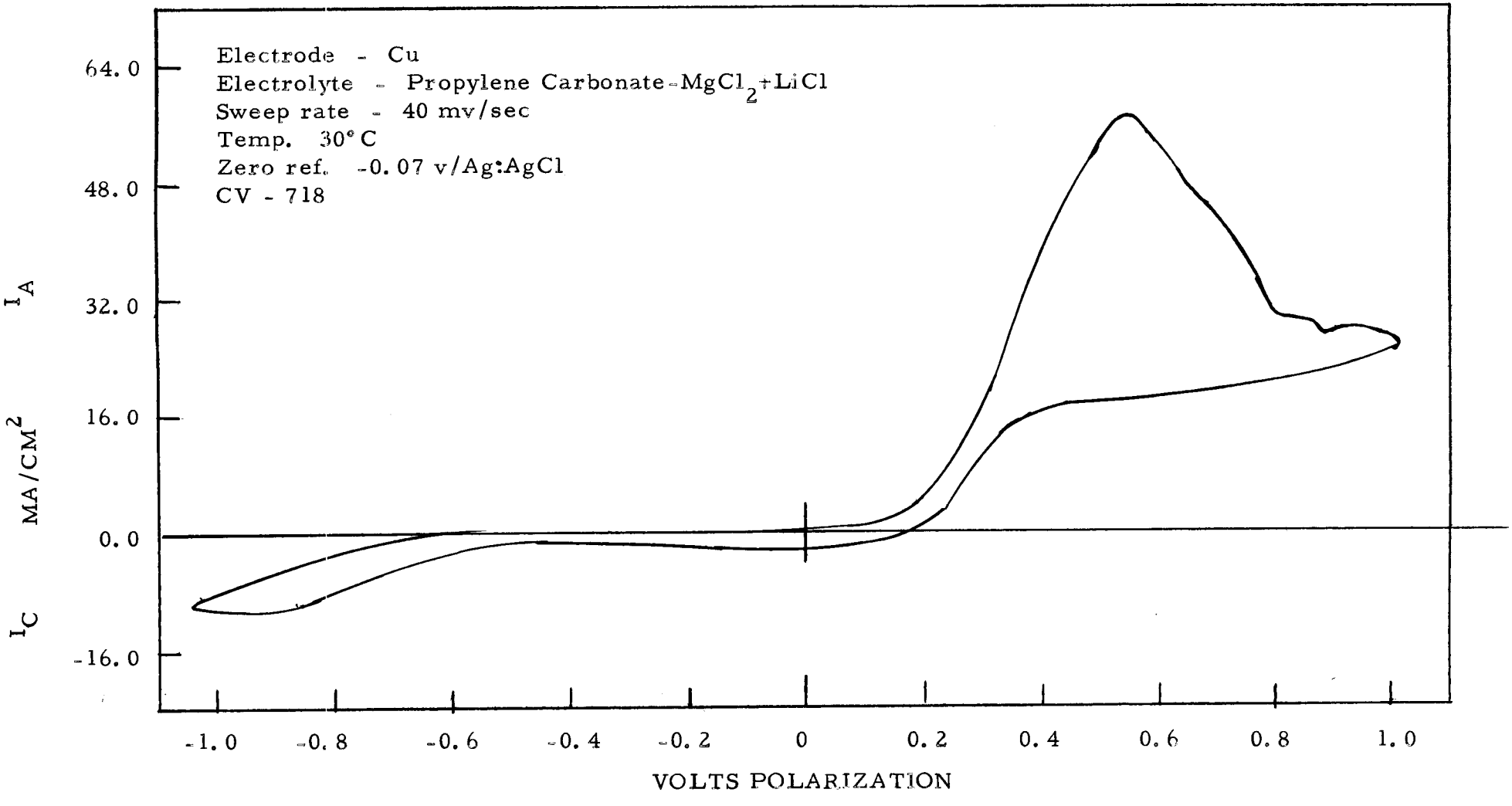
Electrode - Cu
Electrolyte - Propylene Carbonate-$MgCl_2$+LiCl
Sweep rate - 40 mv/sec
Temp. 30° C
Zero ref. -0.07 v/Ag:AgCl
CV - 718
64.0
48.0
32.0
16.0
0.0
-16.0
I_A
MA/CM^2
I_C
-1.0
-0.8
-0.6
-0.4
-0.2
0
0.2
0.4
0.6
0.8
1.0
VOLTS POLARIZATION

Figure 34

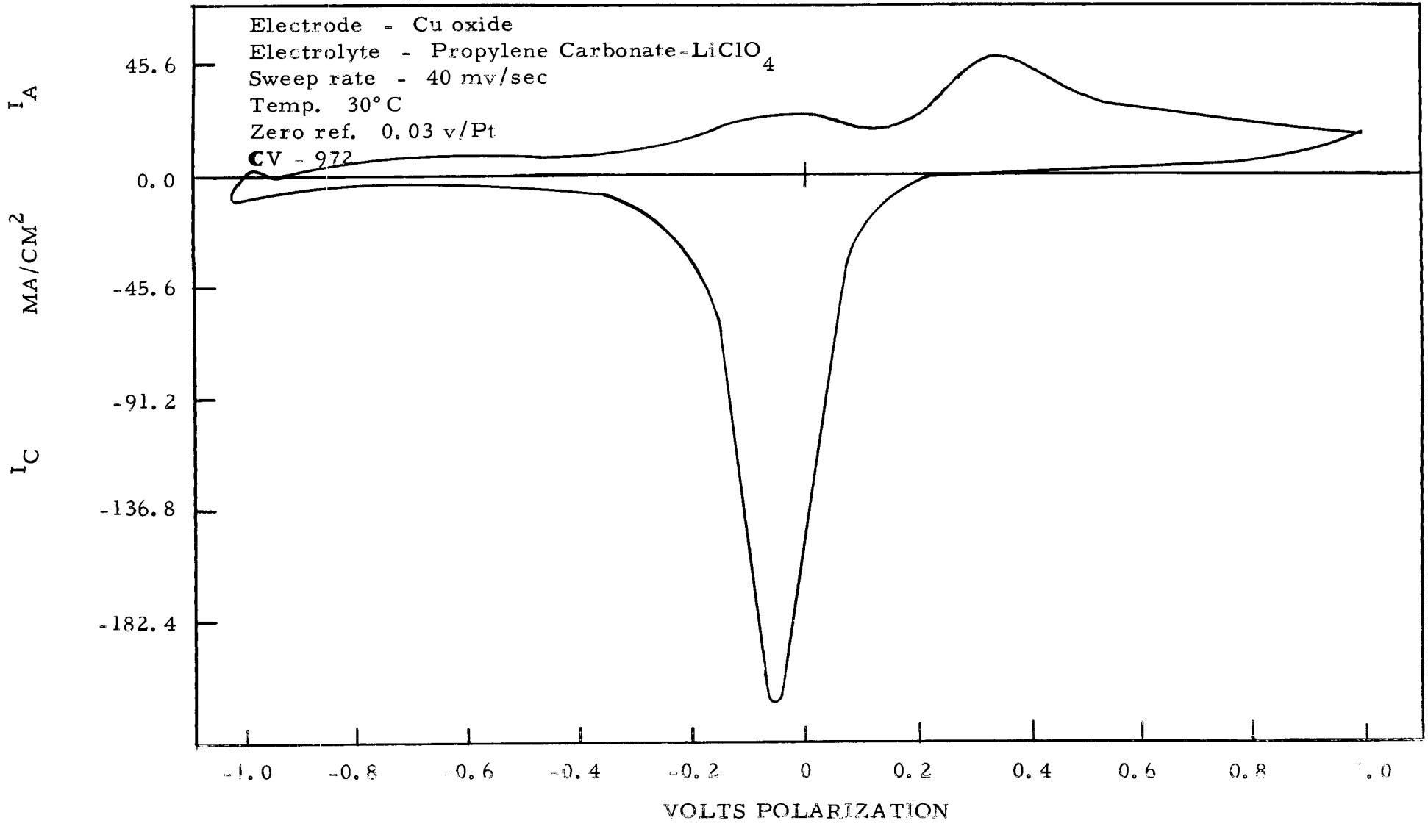
Electrode - Cu oxide
Electrolyte - Propylene Carbonate-$LiClO_4$
Sweep rate - 40 mv/sec
Temp. 30° C
Zero ref. 0.03 v/Pt
CV - 972
I_A
45.6
0.0
MA/CM^2
-45.6
-91.2
I_C
-136.8
-182.4
-1.0
-0.8
-0.6
-0.4
-0.2
0
0.2
0.4
0.6
0.8
.0
VOLTS POLARIZATION

Figure 35

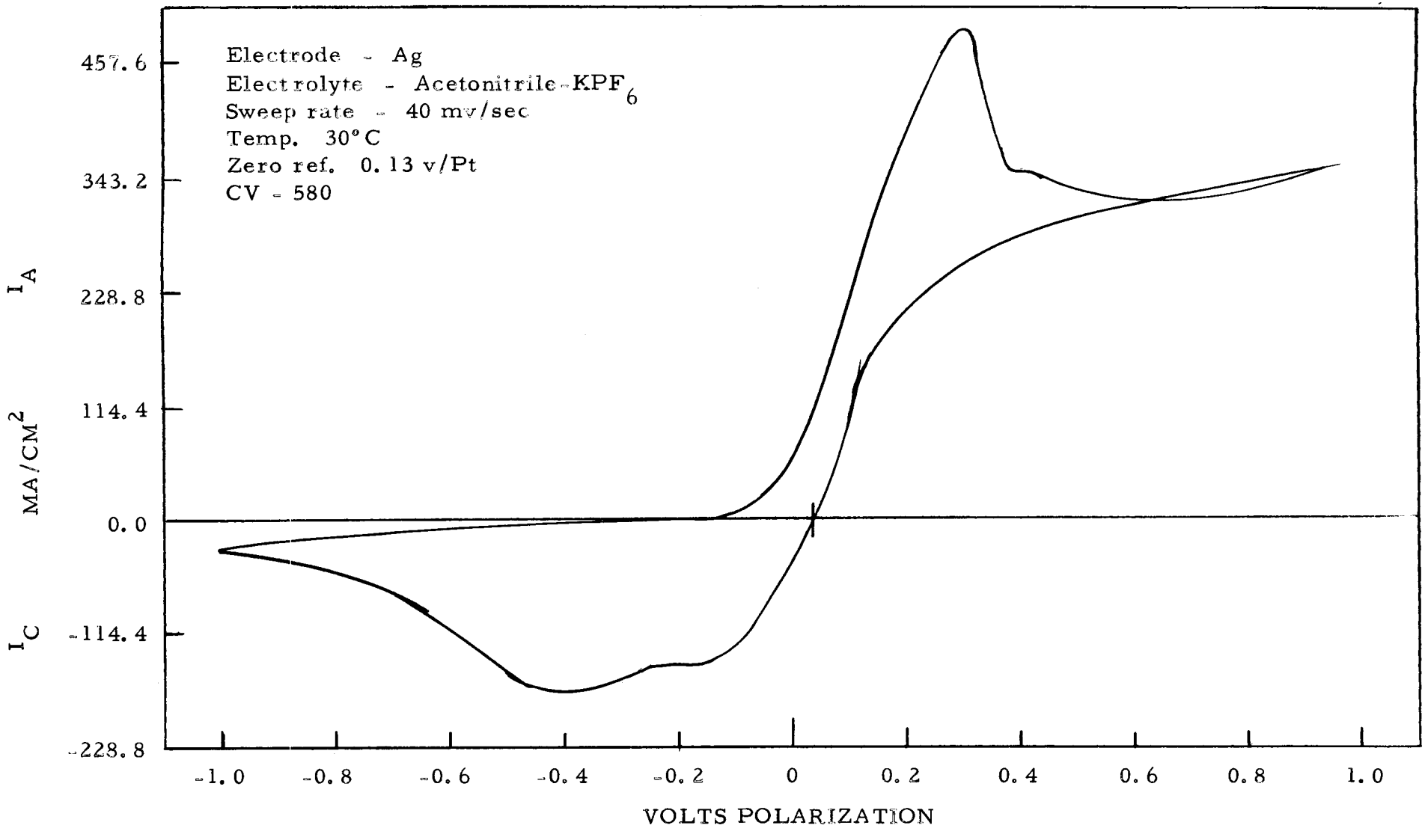
Electrode - Ag
Electrolyte - Acetonitrile-KPF_6
Sweep rate - 40 mv/sec
Temp. 30°C
Zero ref. 0.13 v/Pt
CV - 580
457.6
343.2
228.8
114.4
0.0
-114.4
-228.8
I_A
MA/CM^2
I_C
-1.0
-0.8
-0.6
-0.4
-0.2
0
0.2
0.4
0.6
0.8
1.0
VOLTS POLARIZATION

Figure 36

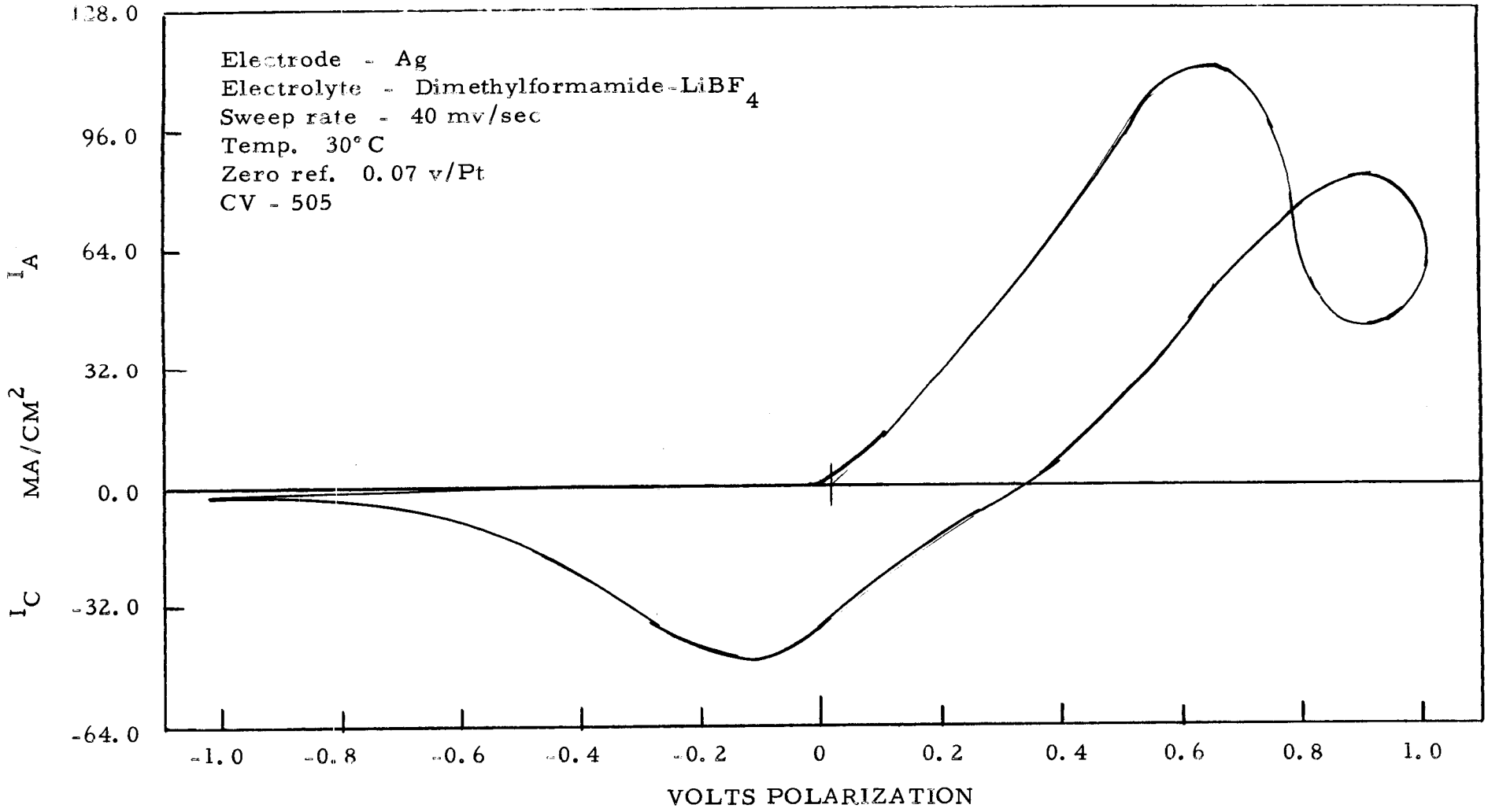
128.0
96.0
64.0
32.0
0.0
-32.0
-64.0
I_A
I_C
MA/CM^2
Electrode - Ag
Electrolyte - Dimethylformamide-$LiBF_4$
Sweep rate - 40 mv/sec
Temp. 30° C
Zero ref. 0.07 v/Pt
CV - 505
-1.0
-0.8
-0.6
-0.4
-0.2
0
0.2
0.4
0.6
0.8
1.0
VOLTS POLARIZATION

Figure 37

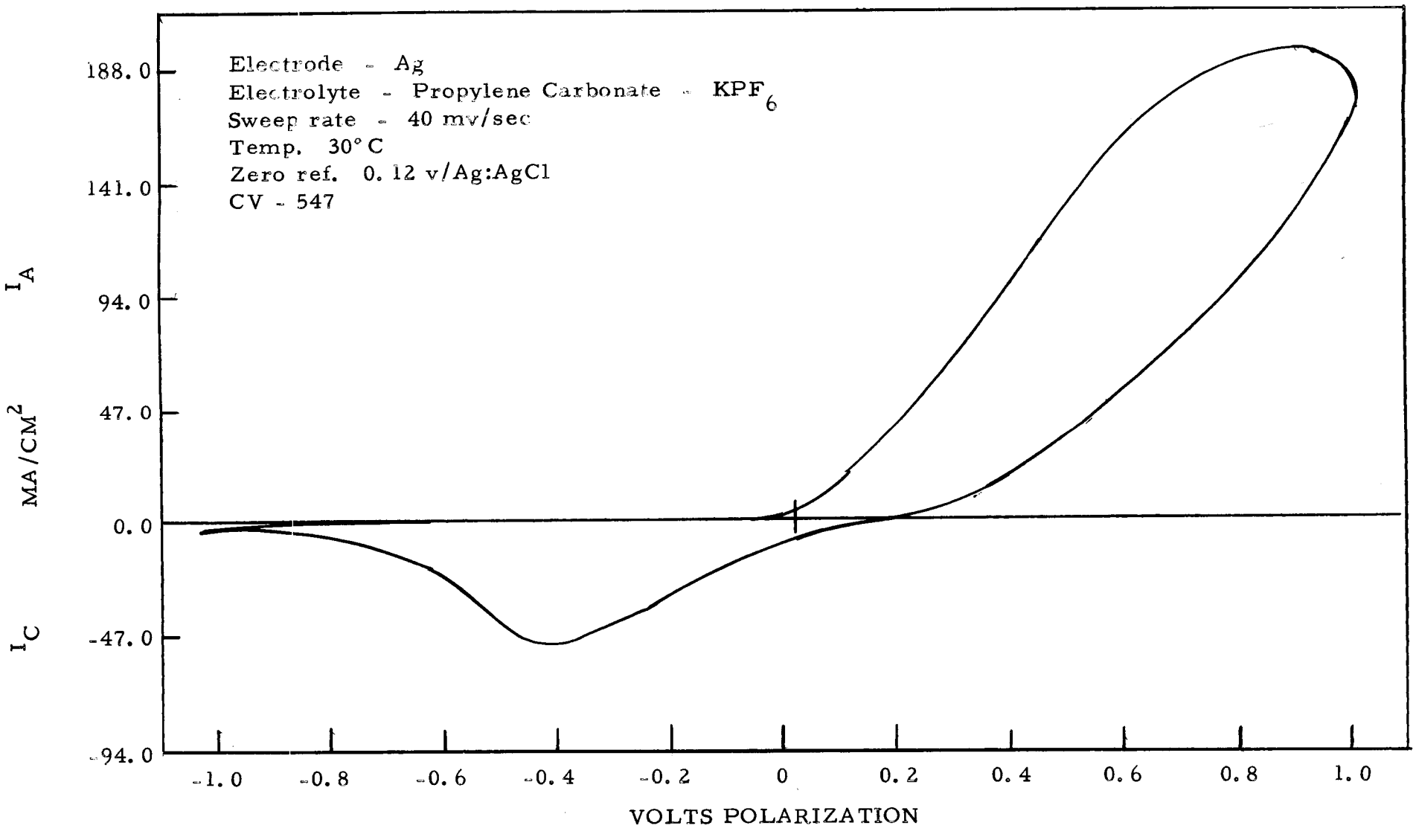
Electrode - Ag
Electrolyte - Propylene Carbonate - KPF_6
Sweep rate - 40 mv/sec
Temp. 30° C
Zero ref. 0.12 v/Ag:AgCl
CV - 547
188.0
141.0
94.0
47.0
0.0
-47.0
-94.0
I_A
MA/CM^2
I_C
-1.0
-0.8
-0.6
-0.4
-0.2
0
0.2
0.4
0.6
0.8
1.0
VOLTS POLARIZATION

Figure 38

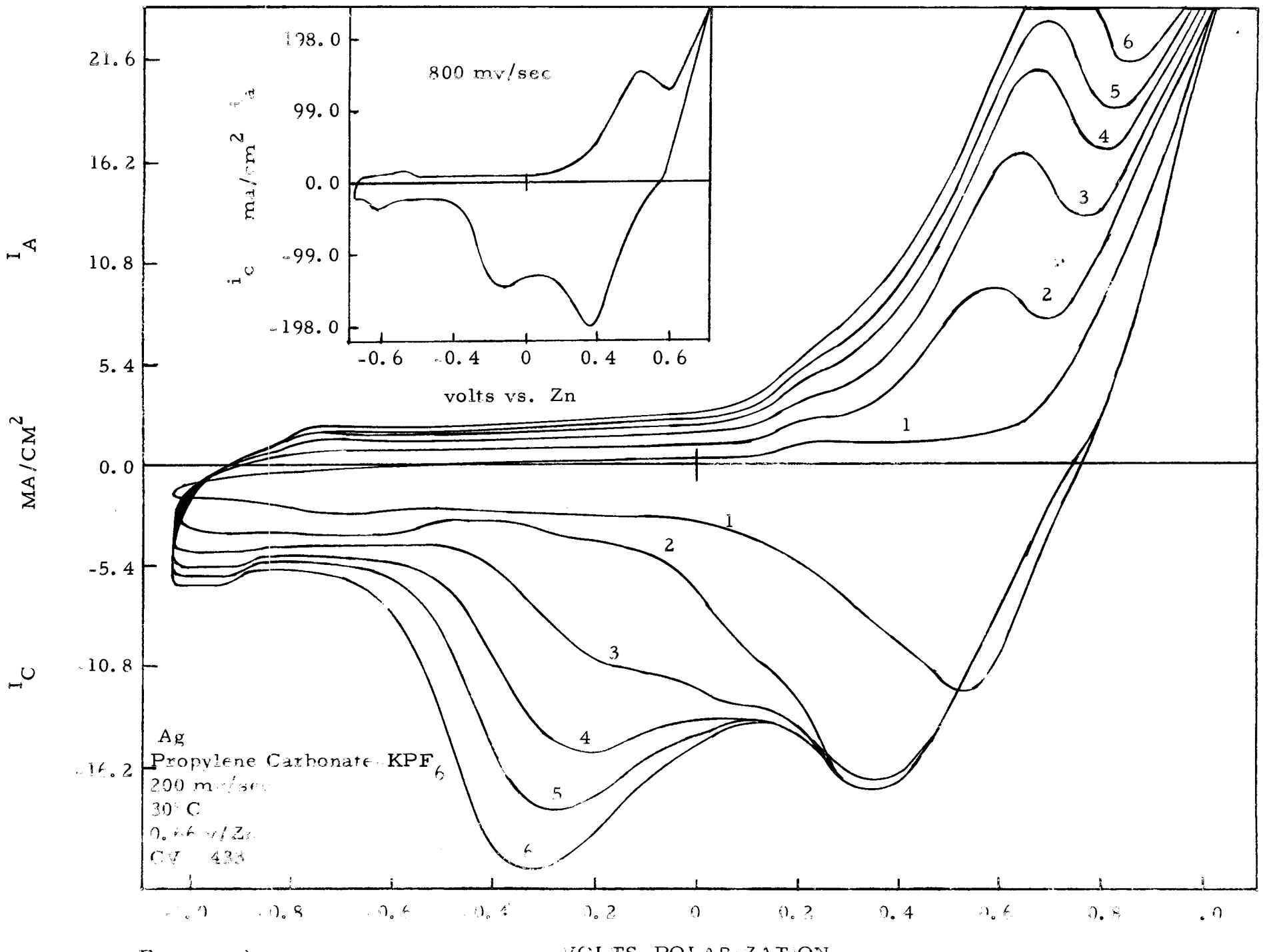
198.0
99.0
0.0
-99.0
-198.0
800 mv/sec
i_c ma/cm^2
-0.6
-0.4
0
0.4
0.6
volts vs. Zn
21.6
16.2
10.8
5.4
0.0
-5.4
-10.8
-16.2
I_A
MA/CM^2
I_C
1
2
3
4
5
6
Ag
Propylene Carbonate-KPF$_6$
200 mv/sec
30° C
0.66 v/Zn
CV 433
-1.0
-0.8
-0.6
-0.4
-0.2
0
0.2
0.4
0.6
0.8
1.0
VOLTS POLARIZATION

Fig. 39

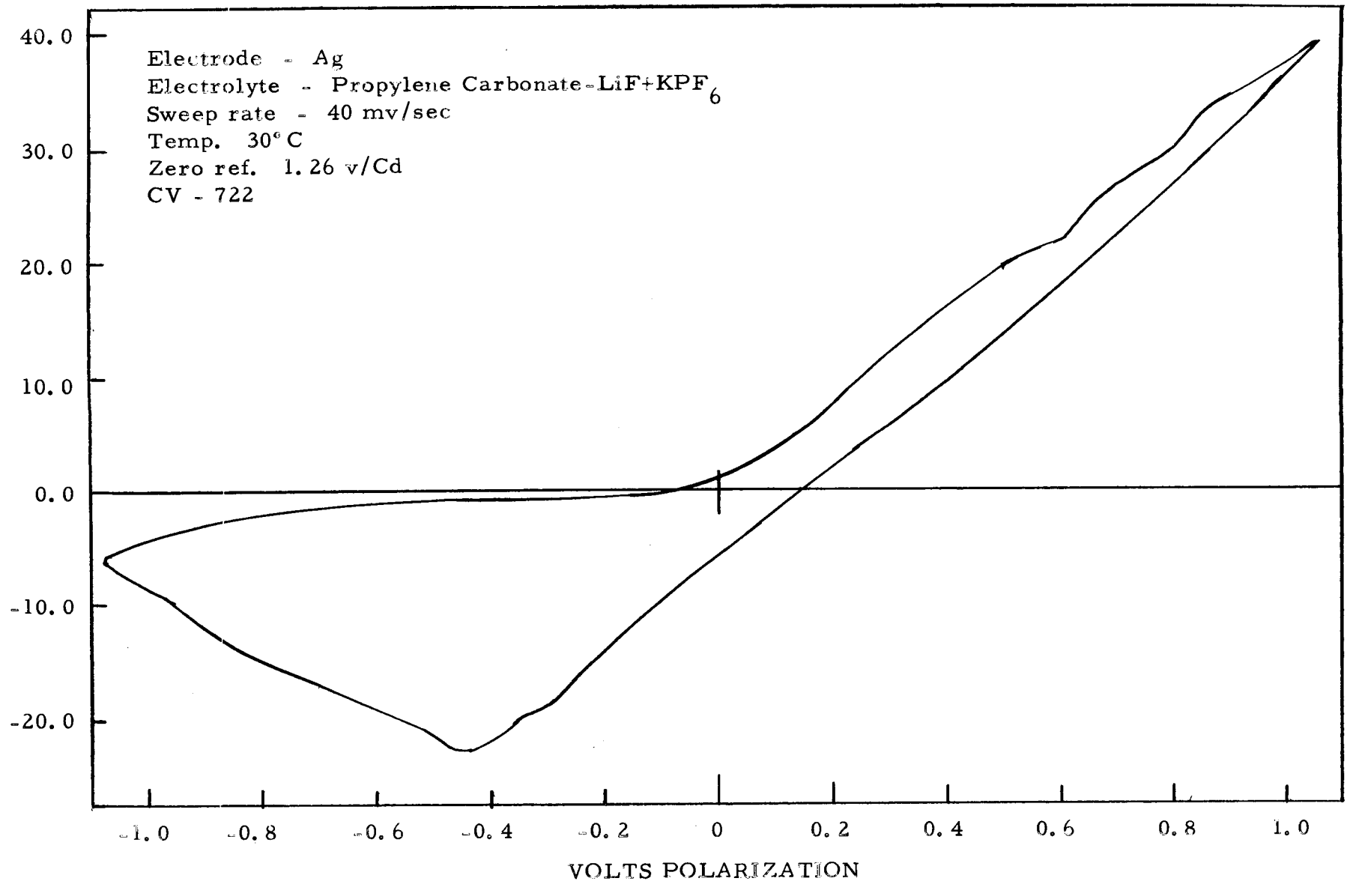
Electrode - Ag
Electrolyte - Propylene Carbonate-LiF+KPF6
Sweep rate - 40 mv/sec
Temp. 30° C
Zero ref. 1.26 v/Cd
CV - 722
40.0
30.0
20.0
10.0
0.0
-10.0
-20.0
IA
MA/CM2
IC
-1.0
-0.8
-0.6
-0.4
-0.2
0
0.2
0.4
0.6
0.8
1.0
VOLTS POLARIZATION

Figure 40

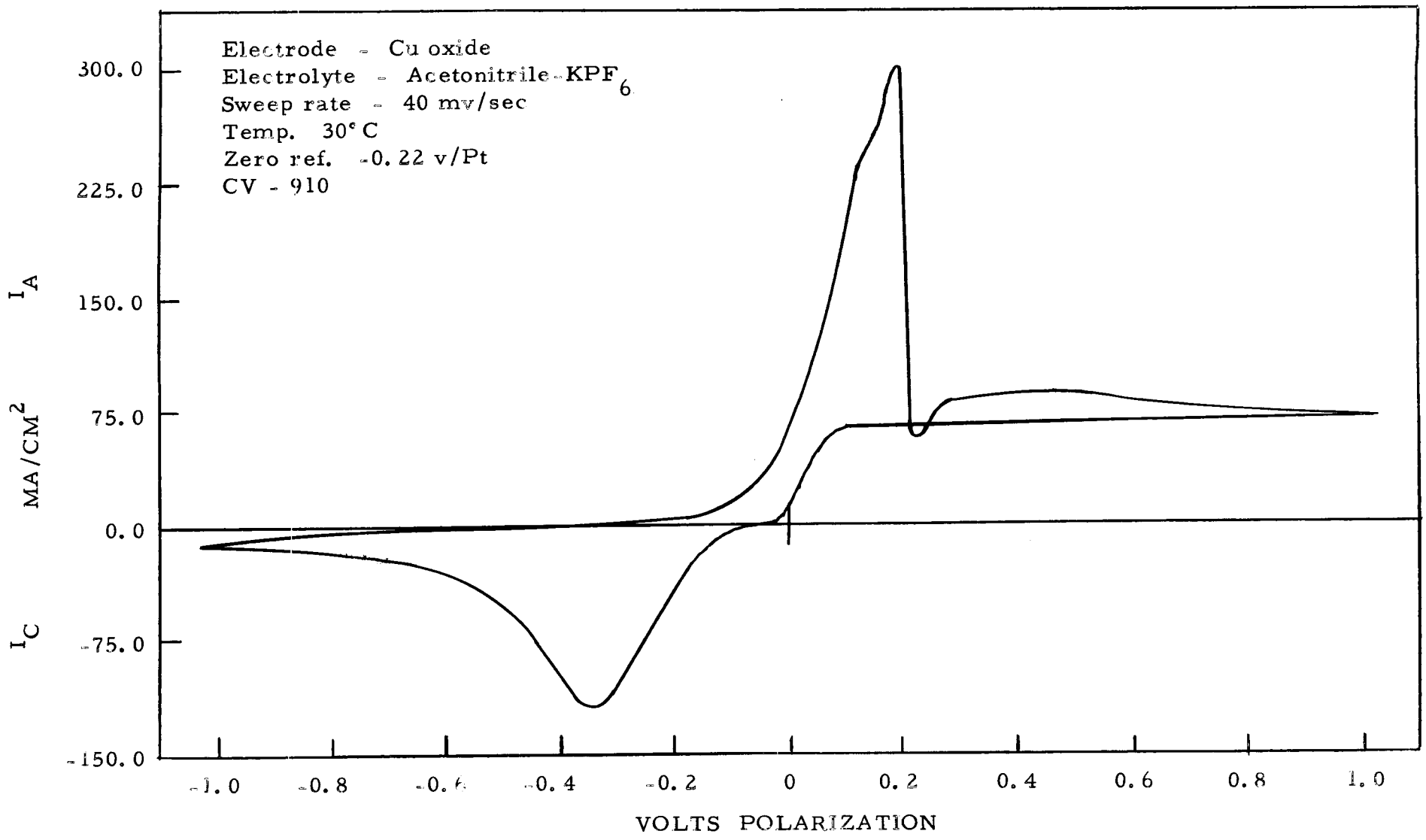
Electrode - Cu oxide
Electrolyte - Acetonitrile-KPF_6
Sweep rate - 40 mv/sec
Temp. 30° C
Zero ref. -0.22 v/Pt
CV - 910
300.0
225.0
150.0
75.0
0.0
-75.0
-150.0
I_A
MA/CM^2
I_C
-1.0
-0.8
-0.6
-0.4
-0.2
0
0.2
0.4
0.6
0.8
1.0
VOLTS POLARIZATION

Figure 41

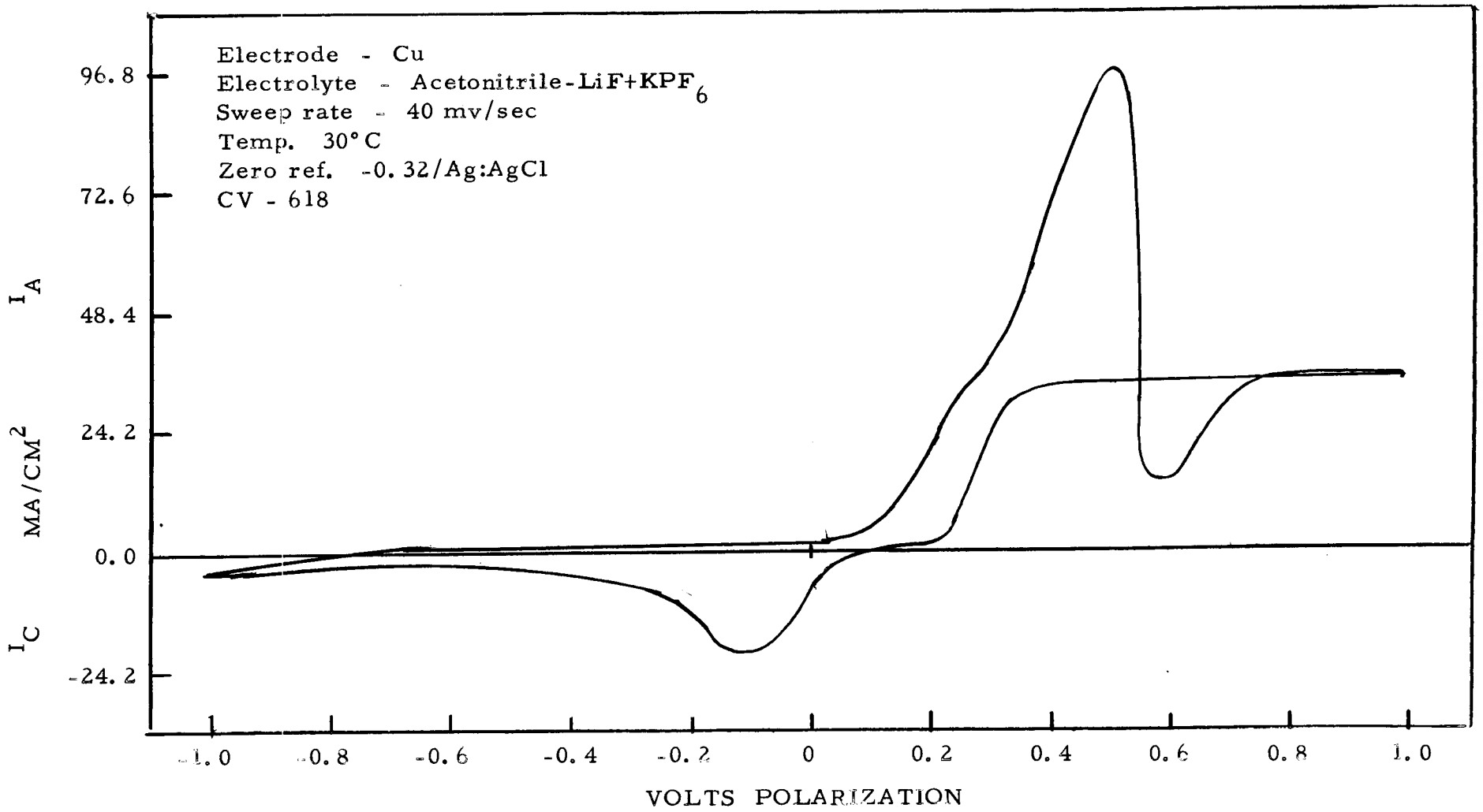
Electrode - Cu
Electrolyte - Acetonitrile-LiF+KPF6
Sweep rate - 40 mv/sec
Temp. 30° C
Zero ref. -0.32/Ag:AgCl
CV - 618
96.8
72.6
48.4
24.2
0.0
-24.2
IA
MA/CM2
IC
-1.0
-0.8
-0.6
-0.4
-0.2
0
0.2
0.4
0.6
0.8
1.0
VOLTS POLARIZATION

FIGURE 42

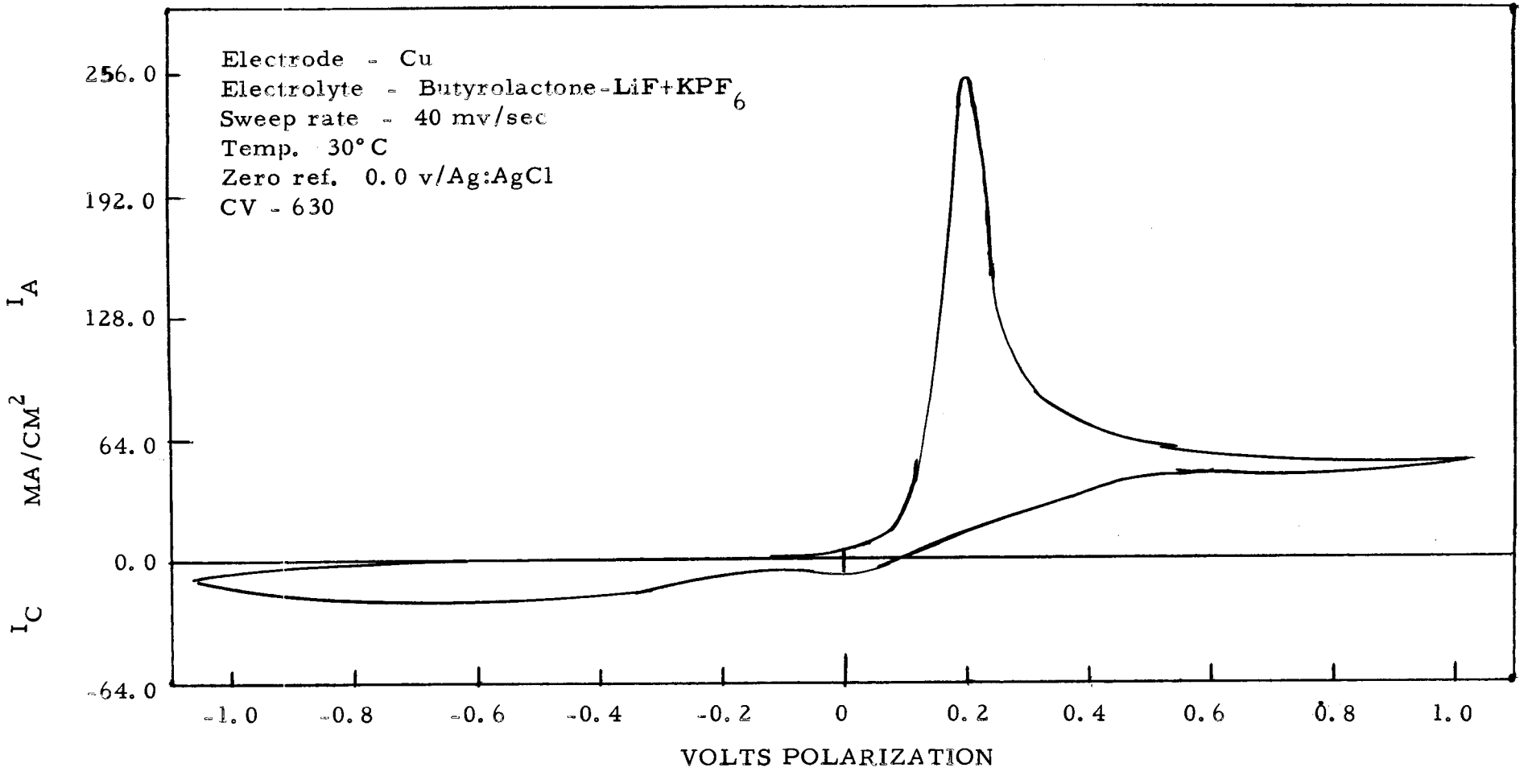
Electrode - Cu
Electrolyte - Butyrolactone-LiF+KPF6
Sweep rate - 40 mv/sec
Temp. 30° C
Zero ref. 0.0 v/Ag:AgCl
CV - 630
256.0
192.0
128.0
64.0
0.0
-64.0
IA
MA/CM2
IC
-1.0
-0.8
-0.6
-0.4
-0.2
0
0.2
0.4
0.6
0.8
1.0
VOLTS POLARIZATION

Figure 43

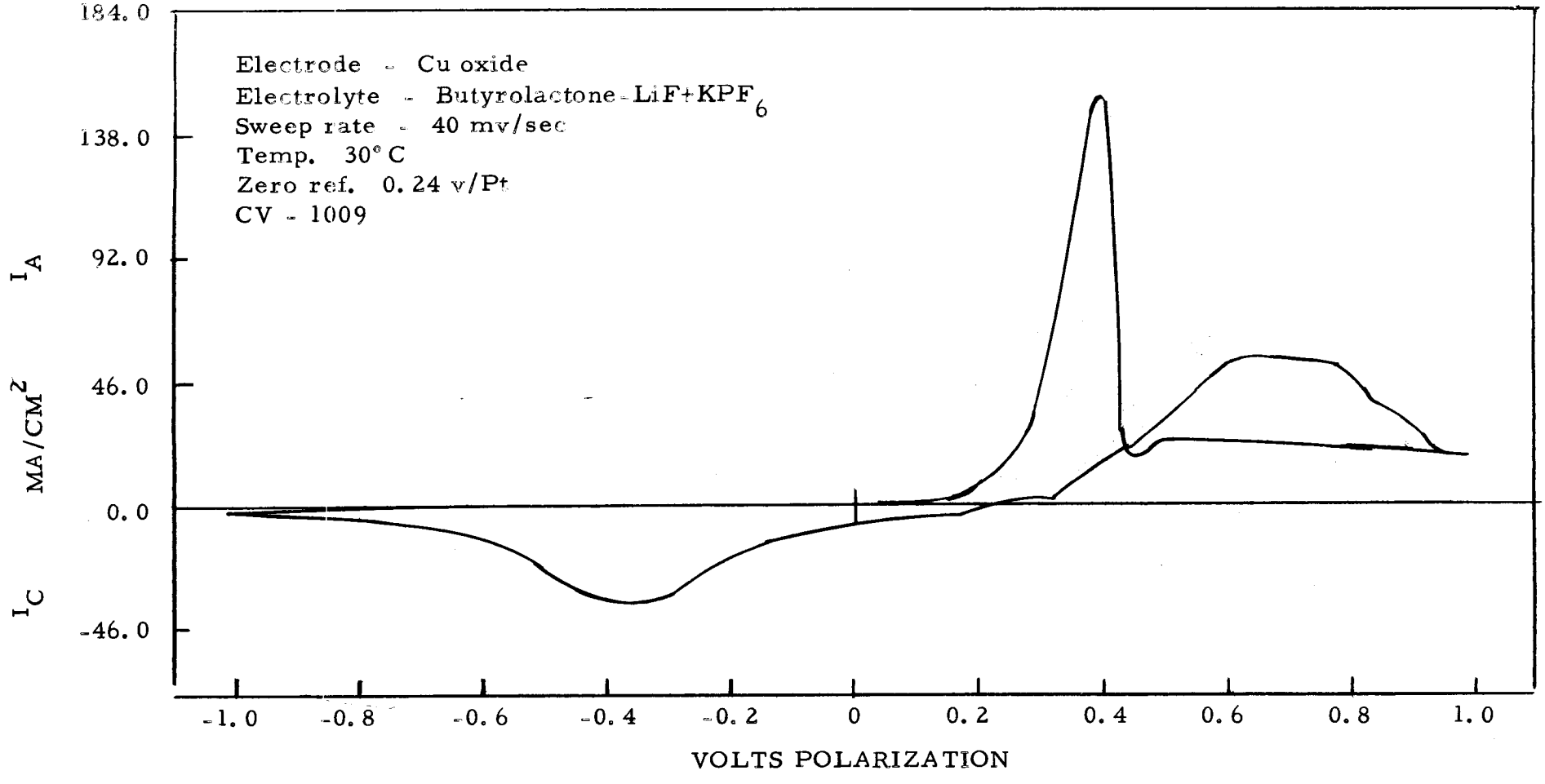
184.0
138.0
92.0
46.0
0.0
-46.0
Electrode - Cu oxide
Electrolyte - Butyrolactone-LiF+KPF6
Sweep rate - 40 mv/sec
Temp. 30° C
Zero ref. 0.24 v/Pt
CV - 1009
IA
MA/CM2
IC
-1.0
-0.8
-0.6
-0.4
-0.2
0
0.2
0.4
0.6
0.8
1.0
VOLTS POLARIZATION

Figure 44

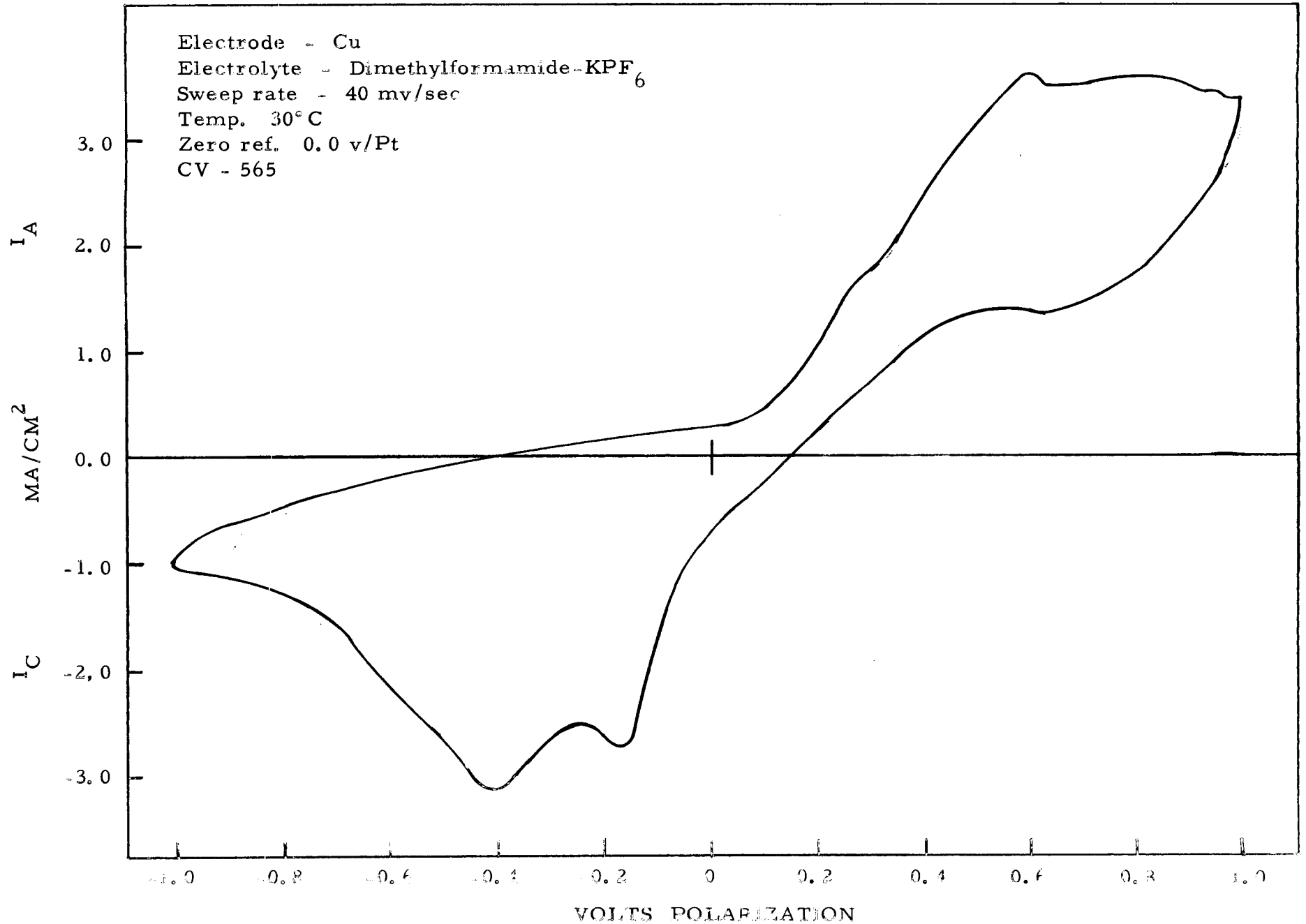
Electrode - Cu
Electrolyte - Dimethylformamide-KPF_6
Sweep rate - 40 mv/sec
Temp. 30° C
Zero ref. 0.0 v/Pt
CV - 565
3.0
2.0
1.0
0.0
-1.0
-2.0
-3.0
I_A
I_C
MA/CM^2
-1.0
-0.8
-0.6
-0.4
-0.2
0
0.2
0.4
0.6
0.8
1.0
VOLTS POLARIZATION

Figure 45

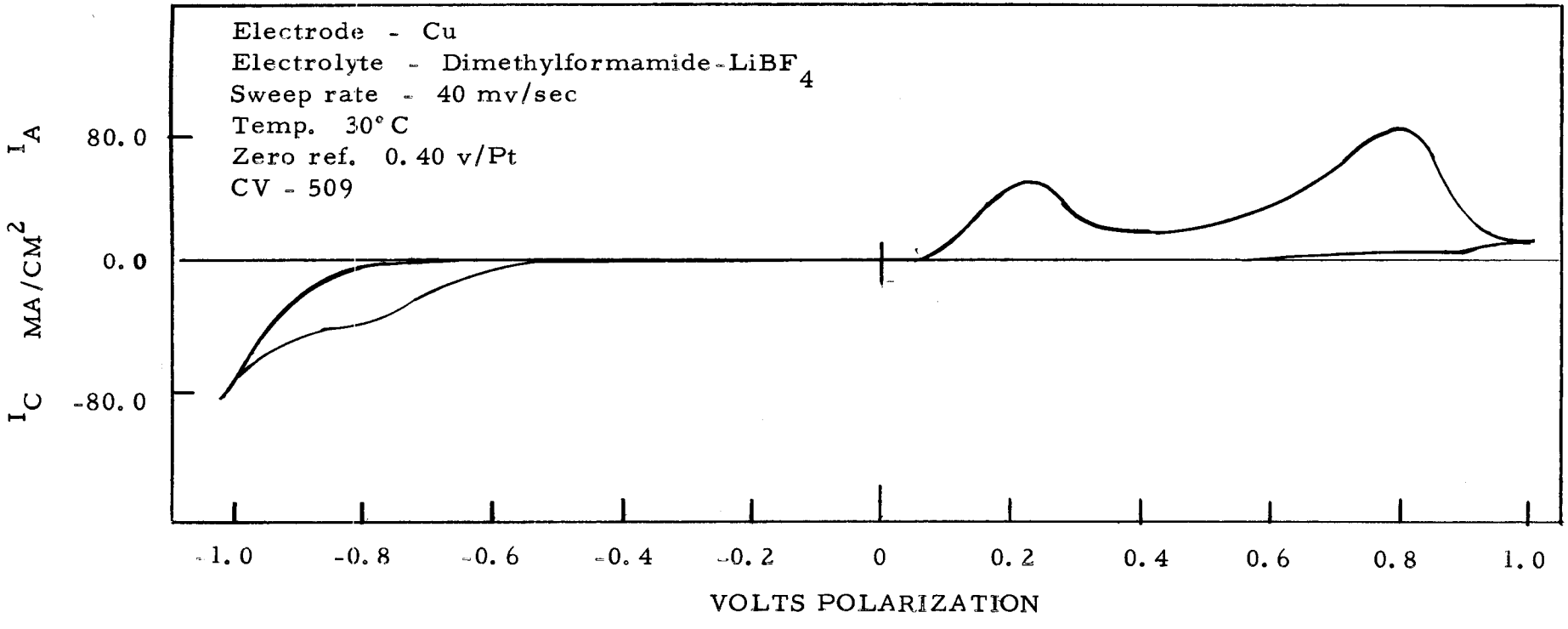
Electrode - Cu
Electrolyte - Dimethylformamide-LiBF4
Sweep rate - 40 mv/sec
Temp. 30° C
Zero ref. 0.40 v/Pt
CV - 509
IA
80.0
0.0
IC MA/CM2
-80.0
-1.0
-0.8
-0.6
-0.4
-0.2
0
0.2
0.4
0.6
0.8
1.0
VOLTS POLARIZATION

Figure 46

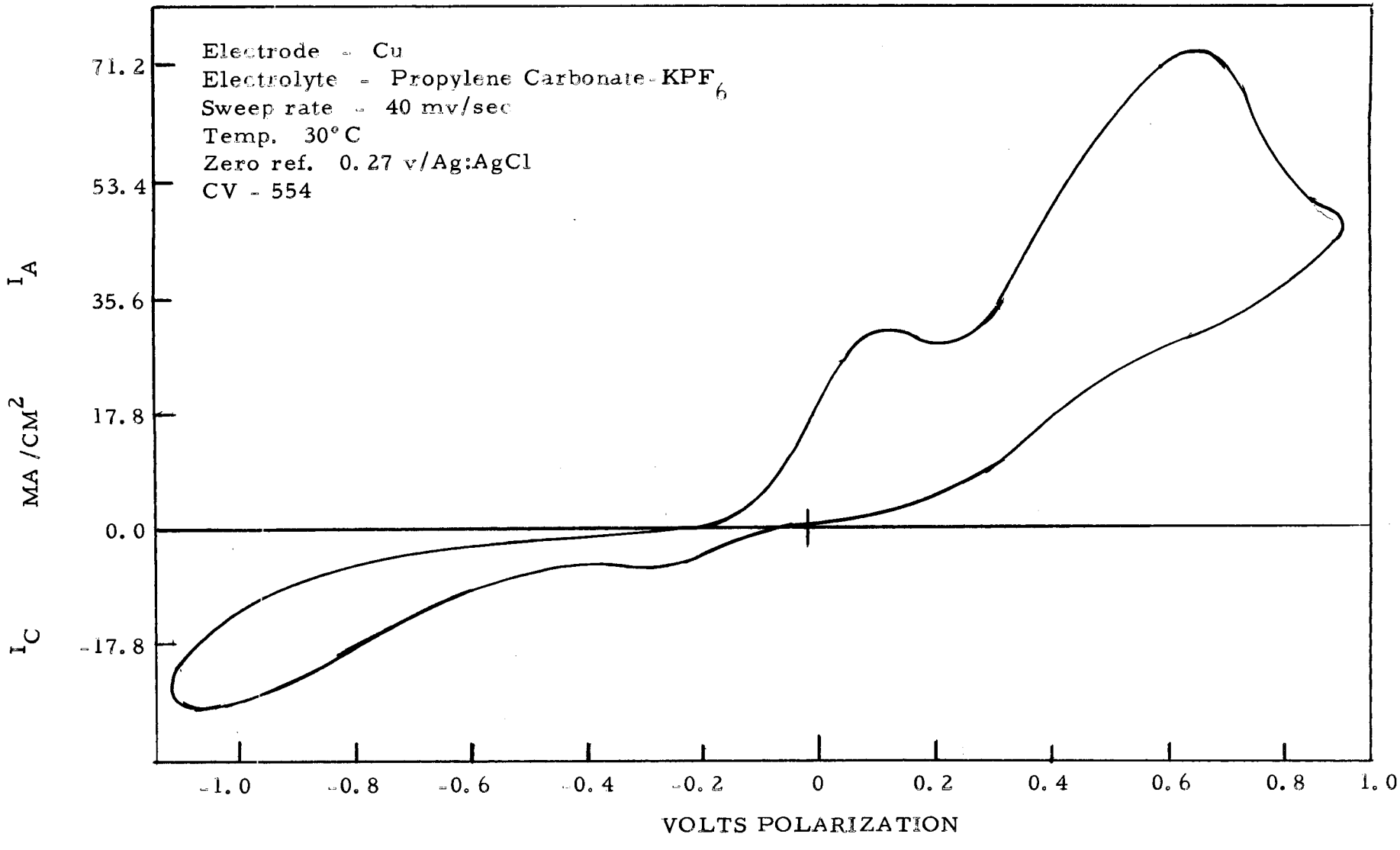
Electrode - Cu
Electrolyte - Propylene Carbonate-KPF_6
Sweep rate - 40 mv/sec
Temp. 30° C
Zero ref. 0.27 v/Ag:AgCl
CV - 554
71.2
53.4
35.6
17.8
0.0
-17.8
I_A
MA /CM^2
I_C
-1.0
-0.8
-0.6
-0.4
-0.2
0
0.2
0.4
0.6
0.8
1.0
VOLTS POLARIZATION

Figure 47

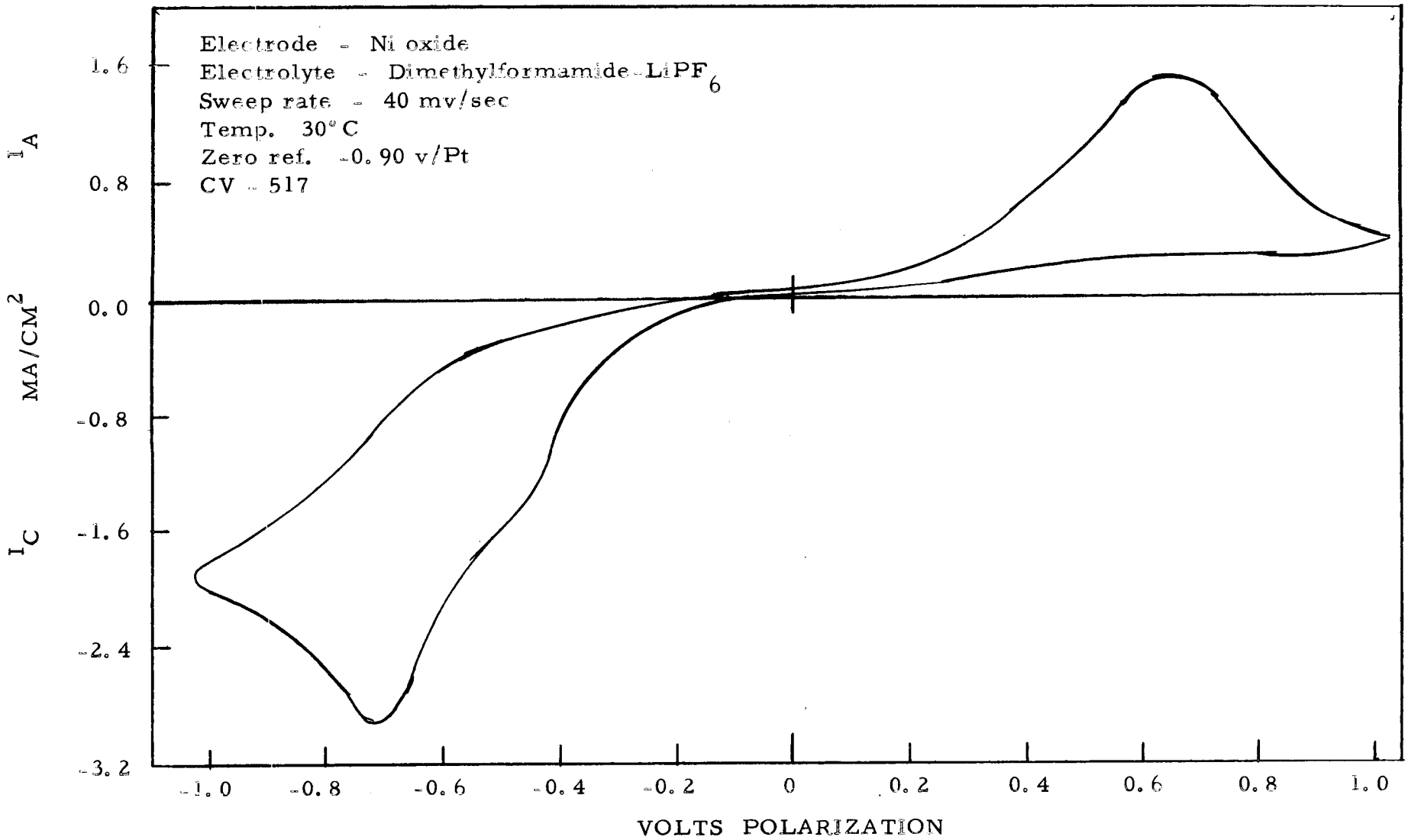
Electrode - Ni oxide
Electrolyte - Dimethylformamide-LiPF6
Sweep rate - 40 mv/sec
Temp. 30° C
Zero ref. -0.90 v/Pt
CV - 517
1.6
0.8
0.0
-0.8
-1.6
-2.4
-3.2
IA
MA/CM2
IC
-1.0
-0.8
-0.6
-0.4
-0.2
0
0.2
0.4
0.6
0.8
1.0
VOLTS POLARIZATION

Figure 48

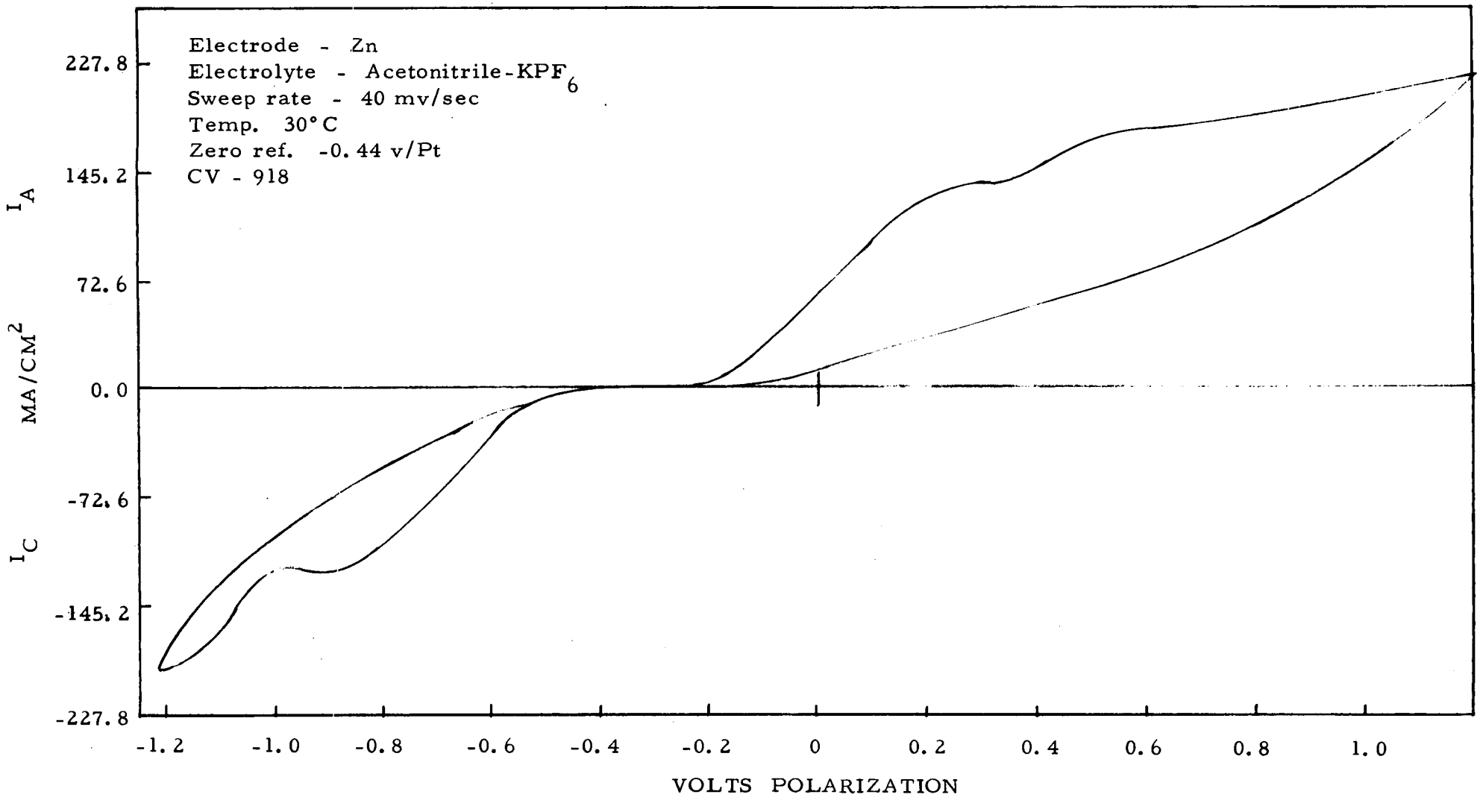
Electrode - Zn
Electrolyte - Acetonitrile-KPF6
Sweep rate - 40 mv/sec
Temp. 30° C
Zero ref. -0.44 v/Pt
CV - 918
227.8
145.2
72.6
0.0
-72.6
-145.2
-227.8
IA
MA/CM2
IC
-1.2
-1.0
-0.8
-0.6
-0.4
-0.2
0
0.2
0.4
0.6
0.8
1.0
VOLTS POLARIZATION

Figure 49

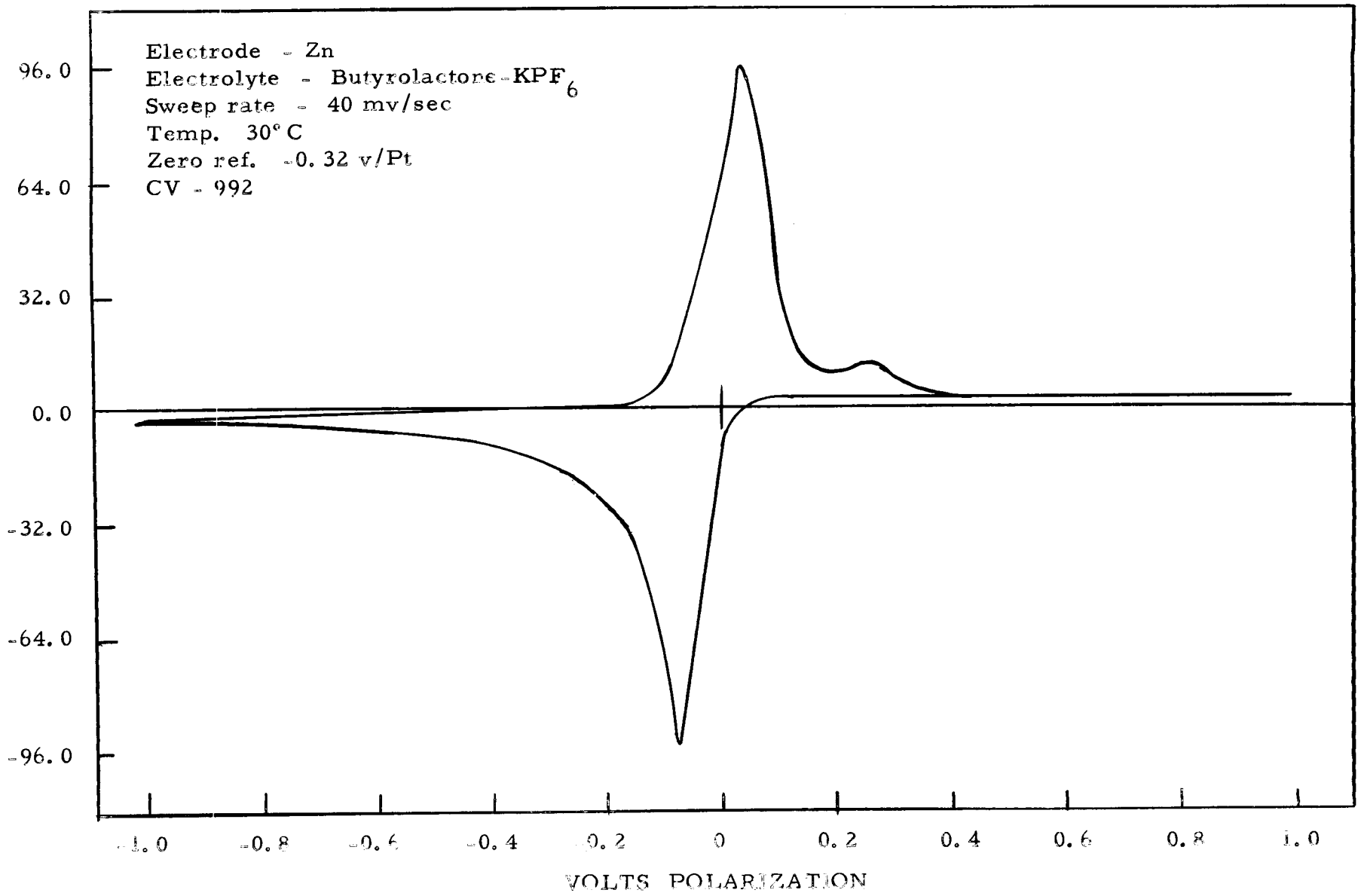
Electrode - Zn
Electrolyte - Butyrolactone-KPF_6
Sweep rate - 40 mv/sec
Temp. 30° C
Zero ref. -0.32 v/Pt
CV - 992
96.0
64.0
32.0
0.0
-32.0
-64.0
-96.0
I_A
I_C
MA/CM^2
-1.0
-0.8
-0.6
-0.4
-0.2
0
0.2
0.4
0.6
0.8
1.0
VOLTS POLARIZATION

F ( )

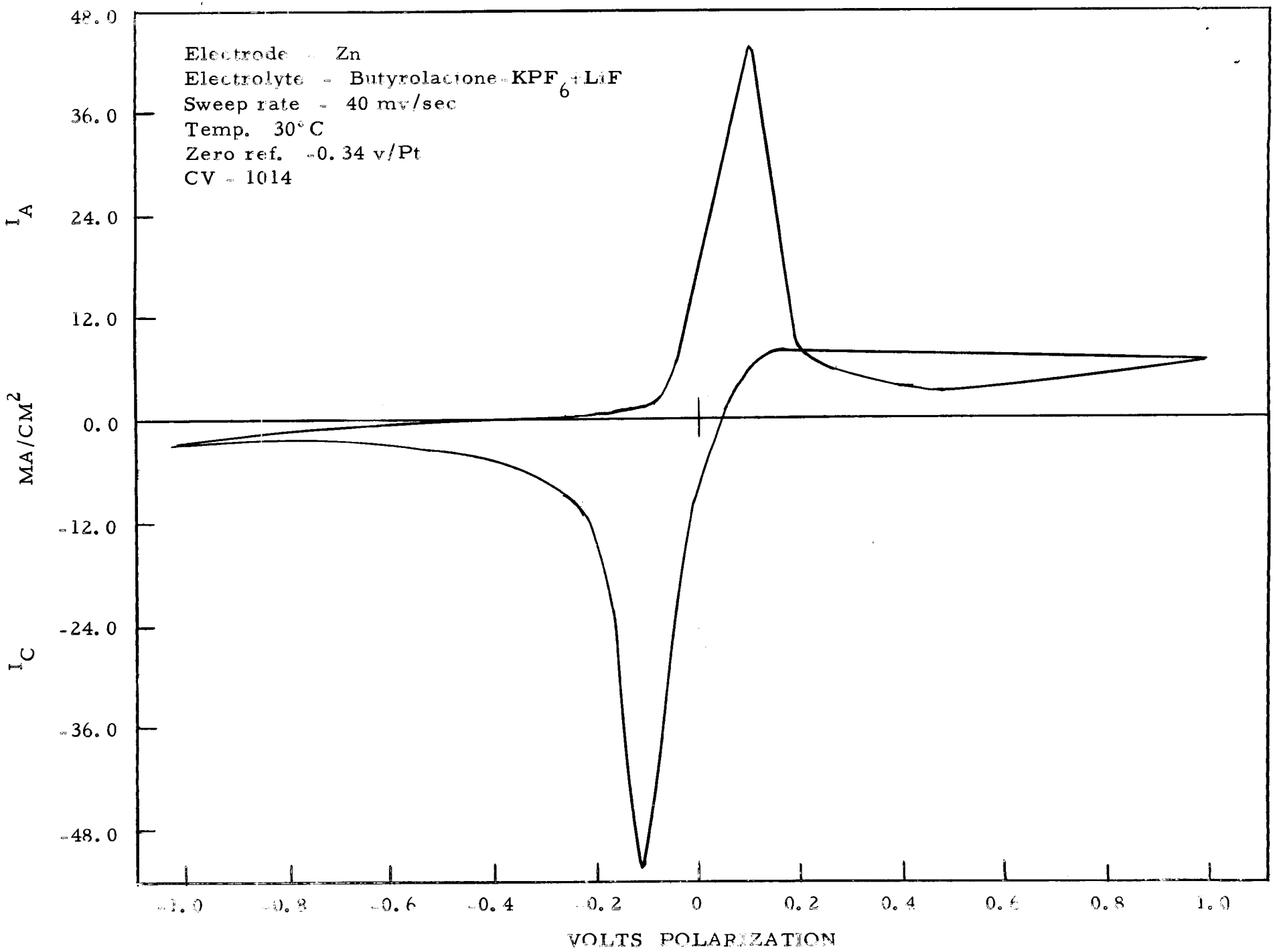
Electrode - Zn
Electrolyte - Butyrolacione-KPF_6+LiF
Sweep rate - 40 mv/sec
Temp. 30° C
Zero ref. -0.34 v/Pt
CV - 1014
48.0
36.0
24.0
12.0
0.0
-12.0
-24.0
-36.0
-48.0
I_A
MA/CM^2
I_C
-1.0
-0.8
-0.6
-0.4
-0.2
0
0.2
0.4
0.6
0.8
1.0
VOLTS POLARIZATION

Figure 5

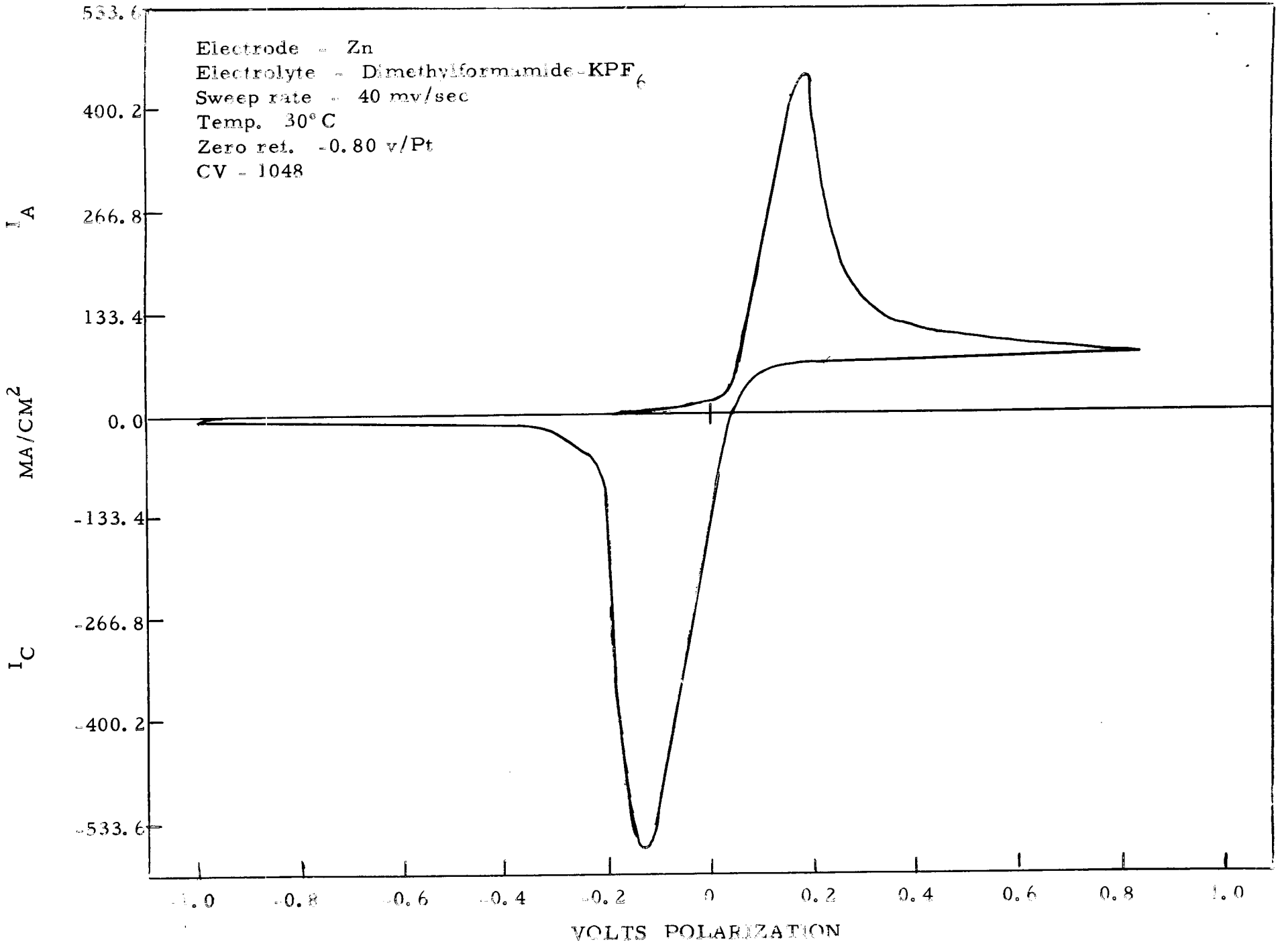
Electrode - Zn
Electrolyte - Dimethylformamide-KPF_6
Sweep rate - 40 mv/sec
Temp. 30° C
Zero ref. -0.80 v/Pt
CV - 1048
533.6
400.2
266.8
133.4
0.0
-133.4
-266.8
-400.2
-533.6
I_A
MA/CM^2
I_C
-1.0
-0.8
-0.6
-0.4
-0.2
0
0.2
0.4
0.6
0.8
1.0
VOLTS POLARIZATION

Figure 52

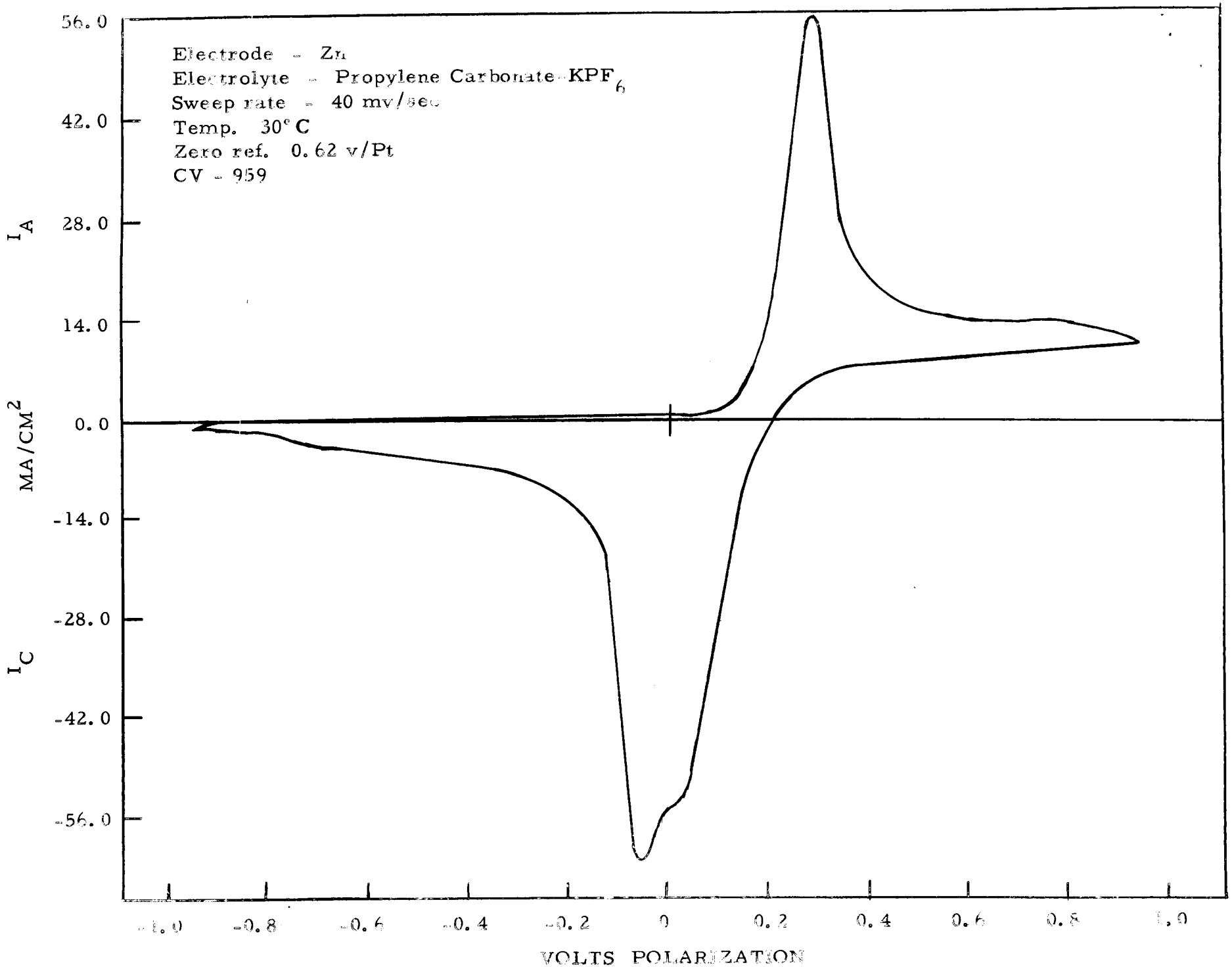
Electrode - Zn
Electrolyte - Propylene Carbonate KPF6
Sweep rate - 40 mv/sec
Temp. 30° C
Zero ref. 0.62 v/Pt
CV - 959
56.0
42.0
28.0
14.0
0.0
-14.0
-28.0
-42.0
-56.0
IA
IC
MA/CM2
-1.0
-0.8
-0.6
-0.4
-0.2
0
0.2
0.4
0.6
0.8
1.0
VOLTS POLARIZATION

Figure 33

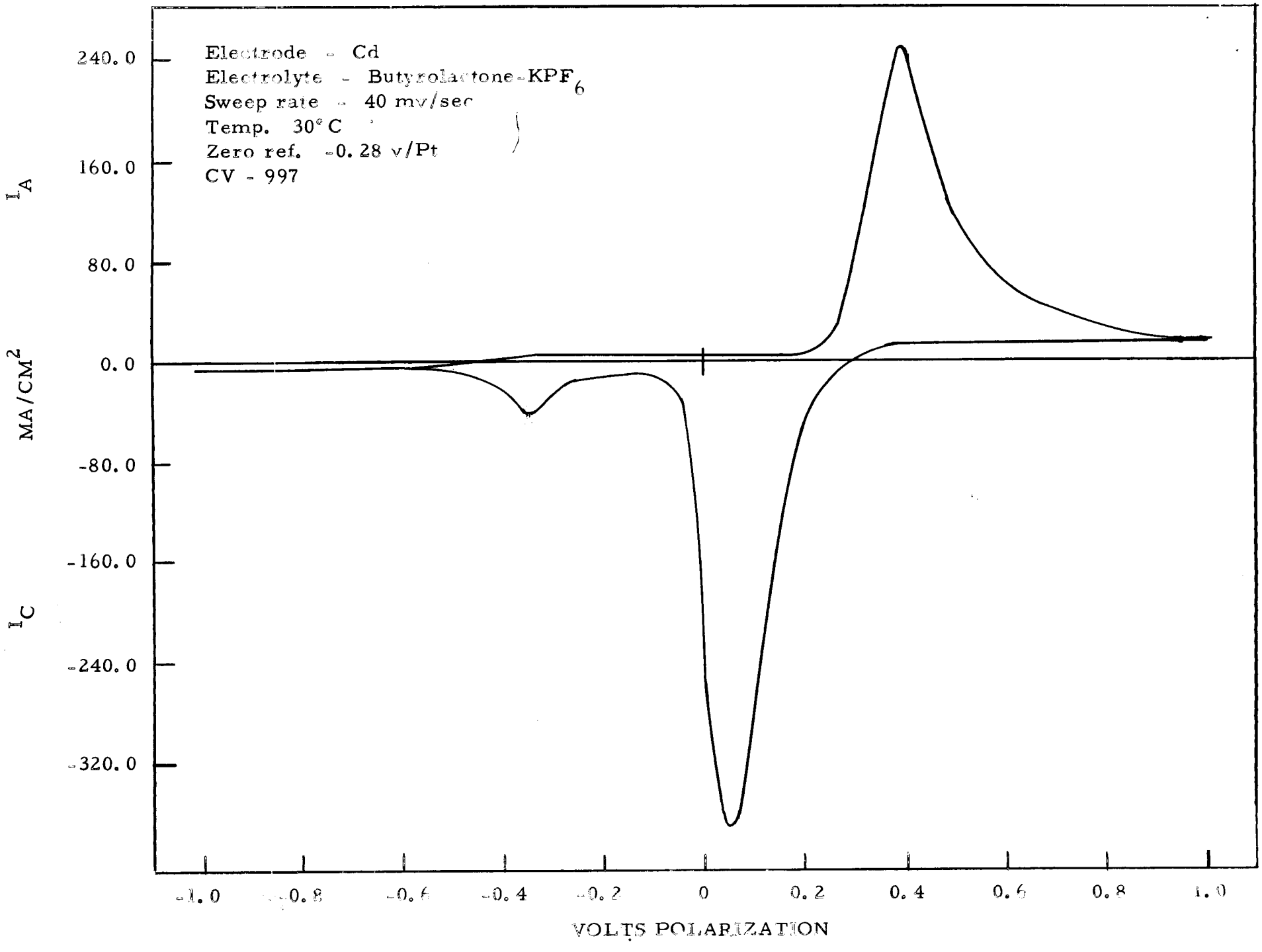
Electrode - Cd
Electrolyte - Butyrolactone-KPF_6
Sweep rate - 40 mv/sec
Temp. 30° C
Zero ref. -0.28 v/Pt
CV - 997
240.0
160.0
80.0
0.0
-80.0
-160.0
-240.0
-320.0
I_A
MA/CM^2
I_C
-1.0
-0.8
-0.6
-0.4
-0.2
0
0.2
0.4
0.6
0.8
1.0
VOLTS POLARIZATION

Figure 54

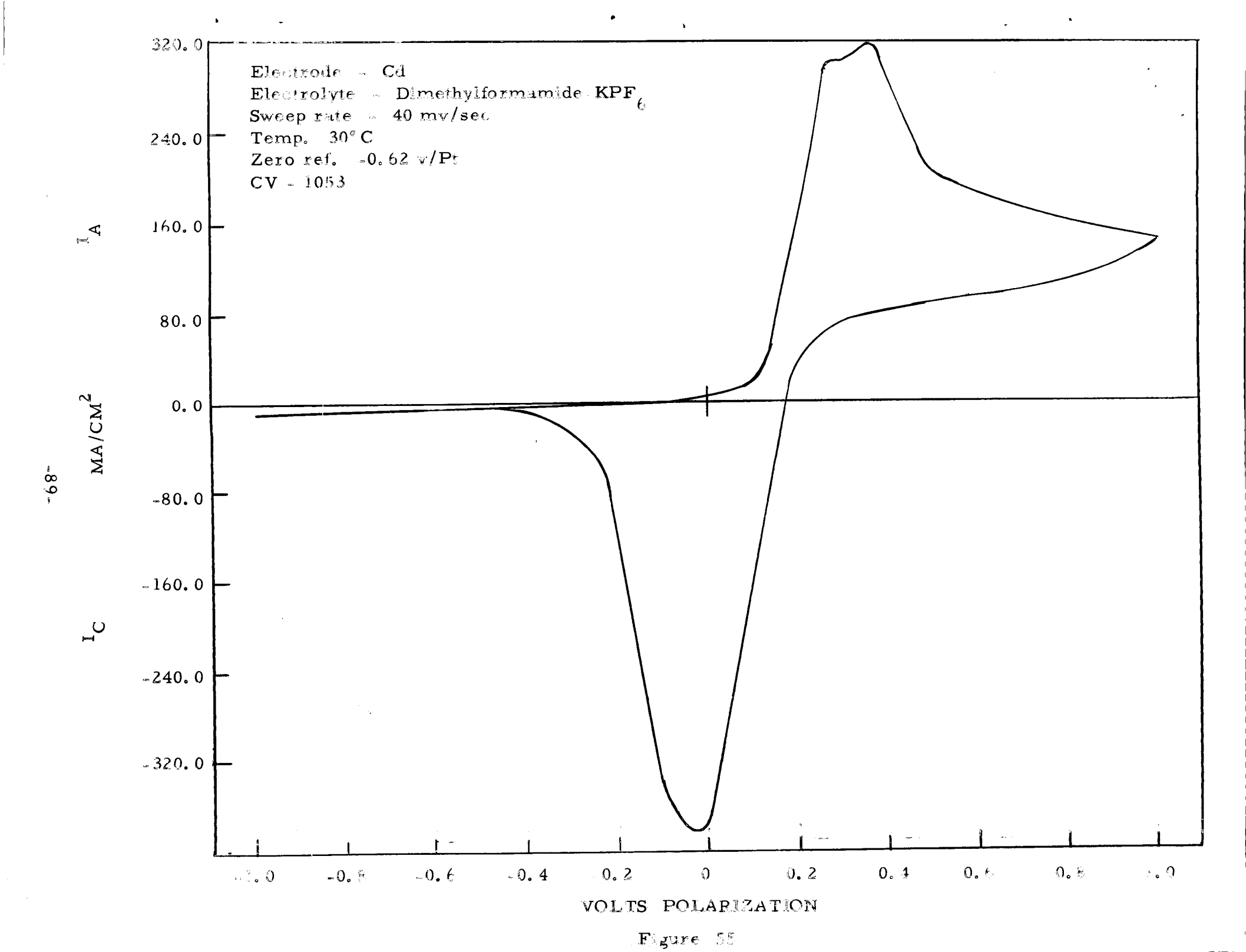
Electrode - Cd
Electrolyte - Dimethylformamide KPF_6
Sweep rate - 40 mv/sec
Temp. 30° C
Zero ref. -0.62 v/Pt
CV - 1053
320.0
240.0
160.0
80.0
0.0
-80.0
-160.0
-240.0
-320.0
I_A
MA/CM^2
I_C
-0.4
0.2
0
0.2
0.4
VOLTS POLARIZATION

Figure 55

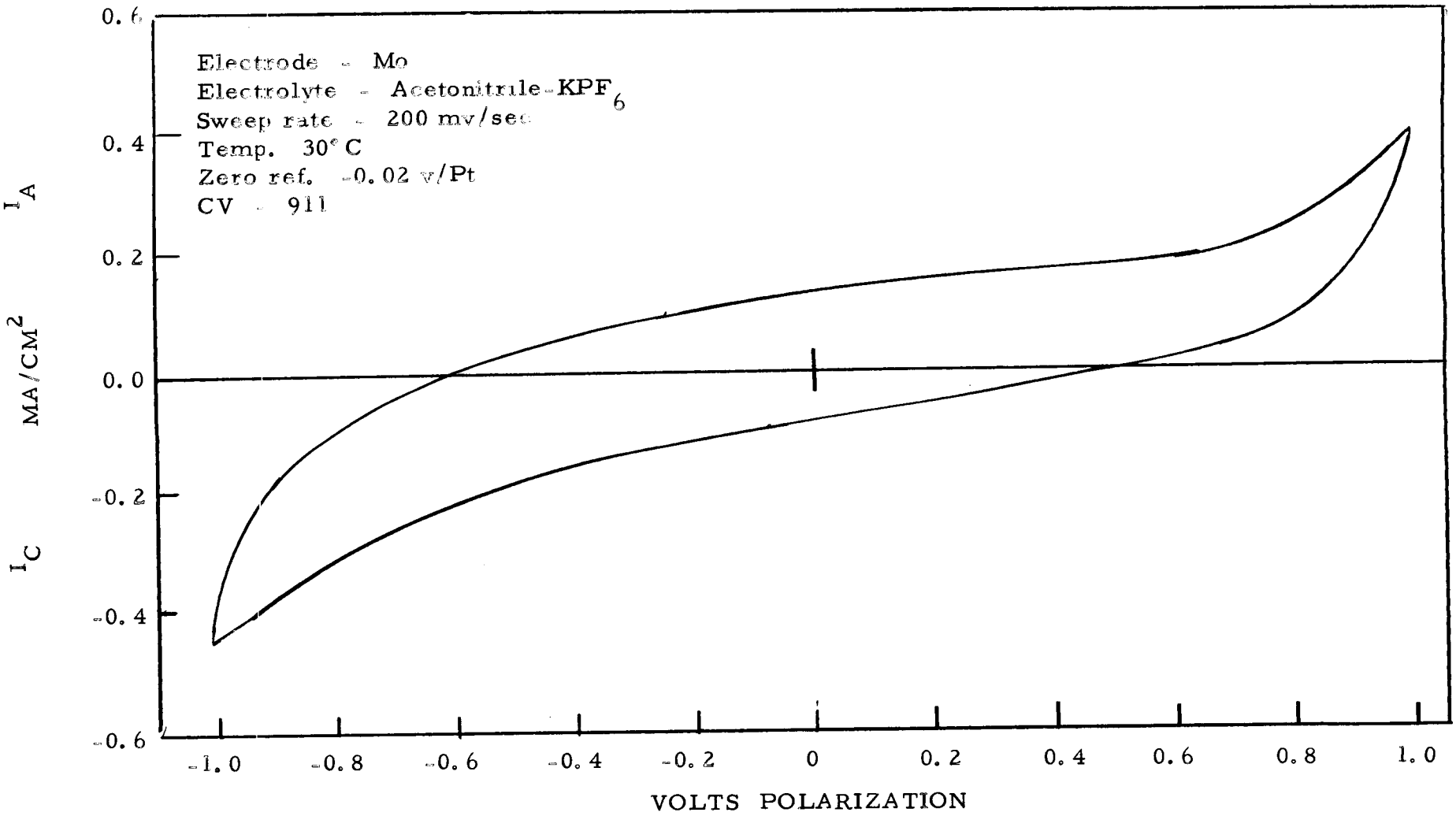
Electrode - Mo
Electrolyte - Acetonitrile-KPF_6
Sweep rate - 200 mv/sec
Temp. 30° C
Zero ref. -0.02 v/Pt
CV - 911
0.6
0.4
0.2
0.0
-0.2
-0.4
-0.6
I_A
I_C
MA/CM^2
-1.0
-0.8
-0.6
-0.4
-0.2
0
0.2
0.4
0.6
0.8
1.0
VOLTS POLARIZATION

Figure 56

C. TABLES OF CYCLIC VOLTAMMETRIC DATA

Included in this section are tables listing parameters derived from the cyclic voltammograms. These parameters are as follows:

1. Sweep index

This is a relative figure of merit taking into account peak height, sweep rate, and discharge capacity. The magnitude of the sweep index is a sensitive function of activation polarization. This parameter is described in more detail in an earlier report (Ref. 1, p. 80).

2. Current density magnitude

3. Cathode reaction type

Described as to whether the reduction reaction involves a dissolved species, or a solid state material formed during the anodic portion of the sweep.

4. Cathode stability

A measure of degree of solubility of the cathode material relative to the cycling time, and hence the sweep rate.

5. Discharge capacity

Amount of cathode material converted per unit area of electrode.

6. Charge-discharge efficiency

Ratio of discharge coulombs to charge coulombs.

7. ΔV_p

Distance between anodic and cathodic peaks in volts, giving a measure of overall electrode reversibility, or in more practical terms, a measure of suitability of the electrochemical system for secondary battery application.

TABLE VI

ANODIC PEAK CURRENT DENSITY AND SWEEP INDEX
CHLORIDE ELECTROLYTES

Systems	Peak Current Density Magnitude	Sweep Index* $ohm^{-1} cm^{-2}$
Ag/Acetonitrile-LiCl	Medium Low	3.2
Ag/Butyrolactone-$AlCl_3$	High	48.2
Ag/Butyrolactone-$MgCl_2$	Medium High	19.0
Ag/Butyrolactone-$MgCl_2$+LiCl	Medium Low	7.1
Ag/Butyrolactone-$LiClO_4$+LiCl	High	-
AgO/Butyrolactone-LiCl+$AlCl_3$	Very High	82.4
AgO/Butyrolactone-$LiClO_4$	Very High	40.2
AgO/Dimethylformamide-LiCl+$AlCl_3$	Medium Low	18.8
Ag/Propylene Carbonate-$MgCl_2$	Medium Low	4.7
Ag/Propylene Carbonate-$MgCl_2$+LiCl	Medium Low	5.5
Ag/Propylene Carbonate-$LiClO_4$	Medium High	-
CuO/Butyrolactone-$LiClO_4$	High	37.6
Cu/Butyrolactone-$LiClO_4$+$AlCl_3$	High	75.3
Cu/Dimethylformamide-LiCl	High	23.2
CuO/Dimethylformamide-LiCl	High	49.6
CuO/Dimethylformamide-LiCl+$AlCl_3$	High	-
Cu/Dimethylformamide-$LiClO_4$+LiCl	High	41.0
Ni/Butyrolactone-$LiClO_4$+LiCl	Medium Low	3.6
Ni/Dimethylformamide-$MgCl_2$+LiCl	Medium Low	6.4

* Relative figure of merit defined as $\frac{(\text{peak c.d.})^2 \times 100}{\text{sweep rate} \times \text{coulombs/cm}^2}$

TABLE VII

CATHODIC PEAK CURRENT DENSITY AND SWEEP INDEX
CHLORIDE ELECTROLYTES

Systems	Peak Current Density Magnitude	Sweep Index * $ohm^{-1} cm^{-2}$
Ag/Acetonitrile-LiCl	Medium Low	8.0
Ag/Butyrolactone-$AlCl_3$	High	76.8
Ag/Butyrolactone-$MgCl_2$	Medium High	21.5
Ag/Butyrolactone-$MgCl_2$+LiCl	Medium Low	9.6
Ag/Butyrolactone-$LiClO_4$+LiCl	High	79.0
AgO/Butyrolactone-LiCl+$AlCl_3$	Very High	594.0
AgO/Butyrolactone-$LiClO_4$	Very High	40.2
AgO/Dimethylformamide-LiCl+$AlCl_3$	High	119.6
Ag/Propylene Carbonate-$MgCl_2$	Medium Low	4.9
Ag/Propylene Carbonate-$MgCl_2$+LiCl	Medium Low	11.2
Ag/Propylene Carbonate-$LiClO_4$	High	
CuO/Butyrolactone-$LiClO_4$	High	27.0
Cu/Butyrolactone-$LiClO_4$+$AlCl_3$	Medium Low	11.4
Cu/Dimethylformamide-LiCl	Medium Low	3.0
CuO/Dimethylformamide-LiCl	Medium High	102.0
CuO/Dimethylformamide-LiCl+$AlCl_3$	Very High	735.2
Cu/Dimethylformamide-$LiClO_4$+LiCl	High	56.9
Ni/Butyrolactone-$LiClO_4$+LiCl	Medium Low	6.8

* See Table VI

TABLE VIII

ANODIC PEAK CURRENT DENSITY AND SWEEP INDEX
FLUORIDE ELECTROLYTES

Systems	Peak Current Density Magnitude	Sweep Index * $ohm^{-1} cm^{-2}$
AgO/Acetonitrile-KPF_6	Very High	30.3
AgO/Acetonitrile-KPF_6+LiF	Very High	151.5
Ag/Dimethylformamide-$LiBF_4$	Low	86.6
AgO/Propylene Carbonate-KPF_6	High	22.8
CuO/Acetonitrile-KPF_6	High	51.6
CuO/Acetonitrile-KPF_6+LiF	High	61.5
Cu/Butyrolactone-MgF_2	High	-
CuO/Butyrolactone-KPF_6	High	22.0
CuO/Butyrolactone-KPF_6+LiF	High	46.2
NiO/Dimethylformamide-$LiPF_6$	Low	0.2
Zn/Butyrolactone-KPF_6	Medium High	47.7
Zn/Butyrolactone-KPF_6+LiF	Medium Low	15.7
Zn/Dimethylformamide-KPF_6	Very High	95.8
Zn/Propylene Carbonate-KPF_6	Medium High	14.1
Cd/Butyrolactone-KPF_6	High	84.2
Cd/Butyrolactone-KPF_6+LiF	Medium High	19.1
Cd/Dimethylformamide-KPF_6	High	26.1

* See Table VI

TABLE IX

CATHODIC PEAK CURRENT DENSITY AND SWEEP INDEX
FLUORIDE ELECTROLYTES

Systems	Peak Current Density Magnitude	Sweep Index * $ohm^{-1} cm^{-2}$
AgO/Acetonitrile-KPF_6	High	24.3
AgO/Acetonitrile-KPF_6+LiF	Very High	175.8
Ag/Dimethylformamide-$LiBF_4$	Medium Low	42.1
AgO/Propylene Carbonate-KPF_6	High	40.7
CuO/Acetonitrile-KPF_6	High	36.2
CuO/Acetonitrile-KPF_6+LiF	Medium High	13.0
Cu/Butyrolactone-MgF_2	Medium Low	
CuO/Butyrolactone-KPF_6	Medium High	16.3
CuO/Butyrolactone-KPF_6+LiF	Medium Low	8.7
NiO/Dimethylformamide-$LiPF_6$	Low	0.4
Zn/Butyrolactone-KPF_6	Medium High	42.0
Zn/Butyrolactone-KPF_6+LiF	Medium High	22.6
Zn/Dimethylformamide-KPF_6	Very High	332.9
Zn/Propylene Carbonate-KPF_6	Medium High	22.4
Cd/Butyrolactone-KPF_6	Very High	193.7
Cd/Butyrolactone-KPF_6+LiF	Medium High	29.4
Cd/Dimethylformamide-KPF_6	Very High	107.4

* See Table VI

TABLE X

CATHODE REACTION TYPE AND COMPATIBILITY
SILVER IN CHLORIDE ELECTROLYTES

System	Cathodic Reaction	Cathode Stability
Ag/Acetonitrile-LiCl	Solid State	Insoluble
Ag/Butyrolactone-$AlCl_3$	Solid State	Insoluble
Ag/Butyrolactone-$MgCl_2$	Solid State	Insoluble
Ag/Butyrolactone-$MgCl_2$+LiCl	Solid State	Insoluble
Ag/Butryolactone-$LiClO_4$+LiCl	Solid State	Insoluble
Ag/Butryolactone-$LiClO_4$+$AlCl_3$	Solid State	Insoluble
Ag/Dimethylformamide-LiCl	Solid State	Insoluble
Ag/Dimethylformamide-LiCl+$AlCl_3$	Solid State	Insoluble
Ag/Dimethylformamide-$MgCl_2$	Solid State	Insoluble
Ag/Dimethylformamide-$MgCl_2$+LiCl	Solid State	Insoluble
Ag/Dimethylformamide-$LiClO_4$	Solid State	Soluble
Ag/Propylene Carbonate-$MgCl_2$	Solid State	Insoluble
Ag/Propylene Carbonate-$MgCl_2$+LiCl	Solid State	Insoluble
AgO/Acetonitrile-$LiClO_4$	Solid State	Soluble
AgO/Butyrolactone-LiCl	Solid State	Insoluble
AgO/Butyrolactone-LiCl+$AlCl_3$	Solid State	Insoluble
AgO/Butyrolactone -$LiClO_4$	Dissolved Species	Soluble
AgO/Dimethylformamide-LiCl+$AlCl_3$	Solid State	Insoluble
AgO/Dimethylformamide-$LiClO_4$+$AlCl_3$	Dissolved Species	Soluble
AgO/Propylene Carbonate-$LiClO_4$	Solid State	Insoluble

TABLE XI

CATHODE REACTION TYPE AND COMPATIBILITY
SILVER IN FLUORIDE ELECTROLYTES

System	Cathodic Reaction	Cathode Stability
Ag/Acetonitrile-KPF_6	Solid State	Insoluble
Ag/Acetonitrile-KPF_6 + 1000 ppm H_2O	Solid State	Soluble
AgO/Acetonitrile-KPF_6	Solid State	Soluble
Ag/Acetonitrile-KPF_6+LiF	Solid State	Insoluble
AgO/Acetonitrile-KPF_6+LiF	Solid State	Soluble
Ag/Butyrolactone-MgF_2	Solid State	Insoluble
Ag/Butyrolactone-MgF_2+LiF	Solid State	Insoluble
Ag/Butyrolactone-KPF_6	Solid State	Soluble
AgO/Butyrolactone-KPF_6	--	Soluble
Ag/Butyrolactone-KPF_6+LiF	Solid State	Soluble
AgO/Butyrolactone-KPF_6+LiF	--	Soluble
Ag/Dimethylformamide-KPF_6	Solid State	Soluble
AgO/Dimethylformamide-KPF_6	Solid State	Soluble
Ag/Dimethylformamide-KPF_6+LiF	Solid State	Soluble
Ag/Dimethylformamide-$LiBF_4$	Solid State	Soluble
Ag/Propylene Carbonate-KPF_6	Solid State	Soluble
AgO/Propylene Carbonate-KPF_6	--	Soluble

TABLE XII

CATHODE REACTION TYPE AND COMPATIBILITY
COPPER IN CHLORIDE ELECTROLYTES

System	Cathodic Reaction	Cathode Stability
Cu/Acetonitrile-$AlCl_3$	Solid State	Soluble
CuO/Acetonitrile-$LiClO_4$	Solid State	Insoluble
Cu/Butyrolactone-$AlCl_3$	Solid State	Soluble
CuO/Butyrolactone-$LiCl+AlCl_3$	Solid State	Insoluble
Cu/Butyrolactone-$MgCl_2$	Solid State	Insoluble
Cu/Butyrolactone-$MgCl_2$+LiCl	Solid State	Soluble
Cu/Butyrolactone-$LiClO_4+AlCl_3$	Solid State	Soluble
Cu/Dimethylformamide-LiCl	Solid State	Soluble
CuO/Dimethylformamide-LiCl	Solid State	Soluble
CuO/Dimethylformamide-$LiCl+AlCl_3$	Dissolved Species	Soluble
Cu/Dimethylformamide-$MgCl_2$	Solid State	Soluble
Cu/Dimethylformamide-$MgCl_2$+LiCl	Solid State	Soluble
Cu/Dimethylformamide-$LiClO_4$	Dissolved Species	Soluble
CuO/Dimethylformamide-$LiClO_4$	Dissolved Species	Soluble
Cu/Dimethylformamide-$LiClO_4$+LiCl	Dissolved Species	Soluble
Cu/Dimethylformamide-$LiClO_4+AlCl_3$	Solid State	Soluble
Cu/Propylene Carbonate-$MgCl_2$+LiCl	Solid State	Soluble
Cu/Propylene Carbonate-$LiClO_4$	Solid State	Insoluble
CuO/Propylene Carbonate-$LiClO_4$	Solid State	Insoluble

TABLE XIII

CATHODE REACTION TYPE AND COMPATIBILITY
COPPER IN FLUORIDE ELECTROLYTES

System	Cathodic Reaction	Cathode Stability
Cu/Acetonitrile-KPF_6	Solid State	Insoluble
CuO/Acetonitrile-KPF_6	Solid State	Insoluble
Cu/Acetonitrile-KPF_6+LiF	Solid State	Insoluble
CuO/Acetonitrile-KPF_6+LiF	Solid State	Insoluble
Cu/Butyrolactone-MgF_2	Solid State	Soluble
Cu/Butyrolactone-MgF_2+LiF	Solid State	Insoluble
Cu/Butyrolactone-KPF_6	Solid State	Soluble
CuO/Butyrolactone-KPF_6	Solid State	Insoluble
Cu/Butyrolactone-KPF_6+LiF	Solid State	Soluble
CuO/Butyrolactone-KPF_6+LiF	Solid State	Insoluble
Cu/Dimethylformamide-KPF_6	Solid State	Insoluble
Cu/Dimethylformamide-$LiBF_4$	Solid State	Soluble
Cu/Propylene Carbonate-KPF_6	Solid State	Soluble

TABLE XIV

CATHODE REACTION TYPE AND COMPATIBILITY
ZINC, CADMIUM IN FLUORIDE ELECTROLYTES

System	Cathodic Reaction	Cathode Stability
Zn/Acetonitrile-KPF_6	Solid State	Insoluble
Zn/Butyrolactone-KPF_6	Solid State	Insoluble
Zn/Butyrolactone-KPF_6+LiF	Solid State	Insoluble
Zn/Dimethylformamide-KPF_6	Solid State	Insoluble
Zn/Propylene Carbonate-KPF_6	Solid State	Insoluble
Cd/Butyrolactone-KPF_6	Solid State	Insoluble
Cd/Butyrolactone-KPF_6+LiF	Solid State	Insoluble
Cd/Dimethylformamide-KPF_6	Solid State	Insoluble
Cd/Propylene Carbonate-KPF_6	--	Soluble

TABLE XV

ΔV_p*, CHARGE-DISCHARGE EFFICIENCY AND DISCHARGE CAPACITY
SILVER ELECTRODES

System	ΔV_p* Volt	Charge-Discharge Efficiency %	Discharge Capacity Coulomb/cm^2
Ag/Acetonitrile-LiCl	0.80	90.0	0.3
AgO/Acetonitrile-KPF_6	0.54	23.0	1.0
AgO/Butyrolactone-LiCl	1.10	67.0	0.8
AgO/Butyrolactone-LiCl+$AlCl_3$	0.23	100.0	4.4
Ag/Butyrolactone-$MgCl_2$	0.70	100.0	0.7
Ag/Butyrolactone-$MgCl_2$+LiCl	0.40	100.0	3.0
AgO/Butyrolactone-$LiClO_4$	0.98	34.4	4.1
Ag/Butyrolactone-$AlCl_3$	0.87	96.0	2.2
Ag/Butyrolactone-$LiClO_4$+LiCl	0.55	--	-
Ag/Butyrolactone-$LiClO_4$+$AlCl_3$	0.85	79.6	1.5
AgO/Dimethylformamide-LiCl+$AlCl_3$	0.02	42.6	0.3
Ag/Dimethylformamide-$LiClO_4$	0.72	--	-
AgO/Dimethylformamide-$LiClO_4$+$AlCl_3$	0.02	40.0	0.2
Ag/Propylene Carbonate-$MgCl_2$	1.10	100.0	0.7
Ag/Propylene Carbonate-$MgCl_2$+LiCl	0.93	74.0	0.3
Ag/Propylene Carbonate-$LiClO_4$	1.40	--	-
AgO/Propylene Carbonate-$LiClO_4$	--	62.8	0.1

* Voltage separating anodic and cathodic peaks.

TABLE XVI

ΔV_p*, CHARGE-DISCHARGE EFFICIENCY AND DISCHARGE CAPACITY
COPPER ELECTRODES

System	ΔV_p* Volt	Charge-Discharge Efficiency %	Discharge Capacity Coulomb/cm^2
CuO/Acetonitrile-$LiClO_4$	1.14	--	-
CuO/Acetonitrile-KPF_6+LiF	0.70	49.7	1.1
Cu/Butyrolactone-MgF_2	0.22	--	-
CuO/Butyrolactone-KPF_6	1.28	26.2	1.2
CuO/Butyrolactone-KPF_6+LiF	0.75	34.2	0.4
Cu/Butyrolactone-$AlCl_3$	0.33	--	-
Cu/Butyrolactone-$MgCl_2$	--	10.5	-
CuO/Butyrolactone-$LiClO_4$	1.27	46.5	1.9
CuO/Butyrolactone-LiCl+$AlCl_3$	0.30	31.1	0.4
Cu/Butyrolactone-$LiClO_4$+$AlCl_3$	0.20	46.7	0.3
Cu/Dimethylformamide-LiCl	0.50	6.9	0.1
CuO/Dimethylformamide-LiCl	0.30	6.7	-
CuO/Dimethylformamide-LiCl+$AlCl_3$	0.17	--	-
CuO/Dimethylformamide-$LiClO_4$+LiCl	0.25	28.4	0.9
Cu/Dimethylformamide-$LiClO_4$+$AlCl_3$	0.23	8.2	4.2
Cu/Propylene Carbonate-$LiClO_4$	1.30	--	-
CuO/Propylene Carbonate-$LiClO_4$	0.39	100.0	0.6

* Voltage separating anodic and cathodic peaks.

TABLE XVII

ΔV_p*, CHARGE-DISCHARGE EFFICIENCY AND DISCHARGE CAPACITY ZINC, CADMIUM IN FLUORIDE ELECTROLYTES

System	ΔV_p* Volt	Charge-Discharge Efficiency %	Discharge Capacity Coulomb/cm^2
Zn/Acetonitrile-KPF_6	1.20	--	-
Zn/Butyrolactone-KPF_6	0.13	100.0	0.5
Zn/Butyrolactone-KPF_6+LiF	0.24	--	-
Zn/Dimethylformamide-KPF_6	0.32	48.3	2.4
Zn/Propylene Carbonate-KPF_6	0.34	74.1	0.4
Cd/Butyrolactone-KPF_6	0.34	94.7	1.7
Cd/Butyrolactone-KPF_6+LiF	0.27	--	-
Cd/Dimethylformamide-KPF_6	0.40	49.9	2.8
Cd/Propylene Carbonate-KPF_6	0.70	--	-

* Voltage separating anodic and cathodic peaks.

II. EXPERIMENTAL

A. MATERIAL PURIFICATION AND CHARACTERIZATION

1. Distillation of Solvents

With the exception of propylene carbonate, the solvents were distilled as previously described. Although initially a single distillation had sufficed for the purification of propylene carbonate, this method did not suffice for the purification of later quantities. It was found that water apparently reached a constant level in all fractions obtained in the distillation. Since it was known that the distillation procedure was capable of removing water originally present, it was suspected that an impurity was present in the propylene carbonate which slowly decomposed under the distillation conditions, yielding water as one of the products. Therefore, following the first distillation, the main cuts of propylene carbonate were dried over calcium sulfate, filtered, and carefully redistilled. This procedure afforded propylene carbonate of reproducible purity.

2. Solution Preparation

All materials were stored after drying in closed containers in a glove bag under nitrogen. All manipulation of solvents and solutes was accomplished in a controlled atmosphere chamber under nitrogen. Where necessary, cooling was furnished by a cold-finger which was flame-dried and positioned in the exterior wall of the controlled atmosphere chamber. The flask containing the solvent was positioned around the cold-finger while coolant was added externally. Usually, the rate of addition of solute was controlled so as to maintain the temperature in the solution flask at -5° to 10° C.

In order to facilitate repetitive preparation of solutions for the screening of various electrodes, the method of solution preparation was altered. (Ref. 1)

The procedure used during this period involved the initial mixing of solvent and solute in a proportion so as to yield a 0.5 m solution. If the solute was insufficiently soluble, the solution was allowed to stand overnight, filtered, and the conductivity determined. If the solute was soluble, an increment of solute (sufficient to bring the solution to 0.75 m) was added and the conductivity redetermined. If the conductivity had not changed by 0.5×10^{-n} ohm^{-1} cm^{-1} (n being the same order as that in the initial conductivity measurements) the solution was filtered and used at this concentration for the cyclic voltammetry procedure. If the conductance changed by more than 0.5×10^{-n} ohm^{-1} cm^{-1}, the incremental addition procedure was repeated until the change in conductivity was less than 0.5×10^{-n} ohm^{-1} cm^{-1}.

Conductance measurements during this period were not thermostatted. Ambient temperature in the controlled atmosphere chamber varied between 22 to 28° C. A recirculating gas heating system capable of maintaining the temperature at 30 ± 1° C has been recently installed in the controlled atmosphere chamber.

3. Electrode Preparation

Copper oxide electrodes were prepared by heating copper wire in a vycor tube at 200° C for 20 minutes. Following this, the materials were allowed to cool and then stored under nitrogen. In the case of nickel, it was necessary to heat for 60 minutes at 300° C in order to prepare the oxide.

Silver oxide was prepared at room temperature by electrolytic oxidation at 2.0 ma/cm^2 in a 30% potassium hydroxide solution. After the reaction was completed, the oxidized electrode was washed with water, air dried, and finally dried under vacuum at ambient temperature.

B. CYCLIC VOLTAMMETRIC MEASUREMENTS

A detailed description of the instrumentation, measuring cell, and measurement procedure, is thoroughly described in the First Quarterly Report (Ref. 1). During the present quarter some changes were made in the measurement procedure. Cyclic voltammograms are now obtained at 200, 80, and 40 mv/sec. As before, triplicate measurements are made using a fresh electrode and fresh sample of solution each time. Measurements were made as before in a thermostatted both at 30° C.

The primary modification during this period was the change to an improved measuring cell. The chief modification was the introduction of a notched luggin capillary, for the purpose of reproducible positioning of the working electrode. The new cell is also equipped with a ground glass ball-joint connection for the working electrode compartment of the cell. The ball-joint facilitates the positioning of the electrode into the luggin capillary notch, and the joint clamp holds the electrode rigidly in place during the measurements.

The reproducibility of cyclic voltammograms obtained using the new cell has been significantly improved. This has been brought about by decreasing the working electrode - reference electrode distance to an absolute minimum, and by reproducing this distance for every determination. Any lack of reproducibility in the curves can now be safely attributed to the changing electrode surface of the more soluble electrode materials, this being more pronounced at the lowest sweep rate.

III. REFERENCES

1. Whittaker Corporation, Narmco Research and Development Division, First Quarterly Report, NASA Contract NAS 3-8509, NASA Report CR-72069, August 1966.

2. J. Mitchell and O. Smith, Aquametry, Interscience Publishers, Inc., New York, New York (1948).

DISTRIBUTION LIST

National Aeronautics and Space Admin.
Washington, D. C. 20546
Attn: E. M. Cohn/RNW
A. M. Greg Andrus/PC

National Aeronautics and Space Admin.
Goddard Space Flight Center
Greenbelt, Maryland 20771
Attn: T. Hennigan, Code 716.2
J. Sherfey, Code 735
P. Donnelly, Code 636.2
E. R. Stroup, Code 636.2

National Aeronautics and Space Admin.
Langley Research Center
Instrument Research Division
Hampton, Virginia 23365
Attn: J. L. Patterson, MS 234
M. B. Seyffert, MS 112

National Aeronautics and Space Admin.
Langley Research Center
Langley Station
Hampton, Virginia 23365
Attn: S. T. Peterson
Harry Ricker

National Aeronautics and Space Admin.
Lewis Research Center
21000 Brookpark Road
Cleveland, Ohio 44135
Attn: Library, MS 60-3
N. D. Sanders, MS 302-1
John E. Dilley, MS 500-309
B. Lubarsky, MS 500-201
H. J. Schwartz, MS 500-201
R. B. King, MS 500-202
V. F. Hlavin, MS 3-14 (Final only)
M. J. Saari, MS 500-202
J. J. Weber, MS 3-19
Report Control, MS 5-5
S. Fordyce, MS 302-1

National Aeronautics and Space Admin.
Scientific and Technical Information Facility
P. O. Box 33
College Park, Maryland 20740
Attn: Acquisitions Branch (SQT-34054)
(2 cys. + 1 repro.)

National Aeronautics and Space Admin.
George C. Marshall Space Flight Center
Huntsville, Alabama 35812
Attn: Philip Youngblood
R. Boehme, Bldg. 4487-BB,
M-ASTR-EC

National Aeronautics and Space Admin.
Manned Spacecraft Center
Houston, Texas 77058
Attn: W. R. Dusenbury, Propulsion and
Energy Systems
R. Cohen, Gemini Project Office
R. Ferguson (EP-5)
J. T. Kennedy (EE-5)
F. E. Eastman (EE-4)

National Aeronautics and Space Admin.
Ames Research Center
Pioneer Project
Moffett Field, California 94035
Attn: J. R. Swain
A. S. Hertzog
J. Rubenzer, Biosatellite Project

Jet Propulsion Laboratory
4800 Oak Grove Drive
Pasadena, California 91103
Attn: A. Uchiyama

U. S. Army Engineer R and D Labs.
Fort Belvoir, Virginia 22060
Attn: Electrical Power Branch, SMOFB-EP

Commanding Officer
U. S. Army Electronics R and D Labs.
Fort Monmouth, New Jersey 07703
Attn: Power Sources Div., Code SELRA/PS

Research Office
R and D Directorate
Army Weapons Command
Rock Island, Illinois 61201
Attn: G. Riensmith, Chief

U. S. Army Research Office
Box CM, Duke Station
Durham, North Carolina 27706
Attn: Dr. W. Jorgensen

U. S. Army Research Office
Chief, R and D
Department of the Army
3 D 442, The Pentagon
Washington, D. C. 20546

Harry Diamond Laboratories
Room 300, Bldg. 92
Conn. Ave. and Van Ness St., NW
Washington, D. C. 20438
Attn: N. Kaplan

Army Materiel Command
Research Division
AMCRD-RSCM-T-7
Washington, D. C. 20315
Attn: J. W. Crellin

Army Materiel Command
Development Division
AMCRD-DE-MO-P
Washington, D. C. 20315
Attn: M. D. Aiken

U. S. Army TRECOM
Fort Eustis, Virginia 23604
Attn: Dr. R. L. Echols (SMOFE-PSG)
L. M. Bartone (SMOFE-ASE)

U. S. Army Mobility Command
Research Division
Warren, Michigan 48090
Attn: O. Renius (AMSMO-RR)

U. S. Army R and L Liaison Group (9851 DV)
APO 757
New York, New York 10004
Attn: B. R. Stein

Natick Laboratories
Clothing and Organic Materials Division
Natick, Massachusetts 01760
Attn: N. Fertman

Office of Naval Research
Department of the Navy
Washington, D. C. 20360
Attn: Head, Power Branch, Code 429
H. W. Fox, Code 425

Naval Research Laboratory
Washington, D. C. 20390
Attn: Dr. J. C. White, Code 6160

U. S. Navy
Marine Engineering Laboratory
Annapolis, Maryland 21402
Attn: J. H. Harrison

Bureau of Naval Weapons
Department of the Navy
Washington, D. C. 20360
Attn: W. T. Beatson, Code RAAE-52
M. Knight, Code RAAE-50

Naval Ammunition Depot
Crane, Indiana 47522
Attn: E. Bruess
H. Schultz

Naval Ordnance Laboratory
Department of the Navy
Corona, California 91720
Attn: W. C. Spindler, Code 441

Naval Ordnance Laboratory
Department of the Navy
Silver Springs, Maryland 20900
Attn: P. B. Cole, Code WB

Bureau of Ships
Department of the Navy
Washington, D. C. 20360
Attn: B. B. Rosenbaum, Code 340
C. F. Viglotti, Code 660

Space Systems Division
Los Angeles AF Station
Los Angeles, California 90045
Attn: SSSD

Air Force Cambridge Research Lab.
L. G. Hanscom Field
Bedford, Massachusetts 01731
Attn: Commander (CRO)

Flight Vehicle Power Branch
Aero Propulsion Laboratory
Wright-Patterson AFB, Ohio 45433
Attn: J. E. Cooper

Headquarters, USAF (AFRDR-AS)
Washington, D. C. 20546
Attn: Maj. G. Starkey
Lt. Col. W. G. Alexander

Rome Air Development Center, ESD
Griffis AF Base, New York 13442
Attn: F. J. Mollura (RASSM)

National Bureau of Standards
Washington, D. C. 20234
Attn: Dr. W. J. Hamer

Office, DDR and E, USE and BSS
The Pentagon
Washington, D. C. 20310
Attn: G. B. Wareham

Army Reactors, DRD
U. S. Atomic Energy Commission
Washington, D. C. 20545
Attn: D. B. Hoatson

Institute for Defense Analyses
R and E Support Division
400 Army-Navy Drive
Arlington, Virginia 22202
Attn: R. Hamilton
Dr. G. C. Szego

U. S. Atomic Energy Commission
Auxiliary Power Branch (SNAP)
Division of Reactor Development
Washington, D. C. 20545
Attn: Lt. Col. G. H. Ogburn, Jr.

Advanced Space Reactor Branch
Division of Reactor Development
U. S. Atomic Energy Commission
Washington, D. C. 20545
Attn: Lt. Col. J. H. Anderson

Office of Technical Services
Department of Commerce
Washington, D. C. 20009

Grumman Aircraft
CPGS Plant 35
Beth Page, Long Island, New York 11101
Attn: Bruce Clark

General Electric Company
Research and Development Center
Schenectady, New York 12301
Attn: Dr. H. Liebhafsky
Dr. R. C. Osthoff, Bldg. 37, Rm 2083

General Motors-Defense Research Labs.
6767 Hollister Street
Santa Barbara, California 93105
Attn: Dr. J. S. Smatko/Dr. C. R. Russell

General Telephone and Electronics Labs.
Bayside, New York 11352
Attn: Dr. Paul Goldberg

Globe-Union, Incorporated
900 East Keefe Avenue
Milwaukee, Wisconsin 53201
Attn: Dr. Warren Towle

Gould-National Batteries, Incorporated
Engineering and Research Center
2630 University Avenue, SE
Minneapolis, Minnesota 55418
Attn: D. L. Douglas

Gulton Industries
Alkaline Battery Division
212 Durham Avenue
Metuchen, New Jersey 08840
Attn: Dr. Robert Shair

Hughes Aircraft Corporation
Centinda Avenue and Teale Street
Culver City, California 90230
Attn: T. V. Carvey

Hughes Aircraft Corporation
Building 366, MS 524
El Segundo, California 90245
Attn: R. B. Robinson

Hughes Research Labs. Corp.
3011 Malibu Canyon Road
Malibu, California 90265
Attn: T. M. Hahn

ITT Federal Laboratories
500 Washington Avenue
Nutley, New Jersey 07110
Attn: Dr. P. E. Lightly

IIT Research Institute
10 West 35 Street
Chicago, Illinois 60616
Attn: Dr. H. T. Francis

Idaho State University
Department of Chemistry
Pocatello, Idaho 83201
Attn: Dr. G. Myron Arcand

Institute of Gas Technology
State and 34 Street
Chicago, Illinois 60616
Attn: B. S. Baker

Johns Hopkins University
Applied Physics Laboratory
8621 Georgia Avenue
Silver Springs, Maryland 20910
Attn: Richard Cole

Johns-Mansville R and E. Center
P. O. Box 159
Manville, New Jersey 08835
Attn: J. S. Parkinson

Leesona Moos Laboratories
Lake Success Park, Community Drive
Great Neck, New York 11021
Attn: Dr. H. Oswin

Livingston Electronic Corporation
Route 309
Montgomeryville, Pennsylvania 18936
Attn: William F. Meyers

Lockheed Missiles and Space Co.
3251 Hanover Street
Palo Alto, California 94304
Attn: Library
Dr. G. B. Adams

Lockheed Missiles and Space Co.
Dept. 52-30
Palo Alto, California 94304
Attn: J. E. Chilton

Lockheed Missiles and Space Co.
Dept. 65-82
Palo Alto, California 94304
Attn: Larry E. Nelson

Magna Corporation
Division of TRW, Incorporated
101 South East Avenue
Anaheim, California 92805
Attn: Dr. G. Rohrbach

P. R. Mallory and Co., Incorporated
Technical Services Laboratory
Indianapolis, Indiana 46206
Attn: A. S. Doty

P. R. Mallory and Co., Incorporated
3029 East Washington Street
Indianapolis, Indiana 46206
Attn: Technical Librarian

Marquardt Corporation
16555 Saticoy Street
Van Nuys, California 91406
Attn: Dr. H. G. Krull

Material Research Corporation
Orangeburg, New York 10962
Attn: V. E. Adler

Melpar
Technical Information Center
3000 Arlington Boulevard
Falls Church, Virginia 22046

Metals and Control Division
Texas Instruments, Incorporated
34 Forest Street
Attleboro, Massachusetts 02703
Attn: Dr. E. M. Jost

Midwest Research Institute
425 Volker Boulevard
Kansas City, Missouri 64110
Attn: Dr. B. W. Beadle

Monsanto Research Corporation
Everett, Massachusetts 02149
Attn: Dr. J. O. Smith

North American Aviation, Incorporated
Rocketdyne Division
6633 Canoga Avenue
Canoga Park, California 91303
Attn: Library

North American Aviation, Incorporated
12214 Lakewood Boulevard
Downey, California 90241
Attn: Burden M. Otzinger

Dr. John Owen
P. O. Box 87
Bloomfield, New Jersey 07003

Power Information Center
University of Pennsylvania
Moore School Building
200 South 33rd Street
Philadelphia, Pennsylvania 19104

Philco Corporation
Division of the Ford Motor Company
Blue Bell, Pennsylvania 19422
Attn: Dr. Phillip Cholet

Radiation Applications, Incorporated
36-40 37th Street
Long Island City, New York 11101

Radio Corporation of America
Astro Division
Hightstown, New Jersey 08520
Attn: Seymour Winkler

Radio Corporation of America
P. O. Box 800
Princeton, New Jersey 08540
Attn: I. Schulman

Sonotone Corporation
Saw Mill River Road
Elmsford, New York 10523
Attn: A. Mundel

Texas Instruments, Incorporated
13500 North Central Expressway
Dallas, Texas 75222
Attn: Dr. Isaac Trachtenberg

Thomas A. Edison Research Laboratory
McGraw Edison Company
Watchung Avenue
West Orange, New Jersey 07052
Attn: Dr. P. F. Grieger

TRW Incorporated
TRW Systems Group
One Space Park
Redondo Beach, California 90278
Attn: Dr. A. Krausz, Bldg. 60, Rm 929
R. Sparks

TRW Incorporated
23555 Euclid Avenue
Cleveland, Ohio 44117
Attn: Librarian

Tyco Laboratories, Incorporated
Bear Hill
Hickory Drive
Waltham, Massachusetts 02154
Attn: W. W. Burnett

Union Carbide Corporation
Development Laboratory Library
P. O. Box 6056
Cleveland, Ohio 44101

Union Carbide Corporation
Parma Research Center
P. O. Box 6116
Cleveland, Ohio 44101
Attn: Library

University of California
Space Science Laboratory
Berkeley, California 94720
Attn: Dr. C. W. Tobias

University of Pennsylvania
Electrochemistry Laboratory
Philadelphia, Pennsylvania 19104
Attn: Prof. J. O'M Bockris

Western Electric Company
Suite 802, RCA Building
Washington, D. C. 20006
Attn: R. T. Fiske

Westinghouse Electric Corporation
Research and Development Center
Churchill Borough
Pittsburgh, Pennsylvania 15235
Attn: Dr. A. Langer

Whittaker Corporation
Power Sources Division
3850 Olive Street
Denver, Colorado 80237
Attn: J. W. Reiter

Whittaker Corporation
Narmco Research and Development Division
3540 Aero Court
San Diego, California 92123
Attn: Dr. M. Shaw

Yardney Electric Corporation
40-50 Leonard Street
New York, New York 10013
Attn: Dr. George Dalin

Bell Laboratories
Murray Hill, New Jersey 07971
Attn: U. B. Thomas

The Boeing Company
P. O. Box 3707
Seattle, Washington 98124

Borden Chemical Company
Central Research Laboratory
P. O. Box 9524
Philadelphia, Pennsylvania 19124

Burgess Battery Company
Foot of Exchange Street
Freeport, Illinois 61032
Attn: Dr. Howard J. Strauss

C and D Batteries
Division of Electric Autolite Company
Conshohocken, Pennsylvania 19428
Attn: Dr. Eugene Willihnganz

Calvin College
Grand Rapids, Michigan 49506
Attn: Prof. T. P. Dirkse

Catalyst Research Corporation
6101 Falls Road
Baltimore, Maryland 21209
Attn: J. P. Wooley

ChemCell, Incorporated
3 Central Avenue
East Newark, New Jersey 07029
Attn: Peter D. Richman

Delco Remy Division
General Motors Corporation
2401 Columbus Avenue
Anderson, Indiana 46011
Attn: Dr. J. J. Lander

Douglas Aircraft Company, Incorporated
Astropower Laboratory
2121 Campus Drive
Newport Beach, California 92663
Attn: Dr. Carl Berger

Dynatech Corporation
17 Tudor Street
Cambridge, Massachusetts 02138
Attn: R. L. Wentworth

Eagle-Pitcher Company
P. O. Box 47
Joplin, Missouri 64802
Attn: E. M. Morse

Elgin National Watch Company
107 National Street
Elgin, Illinois 60120
Attn: T. Boswell

Electric Storage Battery Company
Missile Battery Division
2510 Louisburg Road
Raleigh, North Carolina 27604
Attn: A. Chreitzberg

Electric Storage Battery Company
Carl F. Norberg Research Center
19 West College Avenue
Yardley, Pennsylvania 19068
Attn: Dr. R. A. Schaefer

Electrochimica Corporation
1140 O'Brien Drive
Menlo Park, California 94025
Attn: Dr. Morris Eisenberg

Electro-Optical Systems, Incorporated
300 North Halstead
Pasadena, California 91107
Attn: E. Findl

Emhart Manufacturing Company
Box 1620
Hartford, Connecticut 06101
Attn: Dr. W. P. Cadogan

Englehard Industries, Incorporated
497 Delancy Street
Newark, New Jersey 07105
Attn: Dr. J. G. Cohn

Dr. Arthur Fleischer
466 South Center Street
Orange, New Jersey 07050

General Electric Company
Missile and Space Division
Spacecraft Department
P. O. Box 8555
Philadelphia, Pennsylvania 19101
Attn: E. W. Kipp, Rm. T-2513

General Electric Company
Battery Products Section
P. O. Box 114
Gainesville, Florida 32601
Attn: Dr. R. L. Hadley

Aerojet-General Corporation
Von Karman Center
Building 312/Dept. 3111
Azusa, California 91703
Attn: Russ Fogle

Aeronutronic Division
Philco Corporation
Ford Road
Newport Beach, California 92660

Aerospace Corporation
P. O. Box 95085
Los Angeles, California 90045
Attn: Library

Aerospace Corporation
Systems Design Division
2350 East El Segundo Boulevard
El Segundo, California 90246
Attn: John G. Krisilas

Allis-Chalmers Manufacturing Company
1100 South 70th Street
Milwaukee, Wisconsin 53201
Attn: Dr. P. Joyner

American University
Massachusetts and Nebraska Avenues, NW
Washington, D. C. 20016
Attn: Dr. R. T. Foley, Chemistry Department

Arthur D. Little, Incorporated
Acorn Park
Cambridge, Massachusetts 02140
Attn: Dr. Ellery W. Stone

Atomics International Division
North American Aviation, Incorporated
8900 DeSoto Avenue
Canoga Park, California 91304
Attn: Dr. H. L. Recht

Battelle Memorial Institute
505 King Avenue
Columbus, Ohio 43201
Attn: Dr. C. L. Faust